NETWORK MODELLING OF FLOW, STORAGE AND DEFORMATION IN POROUS ROCKS

A DISSERTATION

SUBMITTED TO THE DEPARTMENT OF GEOPHYSICS

AND THE COMMITTEE ON GRADUATE STUDIES

OF STANFORD UNIVERSITY

IN PARTIAL FULFILLMENT OF THE REQUIREMENTS

FOR THE DEGREE OF

DOCTOR OF PHILOSOPHY

By

David Paul Yale

August 1984

ABSTRACT

Existing transport and elastic models of porous rocks with fluids are unable to simultaneously simulate a wide range of experimentally determined petrophysical properties. In this study, a unified network model is constructed which represents the pore space of sedimentary rocks as a three dimensional interconnected network of pore throats and nodal pores. By using realistic pore shapes, one model can simulate both transport and elastic properties of rocks. An experimental apparatus has been constructed to measure the fluid permeability, electrical conductivity, and porosity of rocks at various overburden pressures. These petrophysical properties have been measured for a wide range of sedimentary rocks. By adjusting the distributions of pore sizes and pore shapes in the network model, these and other data from the literature have been accurately simulated. Analysis of the pore sizes and shapes which are required to simulate correctly the data provides the basis for the unified study of the flow, storage and deformation properties of rocks.

The network model is used to gain a fundamental understanding of how the pore space controls the physical properties of rocks and how these properties are interrelated. The model shows that a relationship exits between permeability and formation factor for rocks in which the hydraulic and electrical flow paths are similar; simulation of experimental data helps determine in which rocks the hydraulic and electric

flow paths are similar. Analysis of model simulation shows that wide distributions of pore shapes or pore sizes lead to different hydraulic and electrical flow paths and that the behavior of permeability and conductivity are related to percolation theory in these circumstances. The model explains the strong correlation between the change in permeability with pressure and the absolute value of permeability and it suggests that Archie's exponent, m, is a measure of the decoupling between pore volume and conductivity volume in the pore space.

TABLE OF CONTENTS

LIST OF SYMBOLS

a = radius of contact area for two grains in contact

A = pore tube cross-sectional area

α = aspect ratio of pore tube cross-section at zero pressure = b/c

b = length of semi-minor axis of pore tube cross-section
referred to as "minor width"

$[B]$ = nodal analysis matrix [ ] denotes matrix

$[B^t]$ = transpose of $[B]$

β = displacement of two grains in contact towards each other

c = length of semi-major axis of pore tube cross-section
referred to as "pore tube width" or "major width"

CF = conductivity formation factor = 1/FF
referred to as "conductivity"

E = Young's modulus of rock matrix or grains

ECON = electrical conductance of pore tube

[ECON] = diagonal matrix of electrical conductances of pores

FLRT = dimensionless hydraulic conductance of pore shape

FF = resistivity formation factor = 1/CF
referred to as "formation factor"

[HCON] = diagonal matrix of hydraulic conductances of pores

HCON = hydraulic conductance of pore tube

I_j = current across pore element j (A_j or A_i denotes vector)

J_i = current into node i

k = fluid permeability

K = bulk modulus of rock matrix or grains

K^* = effective bulk modulus of rock with pores

L_e/L = effective flow path length/sample length = tortuosity

ℓ = pore tube length

n = normal force pushing two grains together

m = Archie's exponent where $m = \log (CF)/\log (\Phi)$

μ = fluid viscosity

ν = Poisson's ratio for rock matrix or grains

P = isotropic confining pressure, also Pc

ΔP = pressure drop across a pore

P_{cl} = closure pressure of elliptical pores

P_p = pore pressure

Φ = porosity

Q = volumetric flow rate

r = radius of circular cross-section of pore tube
referred to as "pore tube radius"

r_h = effective hydraulic radius of pore tube

r_e = effective electric radius of pore tube

r* = average radius of grain = pore width for GBP shapes

R* = radius of curvature of grain at the point of contact

R_j = resistance of pore element j

RC = R*/r* ratio of radius of curvature to grain radius

ρ = specific resistivity of pore fluid

s_o = shape factor for "bundle of tubes" model

S = radius of spherical and nodal pores

u = fluid velocity

um = micron = 10^{-6} meter

U_i = voltage at node i

V = volume of rock sample

V_j = voltage across pore element j

VOL = volume of pore

4.5E-3 = 4.5×10^{-3} exponential format is used whenever necessary

$\propto$ = "is proportional to"

π = 3.14159264136847395726310473254872394972304738203453 2...

LIST OF FIGURES AND TABLES

CHAPTER ONE

Introduction and Review of Past Pore Space Models

INTRODUCTION

The pore space of sedimentary rocks controls or influences most of the petrophysical properties of the rock; such as permeability, electrical resistivity, porosity, compressibility and elastic wave velocity. Porous rock has long been treated, macroscopically, as homogeneous continuum; however, in order to understand how the pore space controls the petrophysical properties and how the various properties are interrelated, one must look, microscopically, at the heterogeneous pore space. Because of the complexity and variability of the pore space of a given rock and because of the wide range of pore size, pore shape, and rock matrix composition found between various rocks, realistic and quantitative pore space models that represent a wide range of rock types are difficult to construct.

Petrophysical properties such as permeability and electrical resistivity were first related to the pore space by empirical equations such as the Carmen-Kozeny equation for permeability, k:

$$k = \frac{r_h^2 \Phi}{s_o (L_e/L)^2} \qquad (1)$$

(Kozeny, 1927, Carmen, 1938, Wyllie and Spanger, 1952)

and Archie's equation for resistivity formation factor, FF:

$$FF = \phi^{-m} = \frac{L_e/L}{\phi} \qquad (2)$$

(Archie, 1941, Schopper, 1966)

Both models can be thought of as representing the pore space as a "bundle of pore tubes" where the average pore tube radius is r_h, tube length relative to the sample length is Le/L and pore volume relative to the sample volume is ϕ (s_o is a pore tube "shape factor"and m is an empirical quantity called Archie's exponent). Although the models are useful in representing general trends in the experimental data, they give an unrealistic representation of the pore space. Percolation theory, geometrical considerations and ion tracer studies (Kirkpatrick, 1973, Dullien, 1979, Winsauer et al., 1952) all suggest that the relative fluid path length (Le/L or tortuosity) should be in the range of one to five. Calculations by Wyllie and Spangler (1952) and Dullien (1975b) on twenty-two different sandstones show that equation (2) yields tortuosities of between 5 and 72.

Owen (1952) and Fatt (1956a,b,c) recognized that a more realistic representation of the pore space was needed for accurate modelling. Owen (1952) recognized that the high tortuosities found using Archie's law were unrealistic and devised an alternative view of the pore space. His model consisted of large pores connected to one another via smaller pore tubes (see figure 1). Since resistivity is related to the cross-sectional area of the conductor over its length, Owen postulated that the pore tubes would contribute more to the resistivity of the medium than the nodal pore. He constructed an analog model with pore

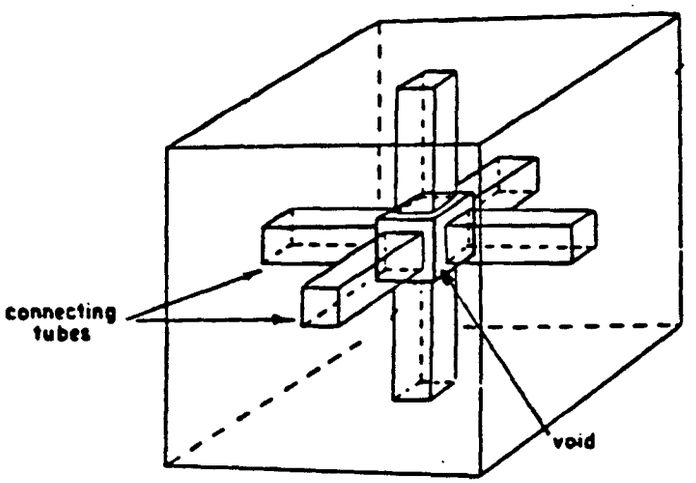

FIGURE 1

Representation of pore space as
nodes (voids) and tubes (Owen 1952)

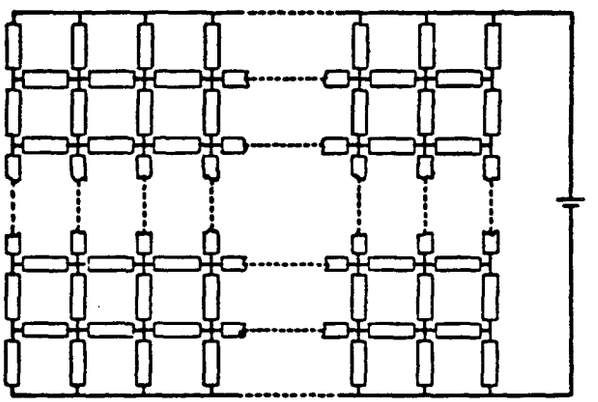

FIGURE 2

Representation of pore space as network
of connected tubes (Fatt 1956a,b,c)

configurations as shown in figure 1 and found that the relative contributions of the pore tube and nodal pores were related inversely to the ratio of their radii. He suggested that a network of these pore elements would give the large formation factor/porosity ratios that are observed without the use of high tortuosities.

Fatt (1956a,b,c) was the first to calculate the permeability and capillary characteristics of a network of pores (see figure 2). The pore elements Fatt used were cylindrical pore tubes whose radii were randomly assigned from a given distribution. Unlike Owen, Fatt's nodes (the pore tube intersections see figure 2) had zero volume. The "permeability" or more strictly speaking the hydraulic conductance of each pore element was assigned according to the Hagen-Pouiselle pipe flow law:

$$Q = \frac{\Delta P \pi r^4}{8 \mu \ell} \qquad (3)$$

where ΔP=pressure drop across pore, ℓ=pore length, r=pore tube radius, μ=fluid viscosity and Q=volumetric flow rate through pore.

Fatt calculated the permeability of a two-dimensional network of pores by constructing a physical network of resistors where the value of each resistor corresponded to the hydraulic resistance of the pore it represented. He simulated relative permeability and capillary displacement by removing resistors whose "pore" had been invaded by the second fluid. These resistors were placed in the same position in a second network so that the relative permeability of each fluid could be calculated.

Fatt's network model proved to be a vast improvement over the bundle of tubes model. The network model correctly predicted the capillary hysteresis and the concavity of the relative permeability versus saturation curve -- two aspects of relative permeability which are always seen in experimental data but not predicted by the simple bundle of tubes model.

Representing the geometry of the pore space as a network is most useful in representing transport properties where the interconnectedness of the real pore space is a controlling factor. Electrical network theory or analogue resistor networks then allow for the exact calculation of the transport properties of the model given the individual pore shapes and sizes. Although interconnectedness is not that important for such petrophysical properties as porosity, compressibility and velocity, the pore shapes and sizes are. In this paper we construct a network pore space model to study both transport properties (permeability and electrical conduction) as well storage (pore volume) and elastic properties (changes in transport and storage properties with pressure) of sedimentary rocks. Just as Owen (1952) found the pore-node-pore model reduced tortuosities to believable levels and Fatt (1956c) found that only a pore network could represent capillary hysteresis, we show that improving the pore geometry and pore shape in a network model allows for the correct representation of a wide range of petrophysical properties. This "unified" pore space model not only allows for the simultaneous modelling of a wide variety of properties, but also leads to a more realistic and unique model of the pore space and to a better understanding of how the pore space controls various properties and how the properties are interrelated.

In this chapter past transport and elastic models are reviewed and the problems confronting the unification of established transport and elastic models are analyzed. The second chapter presents the model which we have developed and analyzes how the model reacts to changes in pore parameters. The third chapter deals with the analysis of simulations which match experimental petrophysical data with a discussion of what information these simulations yield about the pore space and the petrophysical properties that are controlled by the pore space.

REVIEW OF PREVIOUS NETWORK MODELS*

Networks have become standard tools for modelling the transport properties of porous media since they correctly simulate the interconnectedness of the real pore space. Networks have been used most extensively to model immiscible capillary displacement (also known as capillary desaturation and capillary pressure) [1-4, 11, 34, 22, 16, 15, 29, 23, 42, 27, 24, 43, 32]. The notable deviations from Fatt's method are the extension of the simple pore tube network to a more realistic pore tube-nodal pore network similar to Owen's (see figure 7) [4, 27, 1, 43, 32], the extension from immiscible to miscible flow [40, 41, 4], the inclusion of annular flow (two fluids flowing concurrently in the same pore tube) [42] and the extension to three-dimensional networks [34, 22, 29, 43].

Permeability and relative permeability have also been studied using networks [13, 34, 35, 33, 15, 5, 8, 42, 37, 24, 20, 28] with several improvements over Fatt's model. Rose [34] used a three-dimensional model and solved the network flow equations with a computer rather than with an analogue resistor network. Dullien and his co-workers [2, 8, 10] used pore tube radii distributions calculated from real pore size distributions which were obtained from mercury porosimetry and photomicrography of sandstones. Dodds and Lloyd [4] calculated pore tube radii distributions from sphere pack particle size distributions. Seeburger [36, 37] calculated the change in pore tube size with pressure to model permeability variations with confining presstre and Koplik [20] calculated the

* : Reference numbers in this section refer to references listed in Appendix A at the end of this chapter.

flow through spherical pores so that the pore-node-pore model could be extended to permeability.

Electrical resistivity (or formation factor) has not been as widely modelled by the network method [31,35,14,17,18,38,8,25 23] but unlike permeability and capillary pressure, it has been successfully applied to crystalline [14,38,25,26] as well as sedimentary rocks. Networks have also been used to study diffusion, dispersion and surface flow [15,29] as well as second order phase changes in insulator-conductor mixtures and in ferromagnets near the Curie point [39,18].

Pore Geometry

Several different geometries of network models have been proposed. The most popular of these are the two- and three-dimensional regular lattices (see figures 3a,3b). The regular network or lattice allows the construction of analogue models [12,13,14] or the establishment of a set of matrix equations that can be solved for the flow through the network [29,34]. Haring and Greenkorn [15] used a fully random network in which the pore tube radii and lengths are randomly assigned as well as the position of the pore tube in space (in a regular lattice network the position of the pore tube in space remains fixed). This model has the advantage that real pore geometry is more random than allowed for in the regular networks but it has the draw back that random field theory rather than electrical network theory must be used to calculate the properties of the model. This yields exact representations of dispersion [15] but only yields estimates of permeability and electrical resistance and does not allow for any capillary properties to be calculated.

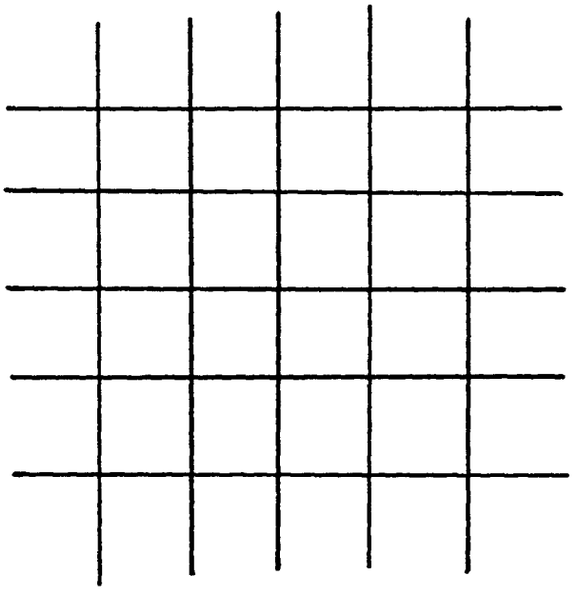

FIGURE 3A

Two-dimensional square lattice

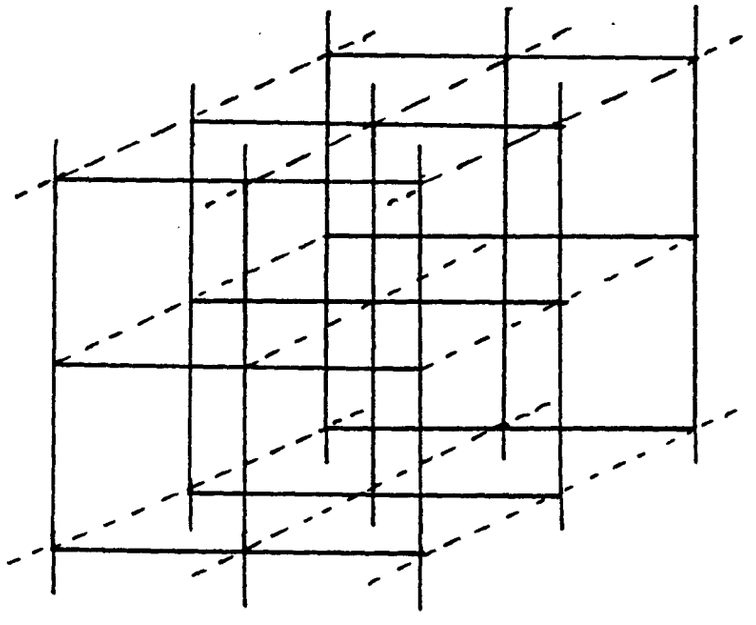

FIGURE 3B

Three-dimensional cubic lattice

Dullien's model [5,8,2,7] is constructed from sets of small networks added together with the permeability and formation factor being calculated from simple statistical equations. Although Dullien gets excellent results, he concedes that the lack of full connectivity in his model leads to problems especially in the capillary characteristics of the model [2].

Two-dimensional network models have been used more frequently than the three-dimensional networks [3,16,35,33,14,40,41,25,42,37,20,1,32] versus [34,22,29,38,26,43] because of simplicity and reduction of computation time, despite the three-dimensional model's more realistic representation of the pore space. Rink and Schopper's [33] use of the Cholesky algorithm further reduces the computation required for the two-dimensional model. However, it has become increasingly evident that two-dimensional networks are not proper representations of three-dimensional porous media. Kirkpatrick [18] and Larson et al. [23] have shown that conduction in three-dimensions is via "clusters" of pores, i.e. flow and conduction are not via single pore channels but rather through clusters of adjacent pores. This "clustering" is much less pronounced in two-dimensional than in three-dimensional networks and it is seen from Seeburger's [37] and Chatizis and Dullien's [2] flow charts that much of the flow is via isolated channels, not clusters, in two-dimensional networks. Another problem in the two-dimensional representation is that percolation thresholds, which are responsible for capillary hysteresis effects and are important in studying two-phase flow, are widely different in two- and three-dimensional networks.

The percolation threshold is defined as the percentage of elements (pore tubes) that need to be present in the network for conduction to occur across the network. Shante and Kirkpatrick [39] found that in square (four tubes meeting at a node) two-dimensional and cubic (six tubes per node) three-dimensional networks, the percolation thresholds are 25% and 50% respectively. Willemson [43] points out that this problem not only results in different saturations at breakthrough but also leads to different residual saturations in two-dimensional networks as compared to three-dimensional networks. We show in the second part of this thesis that even in situations far above percolation threshold, large differences in pore size and shape can lead to the appearance of percolation type phenomena.

Pore tube-nodal pore networks like those of Owen [31] and Koplik [2] have not been used as frequently [31,4,27,20,1] as the simple tube model [30,11,13,34,3,22,16,35,33,14,15,29,40,41,38,5,8,2,7,36,37,24]. Sphere packs [4] and photomicrographs of consolidated sandstones [7,9] show that the pore space can be divided into large "nodal pores" connected to one another via smaller "pore throats" or "pore tubes." The use of the pore tube-nodal pore model is supported further by Owen's [31] explanation (see page 2) for the high resistivity/porosity ratio and by Dullien's [7] theory on the discrepancies between mercury porosimetry and photomicrography pore size distributions (i.e. that the small pore sizes calculated by mercury porosimetry are the connections between the larger pores seen in photomicrography). Both Rink and Schopper [33] and Dullien [5] realize that the constriction of entrances to pores is an important aspect of the pore space but they chose to model this phenomenon by

using bulges in the middle of their pore tube elements while their nodes have zero volume. Dullien [7] mentions that one of the problems with his model is excessive viscous dissipation due to convergent-divergent flow at the nodes. This problem is eliminated in Koplik's [20] pore tube-nodal pore model by assuming slow laminar flow and large pores at the nodes.

Pore Coordination Number

The number of pores that connect together at a node is defined as the coordination number and it has been studied extensively with few conclusive results. For a given size network, increasing the coordination number increases the permeability and decreases the percolation threshold. Two-dimensional networks with coordination numbers of 3,4,6, and 8 (Seeburger 1984, Kirkpatrick 1973, Rink and Schopper 1968, Koplik 1982, Greenberg and Brace 1969) and three-dimensional networks with coordination numbers of 4,6,8,10,12 and 18 (Rose 1956, Kirkpatrick 1971, Greenberg and Brace 1969, Nicholson and Petropoulus 1971) have been studied. Questions remain as to what coordination number exists in the real pore space and what network coordination number best fits experimental data. SEM studies (Wienbrandt and Fatt, 1969, L. Yale personal communication) have shown that the pore coordination number varies from between 3 and 8. Analysis of sphere packs shows that cubic close packing and hexagonal closest packing both yield pore coordination numbers of 6. Yuan (1981) shows that for various packings of spheres of different sizes, the pore coordination number only varies between 4 and 8 in three-dimensions with most of the packings having an average coordination number of 6. We have found that coordination number affects the

nature of two-dimensional networks much more than three-dimensional networks because of the nature of flow path differences in two and three dimensions (Seeburger 1984, Nicholson and Petropoulus 1971).

ELASTIC AND TRANSPORT MODELS:

TWO VIEWS OF THE PORE SPACE

The network models described in the previous section have been used primarily to study how the pore space controls the transport properties of porous media such as permeability, electrical conduction, and two-phase flow. The effect of the pore space on the elastic properties of rocks, such as compressional and shear velocity, pore and bulk compressibility, and changes in transport properties with stress, has been modelled using quite different approaches. One method is the dilute suspension of pores model (Walsh 1965a,b,c, Jaeger and Cook 1976, Watt et al. 1976, Mavko and Nur 1979, Cheng and Toksoz 1979) and a second is the self-consistent embedding of pores model (Walsh 1969, O'Connel and Budiansky 1974, Korringa et al. 1979, Watt et al. 1976, Cleary et al. 1980). Like the network model, both methods begin by calculating the effect of a single pore and embedding an assortment of pores in the rock matrix. The dilute suspension model assumes that the individual pores are far enough apart so that their stress fields do not interact and the effect of all the pores is simply the sum of the effects of each pore. The self-consistent method calculates the effective elastic properties of the rock iteratively as each pore is embedded. In this way, possible interactions between close pores are simulated.

Because the real pore shape and pore geometry are too complex to lend themselves to exact transport and elastic modelling, we must resort to simplified shapes and geometries for which we can calculate the flow and elastic equations and at the same time model the real rock response

that we observe in experimental petrophysics. Unfortunately, network and elastic models have used pore space representations which are very different from each other thus making it difficult to unify transport and elastic models. One difference is that in the network model a highly interconnected pore geometry is used to simulate transport across the rock whereas in elastic embedding models, the pores are assumed not to have any physical connection.

The major difference between the transport and elastic models is that they use pore shapes which are incompatible with the other model. The simplest representation of a pore for both flow and elastic modelling is a cylindrical pore tube or spherical pore (see figures 4a and 4b). The elastic equations for the deformation of a circular inclusion in an otherwise solid matrix have been solved by Muskhelishvili (1953) and others and have been extended to three dimensions for circular cylinders and spheres by Goodier (1933) and Jaeger and Cook (1976). The change in radius of the sphere or tube of circular cross-section from an isotropic pressure, P, is given by:

$$r(P) = \left[1 - \frac{2\,(1-\nu^2)}{E}P\right] \qquad (4)$$

where E=Youngs modulus and ν=Poissons ratio of the matrix. The effect of a set of pores of this shape on the bulk modulus is calculated from equation (4) to be:

$$\frac{1}{K^*} = \frac{1}{K}\left[1 + \frac{16(1-\nu^2)\Sigma S_i^3 + \Sigma\, r_i^2 \ell}{9(1-2\nu)V}\right] \qquad (5)$$

O'Connel and Budiansky (1976)

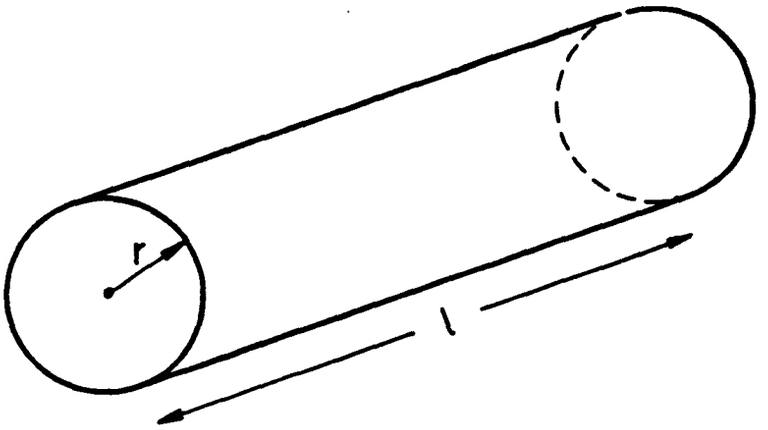

FIGURE 4A

Pore tube with circular cross-section
(cylindrical pore tube)
r = pore tube radius
l = pore tube length

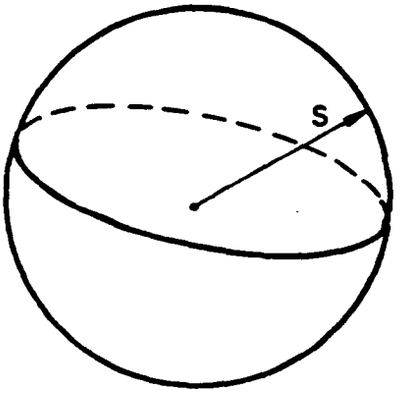

FIGURE 4B

Spherical or nodal pore with S = pore radius

Here K=bulk modulus of grains or matrix, K*=effective bulk modulus of the rock with pores, r_i=pore tube radius, S_i=spherical pore radius, ℓ=pore length and V=volume of sample. It can be seen from equation (4), that the change in radius of pores of these shapes will not be great until the isotropic pressure P approaches the order of Young's modulus, E. Since Youngs modulus is about 5E+5 bars for quartz (Birch 1966), a change in pressure of 10,000 bars is needed to change the bulk modulus by 8% and the permeability by 15% (using equations 3 and 4) for a rock with cylindrical pores. However, most rocks show changes in elastic and transport properties of 10% or more at pressures between 100 and 500 bars (Cheng and Toksoz 1979, Yale 1980, Jones 1978, Han personal communication , Fatt and Davis 1952, Gray et al. 1963, Chierici et al. 1967, Yale 1984, Dobrynin 1962, Wyble 1958).

Almost all of the network models reviewed here used pore tubes of circular cross-section. This is because the flow and capillary characteristics of pores of this shape are simple to calculate and because most of the models were not concerned with how the transport properties change with pressure. However, the stiffness of the circular pore tubes and spherical pores precludes their exclusive use in correctly modelling the changes in elastic moduli and permeability at stresses found in the upper 1000 kilometers of the Earth's crust.

Most velocity models have concentrated on pore shapes which are more compliant but still simple enough so that the elastic equations can be solved exactly. The pore shape used most often in modelling velocities is the thin elliptical crack (Jaeger and Cook 1976, Walsh 1965a,b, O'Connel and Budiansky 1974, Bruner 1976, Korringa et.al. 1979, Cheng

and Toksoz 1979, Watt et.al. 1976) (see figure 5a). The elastic equations for elliptical cracks in two-dimensions and ellipsoidal and oblate spheroidal cavities in three-dimensions (see figure 5b) have been calculated by Eshelby (1957) and Pollard (1973). Elliptical inclusions are elastically convenient pore shapes because the strain field within the ellipse is uniform. The elastic equations for ellipses of large aspect ratio (b>.1c) are similar to those for circles (Pollard 1973), but the equations for thin ellipses (b<<c) depend upon aspect ratio (Berg 1969):

$$b(P) = b_o\left[1 - \frac{2(1-\nu^2)P}{\alpha E}\right] \tag{6}$$

$$c(P) = c_o \quad \text{until pore closing pressure then } c(P_{cl})=0 \tag{7}$$

where b and c are the semi-minor and semi-major widths of the pore and α is the aspect ratio= b_o/c_o. Aspect ratio, α, is defined throughout this report as b/c at zero stress and therefore α does not change with pressure despite changes in b and c with pressure.

Although P is isotropic pressure, the thin nature of the ellipse lets it behave as if it were under a uniaxial stress perpendicular to the semi-minor axis. Using the dilute suspension approximation, the effective modulus of a rock with elliptically shaped pores is:

$$\frac{1}{K^*} = \frac{1}{K}\left[1 + \frac{2(1-\nu^2)\Sigma c_i^2 \ell}{(1-2\nu)V}\right] \tag{8}$$

(Jaeger and Cook 1976)

where ℓ is the length in the third dimension of a pore tube of elliptical cross-section and V is the volume of the rock. There will be a change in the modulus of the rock when the pressure P equals P_{cl}, the pore closing pressure:

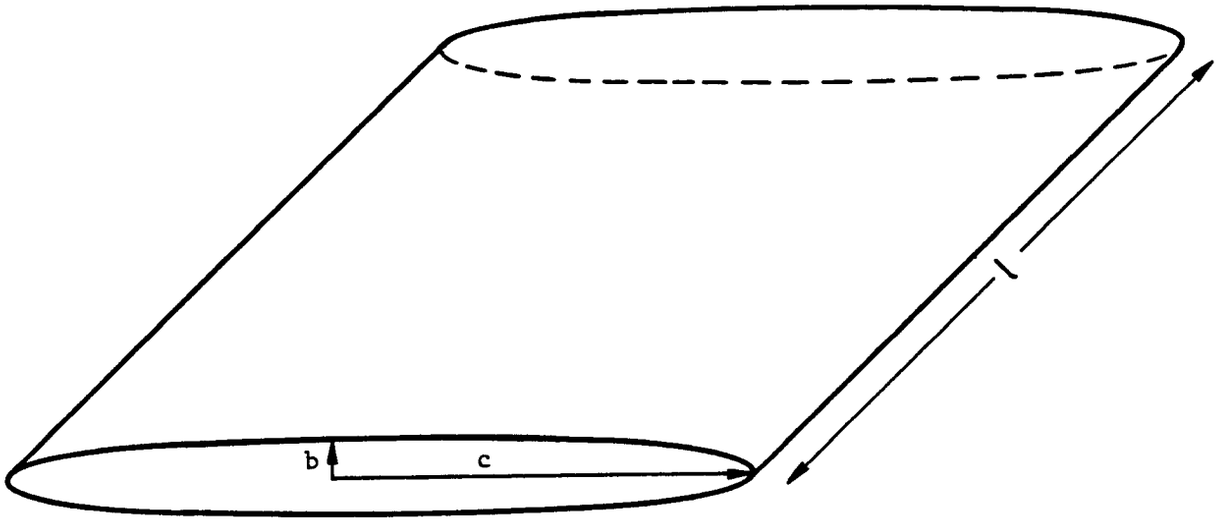

FIGURE 5A

Pore tube of thin elliptical cross-sectional shape
c = pore tube width
b = minor width
l = pore tube length
b/c = aspect ratio of pore tube

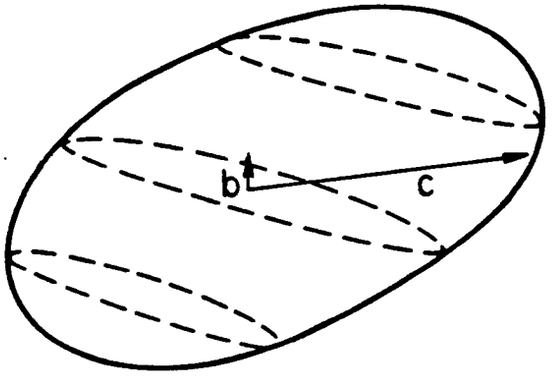

FIGURE 5B

Oblate spheroidal pore
c = pore radius
b = minor width

$$P_{cl} = \frac{\alpha E}{2(1-\nu^2)} \qquad (9)$$

Therefore, a pore space where there is a continuous distribution of aspect ratios among the pores will show a continuous change in velocity and bulk modulus with pressure which is seen in the experimental data.

Cheng and Toksoz (1979) calculated the aspect ratio distribution needed to match P and S wave velocities for several different rocks. Their results are summarized in Table 1, where α is the aspect ratio of the elliptical pores and con(α) is the volumetric concentration of the pores of that aspect ratio. We translate this volumetric concentration to the fraction of the total number of pores that have a given aspect ratio. This fraction is calculated by dividing the volumetric concentration by the aspect ratio and normalizing the sum to 100 percent. We make the assumption that the average pore width, c, does not vary substantially with aspect ratio, an assumption made by Cheng and Toksoz in their calculations of con(α).

Table 1 shows that in Westerly granite, 99.5% of the model pores must have aspect ratios less than or equal to .01. This is very different from Boise sandstone where 63% of the pores have aspect ratios greater than .01. This table also points out one of the shortcomings of elliptical pore shape models. The three sandstones in Cheng and Toksoz study are modelled as having 86% to 91% of their pores with aspect ratios 0.1 or less, yet SEM photos show few pores with aspect ratios less than .1 for rocks within the Berea, Boise and Navajo formations (L. Yale ,1984 and personal communication). Even in Westerly granite, microscopic study has failed to show as many pores with aspect ratios less than 1E-3, as Cheng and Toksoz model predicts (Hadley 1976).

TABLE 1

Aspect Ratio Spectra from Inverted Velocity versus Pressure Profiles (Cheng and Toksoz 1979)

Navajo Sandstone por=.161

α	con(α)	percent
1.0	.1416	9
0.1	.0210	13
.01	.24E-3	1.5
2E-3	.81E-3	30
5E-4	.28E-3	47

Westerly Granite por=.009

α	con(α)	percent
1.0	.69E-2	0.5
.01	.160	12
1E-3	.30E-3	21
4E-4	.12E-3	35
1E-4	.40E-4	30

Berea Sandstone por=.163

α	con(α)	percent
1.0	.140	10
0.1	.022	17
.01	.37E-3	3
1E-3	.44E-3	26
5E-4	.26E-3	44

Boise Sandstone por=.250

α	con(α)	percent
1.0	.1877	14
0.1	.062	49
3E-3	.16E-3	5
1E-3	.33E-3	21
5E-4	.62E-4	10

Note : α = aspect ratio of pores, b/c
con(α) = volumetric concentration of pores of that aspect ratio
percent = percent of all pores with given aspect ratio

Just as the pores of circular cross-section were ineffective in the elastic models, a pore space with a log distribution in aspect ratio of thin ellipses does not model transport properties well. Lamb (1932) has shown the flow equation for pipes (or pore tubes) (see figure 5a) of elliptical cross-section to be:

$$Q = \frac{\Delta P \, \pi \, b^3 c^3}{4\mu\ell(b^2+c^2)} \tag{10}$$

where b and c are the length of the semi-minor and -major axis of the ellipse and ℓ is the pore tube's length. For thin elliptical pore tubes where $b \ll c$, this equation reduces to:

$$Q = \frac{\Delta P}{4\mu\ell} b^3 c = \frac{\Delta P}{4\mu\ell} \alpha^3 c^4 \tag{11}$$

where α=aspect ratio or b/c of the cross-section of the pore. Assuming that the pore width (c) and pore length (ℓ) are kept constant, a pore with aspect ratio 1E-3 conducts 9 orders of magnitude less fluid for a given pressure drop than a pore of aspect ratio 1E-0. Thin pores may have a large pore width but one would need to increase the width of an aspect ratio 1E-3 pore 200 times to have it conduct as much fluid as an aspect ratio 1 pore.

Percolation theory (Kirkpatrick 1973, Koplik 1981b) has shown that in a three-dimensional cubic network, 25% of the pores must have a non-zero conductance for a pore conduction path to exist across the network. If we assume that a set of aspect ratios (as found by Cheng and Toksoz (1979) for Navajo sandstone) are distributed in a cubic network then we can perform the following thought experiment. Starting with a blank or empty lattice of pores we randomly add pores to the lattice beginning

with the pores of highest aspect ratio. After adding the α=1 and α=0.1 pores to the network we find that only 22% percent of the pores are in place and there is no conduction path through the rock. Only after some of the α=0.002 pores have been added do we have a non-zero probability that there is a conduction path across the rock. In other words, we can say that all the fluid that flows through the model rock must pass through pores that have aspect ratio 0.002 or less. We have run computer simulations of networks with this type of log distribution of aspect ratios, and for realistic pore widths (10-100 um), the permeability of these networks is not above 500 microDarcy. The Navajo sandstone generally has a permeability of about 10 to 100 times that value suggesting that thin elliptical pores do not conduct enough fluid to simultaneously match elastic and transport properties of rocks.

Another problem with models that use log distributions of aspect ratios is that they do not model changes in transport properties with pressure properly. A network we constructed with Cheng and Toksöz' (1979) distribution of aspect ratios for Berea sandstone yielded a decrease in permeability and electrical conductivity of 70% and 40% respectively for a pressure change of 500 bars. Experiments on Berea sandstone (Yale 1984a) show changes of only 10% and 5% at 500 bars in permeability and electrical conductivity respectively (see figure 21b and Appendix C).

One could argue that although the pore space may approximate a network of pores, a substantial part of the thin pores may be located between the main network elements, i.e. they may not participate in the flow at all. If this is assumed, we must also assume that the thin pores are smaller (smaller widths and lengths) than the pores of higher

aspect ratio. This would substantially increase the fraction of the pores of low aspect ratio as calculated in Table 1 (where we assume the width and length of the pores to be independent of aspect ratio). If the pores of aspect ratio less then 0.1 are half the size of the pores of aspect ratio 1.0 and 0.1 for the Navajo sandstone then there must be 14 times as many thin pores ($\alpha<0.1$) as wide pores ($\alpha>=.1$). With this many thin pores we can not sustain the assumption that the thin pores do not connect to the network of larger pores. We conclude that the number of very thin pores needed to match velocity versus pressure data are not compatible with experimental results on the transport of fluids through rocks.

Mavko and Nur (1978) introduced a thin tapered pore shape because of the unrealistic behavior of the thin elliptical pore. A pore tube with this shape shown in figure 6. The deformation equations are again calculated in the thin crack approximation ($\alpha<.1$). The change in minor and major widths are given as:

$$b(P) = b_0\left[1- \frac{4(1-\nu^2)}{3\alpha E}P\right]^{3/2} \tag{12}$$

$$c(P) = c_0\left[1- \frac{4(1-\nu^2)}{3\alpha E}P\right]^{1/2} \tag{13}$$

The variation in bulk modulus with pressure due to these cracks is given by:

$$\frac{1}{K^*} = \frac{1}{K}\left[1 + \frac{2\pi(1-\nu^2)\Sigma c_i^2 \ell}{(1-2\nu)\quad V}\right] \tag{14}$$

(Mavko and Nur, 1978)

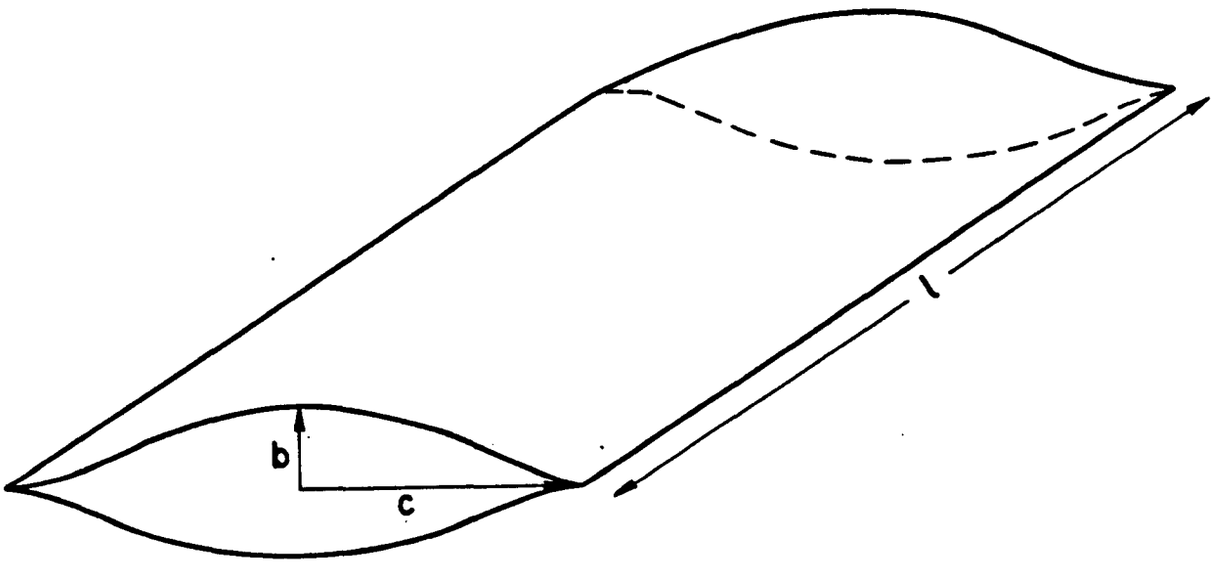

FIGURE 6

Pore tube with tapered (TAP) cross-sectional shape (from Mavko and Nur, 1978)
c = pore tube width
b = minor width
l = pore tube length
b/c= aspect ratio of pore tube

where c=major width, ℓ=length of pore tube in third dimension, and V=volume of rock. Notice that this equation is almost identical to the elliptical and circular cases. The two differences between this shape and the elliptical pore are first, the more realistic shape; most pores end in grain-to-grain boundaries which are better represented by Mavko's pointed cracks than by the rounded ellipses. Secondly, equation 13 shows that the tapered pores major width changes with pressure allowing the modulus and elastic wave velocities to change gradually with pressure without having to close completely before effecting the modulus as elliptical pores must.

Although Mavko's tapered pore shape is an improvement over the elliptical shape because it allows K* to change continuously with pressure, the aspect ratios needed to model changes in elastic properties as well as changes in transport properties such as permeability and electrical conductivity are on the order of 1E-4 to 1E-2. With pores this thin it becomes very difficult to model rocks with permeabilities of greater than 1 to 10 milliDarcy or to model changes in transport properties with pressure. In order to unify transport and elastic models, we must first specify a family of pore shapes which is compatible with both the network and elastic models. These shapes must have large enough aspect ratios to account for observed permeabilities and formation factors but they must also be compliant enough to allow for the changes in permeability, formation factor and modulus that are found experimentally. In chapter 2 we introduce a family of pore shapes which satisfy these criteria.

APPENDIX A

BIBLIOGRAPHY OF NETWORK MODELS

1. Chandler,R., J.Koplik, K.Lerman and J.F.Willensen, Capillary Displacement and Percolation in Porous Media, Schlumberger-Doll preprint, 1981

2. Chatzis,I. and F.A.L.Dullien, Modelling Pore Structure by 2-D and 3-D Networks with Application to Sandstones, J. Cand. Pet. Tech., vol.16, p.97, 1977

3. Dodd,C.G. and O.G.Kiel, Evaluation of Monte Carlo Methods in Studying Fluid-Fluid Displacement and Wettability in Porous Rocks, J. Phys. Chem, vol.63, p.1646, 1959

4. Dodds,J.A. and P.S.Lloyd, A Model for the Void Structure in Multi-Component Sphere Packs Applied to Capillary Pressure Curves, Powder Tech., vol.5, p.69, 1971/72

5. Dullien,F.A.L., New Network Permeability Model of Porous Media, AIChE Jour., vol.21, p.299, 1975a

6. Dullien,F.A.L., Prediction of 'Tortuosity Factors' from Pore Structure Data, AIChE Jour., vol.21, p.820, 1975b

7. Dullien,F.A.L., Porous Media: Fluid Transport and Pore Structure, Acedemic Press, New York, 1979

8. Dullien,F.A.L., I.Chatizis and M.S.El-Sayed, Modelling Transport Phenomena in Porous Media by Networks Consisting of Non-Uniform Capillaries, SPE paper 6191, 1976

9. Dullien,F.A.L. and G.K.Dhawan, Characterization of Pore Structure by a Combination of Qualitative Photomicrography and Mercury Porosimetry, J. Coll. Interfac. Sci., vol.47, p.337, 1974

10. Dullien,F.A.L. and G.K.Dhawan, Bivariate Pore-Size Distributions of Some Sandstones, J.Coll. Interfac. Sci., vol.52, p.129, 1975

11. Fatt,I., The Network Model of Porous Media: I. Capillary Pressure Characteristics, Trans. AIME, vol.207, p.144, 1956a

12. Fatt,I., The Network Model of Porous Media: II. Dynamic Properties of Single Size Tube Network, Trans. AIME, vol.207, p.160, 1956b

13. Fatt,I., The Network Model of Porous Media: III. Dynamic Properties of Networks with Tube Radius Distribution, Trans. AIME, vol.207, p.164, 1956c

14. Greenberg,R.J. and W.F.Brace, Archie's Law for Rocks Modeled by Simple Networks, J. Geophys. Res., vol.74, p.2099, 1969

15. Haring,R.E. and R.A.Greenkorn, A Statistical Model of a Porous Medium with Nonuniform Pores, AIChE Jour., vol.16, p.477, 1970

16. Harris,C.C., Latin Square as a Network Model of Random Packing, Nature, vol.205, p.353, 1965

17. Iczkowski,R.P., Electrical Conductivity of Partially Saturated Porous Solids, Ind. Eng. Chem. Fundam., vol.9, p.674, 1970

18. Kirkpatrick,S., Percolation and Conduction, Rev. Mod. Phys., vol.45, p.574, 1973

19. Koplik,J., On Effective Medium Theory of Random Linear Networks, Schlumberger-Doll preprint, 1981a

20. Koplik,J., Creeping Flow in Two-Dimensional Networks, Schlumberger-Doll preprint, 1981b

21. Koplik, J., Note on the Permeability of Random Networks, Schlumberger-Doll preprint, 1982

22. Ksenzhek,O.S., Capillary Equilibrium in Porous Media with Intersecting Pores, Russ. J. Phys. Chem., vol.37, p.691, 1963

23. Larson,R.G., L.E.Scriven and H.T.Davies, Percolation Theory of Residual Phases in Porous Media, Nature, vol.268, p.409, 1977

24. Lin,C.Y. and J.C.Slattery, Three-Dimensional, Randomized, Network Model for Two-Phase Flow through Porous Media, 2nd Joint SPE/DOE Enhanced Oil Recovery Symp., 1981

25. Madden,T.R., Random Networks and Mixing Laws, Geophysics, vol.41, p.1104, 1976

26. Madden,T.R., Microcrack Connectivity in Rocks: A Renormalization Group Approach to the Critical Phenomena in Crystaline Rocks, J. Geophys. Res., vol.88, p.585, 1983

27. Mohanty,K.K., H.T.Davies and L.E.Scriven, Physics of Oil Entrapment in Water-Wet Rock, SPE paper 9406, 1980

28. New Mexico Institute of Mining and Technology, Three-Dimensional Network Analysis of Interconnected Circular and Slit-Shaped Pores, progress report, 1982

29. Nicholson,D. and J.H.Petropoulos, Capillary Models for Porous Media: III. Two-phase flow in a three-dimensional network with Gaussian radius distribution, J.Phys. D: Appl.Phys., vol.4, p.181, 1971

30. Nur,A., Pore Space Models and the Effects of Pressure on the Relation between Physical Properties, SRP report, vol.7, p.125, 1979

31. Owen,J.E., The Resistivity of a FLuid-Filled Porous Body, Trans. AIME,

vol.195, p.169, 1952

32. Payatakes,A.C., Dynamics of Oil Ganglia During Immiscible Displacement in Water-Wet Porous Media, Ann. Rev. Fluid Mech., vol.14, p.365, 1982

33. Rink,M. and J.R.Schopper, Computations of Network Models of Porous Media, Geophys. Prosp., vol.16, p.277, 1968

34. Rose,W., Studies of Waterflood Performance III. Use of Network Models, Ill. State Geol. Surv. Circ., vol.237, p.1, 1957

35. Schopper,J.R., A Theoretical Investigation on the Formation Factor/ Permeability/ Porosity Relationship Using a Network Model, Geophys. Prosp., vol.14, p.301, 1966

36. Seeburger,D., Fluid Flow through Elliptic and Simple Nonelliptic Fractures, SRP report, vol.7, p.104, 1979

37. Seeburger,D., A Pore Space Model for Rock Permeability and Bulk Modulus, Jour. Geophys. Res., vol.89, p.527, 1984

38. Shankland,T.J. and H.S.Waff, Conductivity in Fluid-Bearing Rocks, J. Geophys. Res., vol.79, p.4863, 1974

39. Shante,V.K.S. and S.Kirkpatrick, An Introduction to Percolation Theory, Advan. Phys., vol.20, p.325, 1971

40. Simon,R. and F.J.Kelsey, The Use of Capillary Tube Networks in Reservoir Performance Studies: I. Equal Viscosity Miscible Displacements, Soc. Pet. Eng. J., vol.11, p.99, 1971

41. Simon,R. and F.J.Kelsey, The Use of Capillary Tube Networks in Reservoir Performance Studies: II. Effect of Heterogeneity and Mobility on Miscible Displacement Efficiency, Soc. Pet. Eng. J., vol.12, p.345, 1972

42. Singhal,A.K. and W.H.Somerton, Quantitative Modelling of Immiscible Displacement in Porous Media: A Network Approach, Rev. Inst. Franc. Pet., vol.32, p.897, 1977

43. Willenson,J.F., Percolation Theory and Capillary-Dominated Flow in 3-D, Schlumberger-Doll preprint, 1981

CHAPTER TWO

A Unified Network Model and Its Response to Changes in Pore Parameters

A THREE-DIMENSIONAL PORE SPACE NETWORK MODEL

We have developed a computer network model to simulate and study the following six properties of porous sedimentary rocks.

1) fluid permeability, k
2) conductivity formation factor, CF
3) porosity, ϕ
4) permeability change with stress, k(P)
5) conductivity change with stress, CF(P)
6) porosity change with stress, ϕ(P)

We define the conductivity formation factor as the conductivity of a fluid saturated rock divided by the conductivity of the pore fluid. Conductivity formation factor is equal to one over the resistivity formation factor which is more commonly referred to as simply formation factor. We use "conductivity" when referring to the conductivity formation factor and "formation factor" when referring to its inverse, resistivity formation factor. In addition to the above properties, the model is being extended to study the anisotropy in permeability and electrical conductivity, to examine the effect of pores on elastic wave velocities (with Jorge Mendoza), and to model the effect of pores and frequency on

the dielectric constant and resistance of porous rocks (with Rosemary Knight).

The main difference between our approach and past models is that we simulate several different petrophysical properties in a single pore space model. This unified approach yields a more realistic and unique representation of the pore space than models concerned with only a single property. The unified approach also allows us to study the relationships among various petrophysical properties and helps us better understand how the pore space controls these properties. Another important departure from most previous models is the inclusion of static elastic properties into a model which has predominantly been used to study only transport properties in the past. This allows the model to simulate the changes in permeability, electrical conductivity and porosity due to changes in pore or confining pressure. We have developed a set of pore shapes (called GBP shapes and discussed in the section entitled 'Grain Boundary Pore Shapes') which are compatible with both elastic and transport modeling.

The goals of this project are to develop a model that will correctly simulate the six petrophysical properties for a wide range of sedimentary rocks. Model simulations which match experimental data are used to gain a better understanding of how the pore space controls various petrophysical properties. In other words, we can analyze exactly how the distribution of pores affects the simplified model and then infer what might be happening in the real pore space. Analysis of the model pore space also offers insights into the relationships among various properties and is useful in determining the degree of correlation between properties for a given rock.

The model presented in this paper is a computer simulation of a three-dimensional cubic network of nodal pores and connecting pore tubes (see figure 7). We have extended the more widely used two-dimensional network to three-dimensions because it better simulates the flow characteristics of real porous media (Kirkpatrick 1973, Larson et al. 1977). The nodal pore-pore tube concept used by Owen (1952), Koplik (1981a), and Dodds and Lloyd (1971) is included to model tortuosities, storage capacity and nodal flow more correctly. The regular cubic lattice is used because it yields a pore coordination number of six (which appears realistic for sedimentary rocks (Yuan 1981), it simulates isotropic flow (Kirkpatrick 1973) and it simplifies certain numerical calculations.

In this chapter we develop the pore shapes need to unify transport and elastic models and then describe the unified model we have constructed. The second part of this chapter deals with how the model responds to changes in the pore parameters, i.e. using the network as a forward model to better understand how the pore space controls various properties.

Grain Boundary Pore Shapes

As discussed in a previous section, differences in pore shape make it difficult to combine previous elastic and transport models into a single model. The thin tapered and thin elliptical pore shapes can not be used in models for rocks with permeabilities greater than 1 to 10 milliDarcy without unrealistically large pore widths. Similarly, we can not model changes in velocity, porosity, permeability, and conductivity due to pressure with the circular pore tubes used in most transport models.

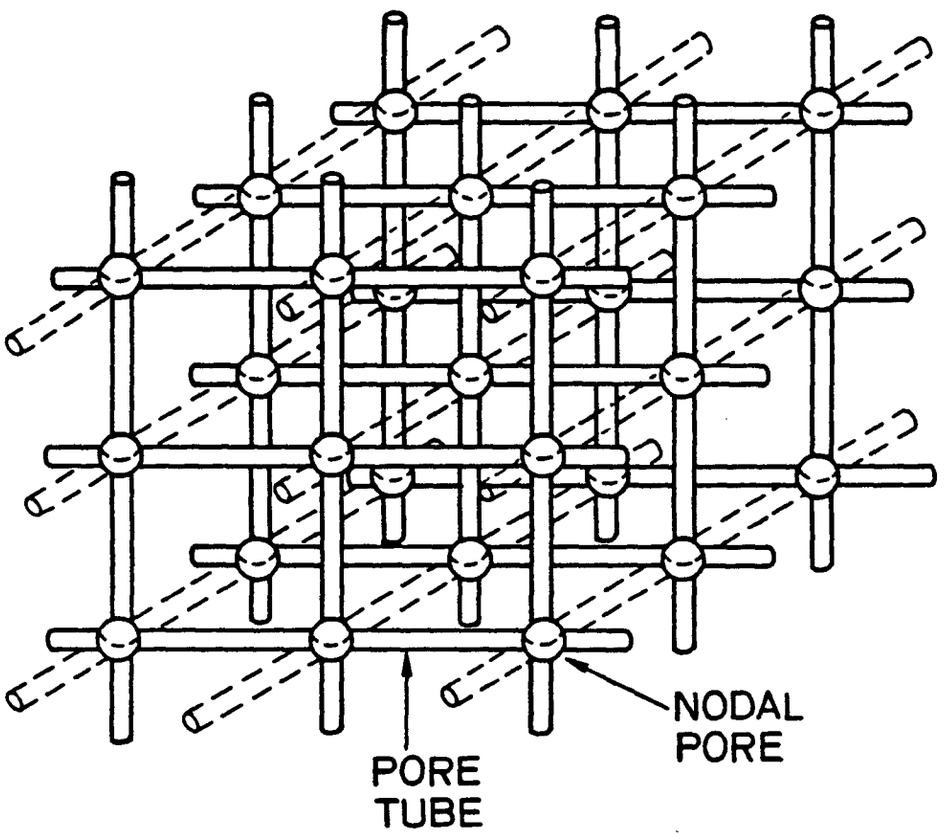

FIGURE 7

Three-dimensional cubic network of
pore tubes and nodal pores
3X3X3 network with 28 nodes and 90
pore tubes

Since most velocity and elastic modulus studies have been approached from the point of view of igneous rocks, thin intergranular cracks as pores have been realistic. But extrapolation to sedimentary rocks, which are collections of grains that have been cemented together, does not appear valid. A better approach is to use the properties of an unconsolidated packing of grains. Hertz-Midlen contact theory (Timoshenko and Goodier 1971) has been used to calculate the elastic moduli of ordered and disordered packings of grains (Murphy 1982, Duffy and Mindlin 1957). In these models velocities and elastic moduli are related to the grain shape and size rather than the pore shape and size.

The flow of fluids through grain packings has an extensive literature and the flow equations for unit cells of various single sized grain packings has been calculated approximately by Snyder and Stewart (1966), and Stewart and Sorensen (1974). These equations turn out to be very complex and valid only for packings of equidimensional spheres. No investigation of how changes in pressure would effect changes in the flow properties of these grain packs has been undertaken. The angular nature of most sandstone grains and the effect of cements and overgrowths on the elastic properties make the extrapolation from grain packs to consolidated sandstones even more difficult.

We have found that although the sphere packs may not represent consolidated sediments exactly, the idea of a pore as bounded by grains and whose elastic properties are dependent upon the deformation of those grains (Hertz contact theory), appears more effective in modelling the transport and elastic properties of a porous sedimentary rock than models where the pore is an isolated inclusion in a homogeneous matrix.

The pore tube shapes we introduce here will be referred to as GBP shapes (grain boundary pore shapes) and they are illustrated in figures 8-12.

The shapes are formed by the smallest opening between four grains in contact. Changing the roundness or angularity of the grains surrounding the pore change the shape and deformation of the pore with pressure. We can envision pores formed by cubic close packs (figure 8a) or hexagonal closest pack (figure 8b). The differences between the two are not large and the elastic and flow calculations for the cubic close pack shape are simpler. Our shape is an approximation of the real pore space and an approximation of a real grain pack. Figures 9a and 9b show a unit cell of a sphere pack and its hydraulic equivalent using GBP shaped tubes and spherical nodal pores (as we do in the network model). The flow in the unit cell of a sphere pack is controlled by the smallest opening in the unit cell and is why the GBP shape is modelled as the smallest opening between four grains in contact.

Applying a force pushing all the grains together forces them to deform at the points of contact and forces a change in shape and size of the pore tube cross-section. The equations governing how the grains and thus the pore shape will deform under stress are given by Hertz contact theory (Hertz 1881, Timoshenko and Goodier 1972).

For two grains under a normal force n, whose radius of curvature at their point of contact is R*, the radius of contact, a, is given by:

$$a = \left[\frac{3(1-\nu^2)n}{4E} R^*\right]^{1/3} \tag{15}$$

The displacement of the centers of the two grains is given by ß:

$$\beta = \left[\frac{9(1-\nu^2)^2 n^2}{2E^2 R^*}\right]^{1/3} \tag{16}$$

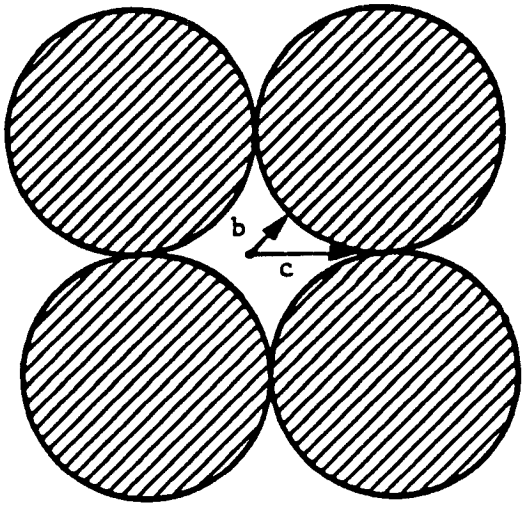

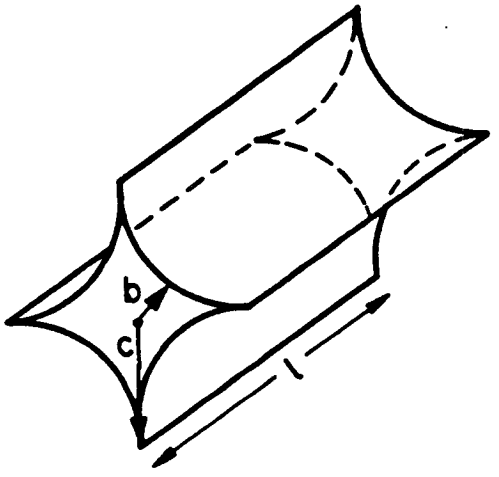

FIGURE 8A

Cross-section of cubic close pack (GBP) pore shape

Pore tube with GBP pore shape
c = pore width
l = pore length
b = minor width
b/c= aspect ratio of pore

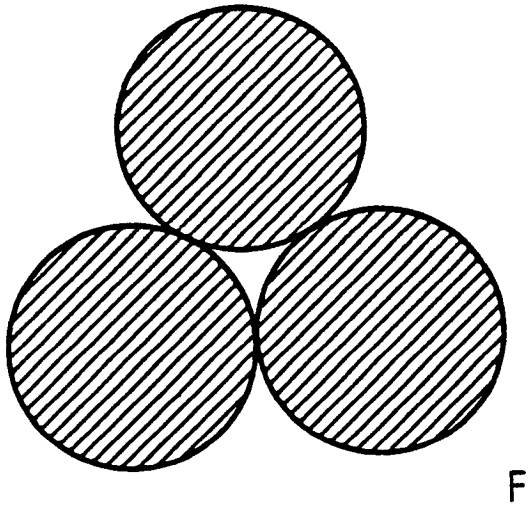

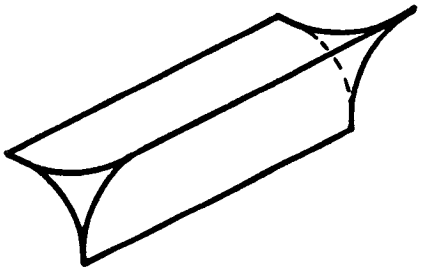

FIGURE 8B

Cross-section of hexagonal closest pack pore shape

Pore tube with hexagonal closest pack shape

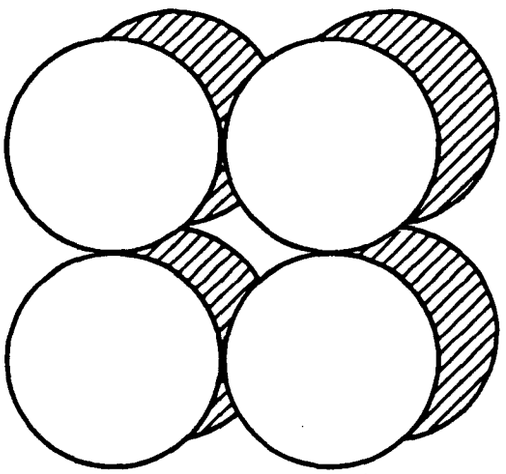

FIGURE 9A

Cubic close packing of spheres

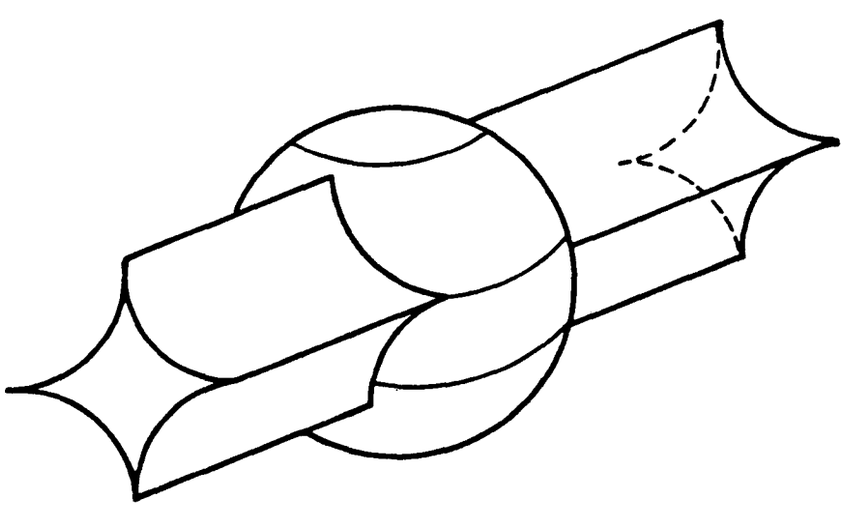

FIGURE 9B

Hydraulic and electrical equivalent of Figure 9a for flow in the z direction using GBP pore tubes and spherical nodal pore.

where ν=Poissons ratio and E= Youngs modulus of the grains. For an isotropic packing of grains, the normal force n can be converted into a hydrostatic pressure P through the equation:

$$n = \sqrt{2} r^{*2} P \qquad \text{(Murphy 1982)} \qquad (17)$$

where r*= the average radius of the grains. Since the radius of the grains can be different from the radius of curvature at the point of contact of the grains, a family of shapes as illustrated in figures 10a,b,c,d can be generated where the thinner (high R*/r* or RC ratio) pore shapes deform more for a given pressure. The Hertz equations can thus be modified and normalized to:

$$\frac{a}{r^*} = \left(\frac{R^*}{r^*}\right)^{1/3} \left(\frac{3\sqrt{2}(1-\nu^2)P}{4E}\right)^{1/3} \qquad (18)$$

$$\frac{\beta/2}{r^*} = \left(\frac{r^*}{R^*}\right)^{1/3} \left(\frac{3\sqrt{2}(1-\nu^2)P}{4E}\right)^{2/3} \qquad (19)$$

where r*=average radius of grain and R*=radius of curvature at contact point; a and β are normalized to the grain radius because the pore width, c, of this shape is equal to our definition of average grain radius, r*. R*/r* is independent of pore width so that the relative deformation of a pore is independent of the absolute size of the pore and is only dependent on the pore shape. The pore shape of the GBP pores is characterized by the R*/r* ratio which we denote as the "RC" ratio of the shape.

Equations 5, 8, and 14 all relate the effective bulk modulus to the pore width and not to the pore shape. Therefore as a first order approximation, we infer that the change in bulk modulus due to a collection of GBP pores is governed by the following equations:

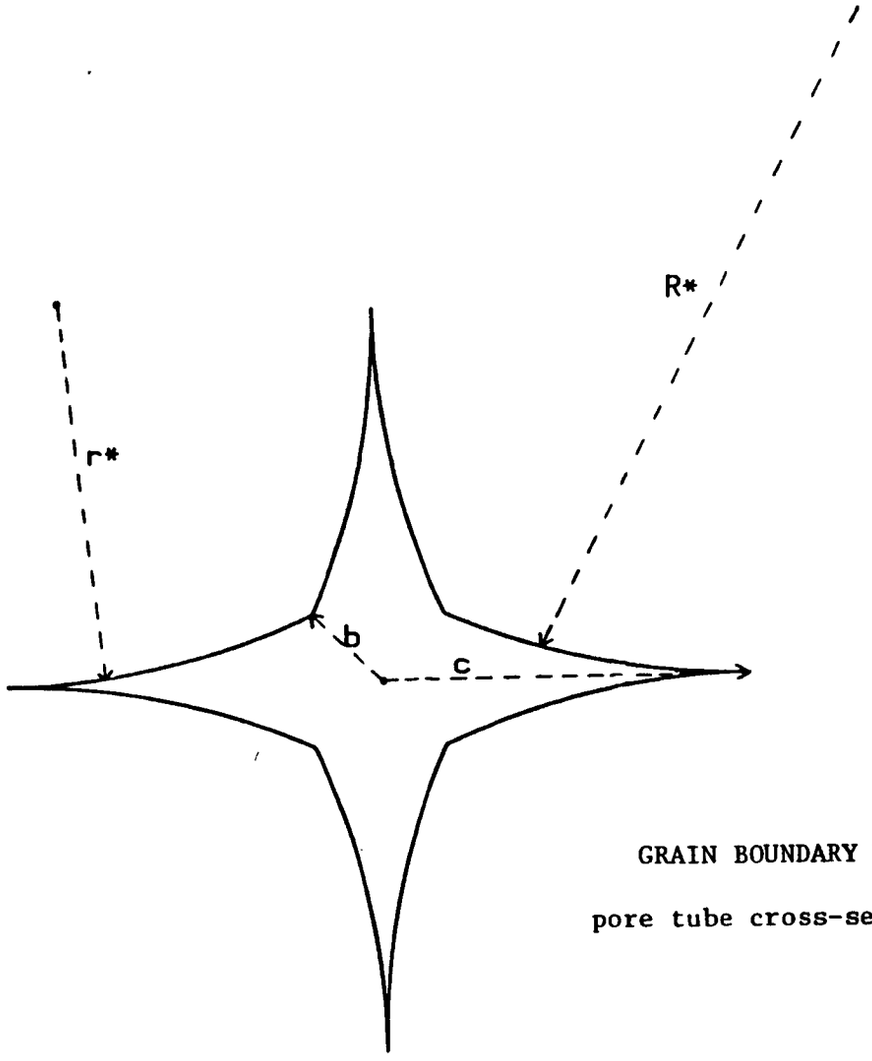

FIGURE 10B

GBP-RC2 pore tube shape
r* = average grain radius
R* = radius of curvature
c = pore shape width
R*/r* = "RC" factor

GRAIN BOUNDARY PORE (GBP)

pore tube cross-sectional shapes

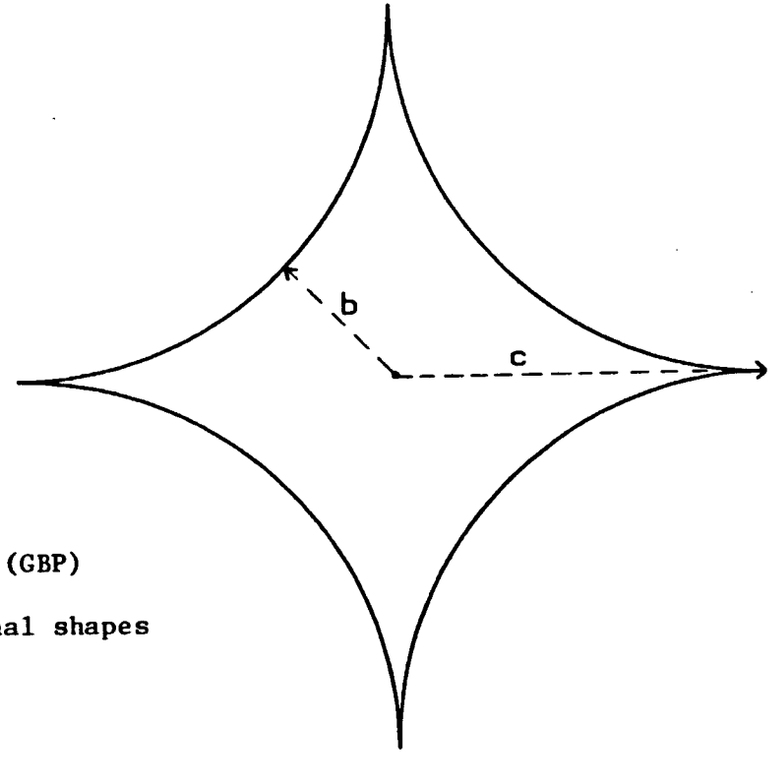

FIGURE 10A

GBP-RC1 pore tube shape
b/c = aspect ratio

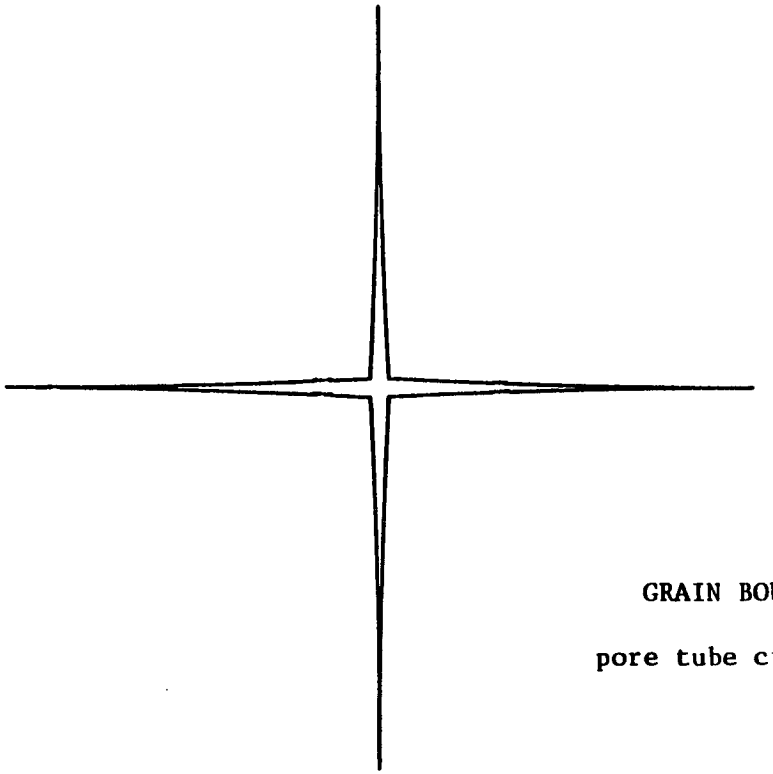

FIGURE 10c

GBP-RC20 pore tube shape

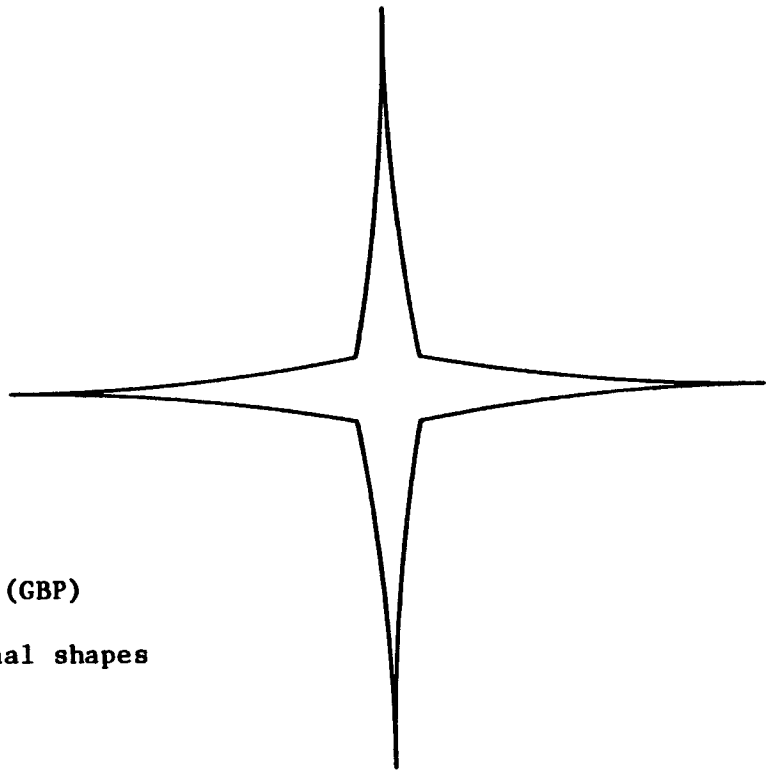

FIGURE 10D

GBP-RC5 pore tube shape

GRAIN BOUNDARY PORE (GBP)

pore tube cross-sectional shapes

$$c(P) = c_0\left(1 - \frac{a(P)}{c_0}\right) \tag{20}$$

$$\frac{1}{K^*} = \frac{1}{K}\left(1 + \frac{4\pi\Sigma c_i^2 \ell}{V}\right) \tag{21}$$

where c= pore width, a=change in pore width from equation 18. This equation is rigorous only for a dilute suspension of non-interacting pores. In our model the pores are close enough to interact but we feel that Hertz contact theory naturally imbeds part of the pore-pore interaction. Mendoza (personal communication) has suggested that the dilute suspension model is rigorous only when the pores are more than one pore radii apart. This is because the stress field caused by the crack tips is almost negligible one pore radius away. In the case of the GBP pores we assume in our deformation calculations that there is another pore adjacent to and in contact with the pore we are studying (see figure 11). Hertz contact theory therefore essentially takes care of the interaction of the stress field of the two pores.

The differences between the thin elliptical, thin tapered and GBP pore shapes are shown in figure 12. Here we show the change in pore width squared (c^2) (which is related to changes in elastic properties) with pressure for the four pore shapes:

$$c(P)^2 \propto \left(1 - \frac{P}{E}\right)^2 \qquad \text{circle} \tag{22}$$

$$c(P)^2 \propto \left(1 - \frac{P}{\alpha E}\right)^2 \qquad \text{ellipse} \tag{23}$$

$$c(P)^2 \propto \left(1 - \frac{P}{\alpha E}\right) \qquad \text{tapered} \tag{24}$$

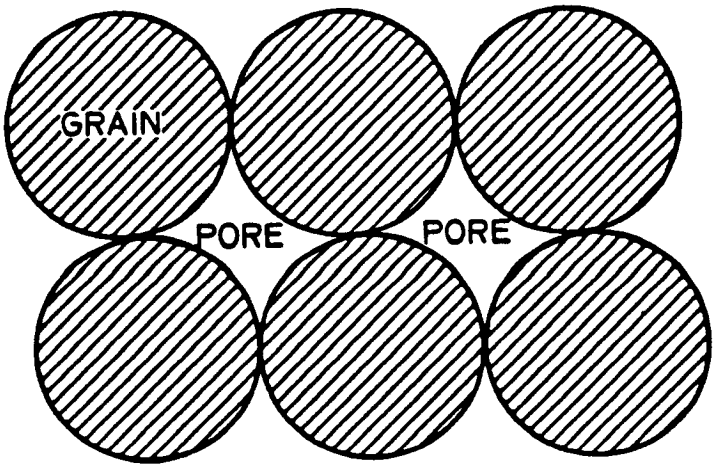

FIGURE 11

Calculation of pore deformation using Hertz contact theory (GBP pores) assumes there are adjacent pores as shown in the above figure.

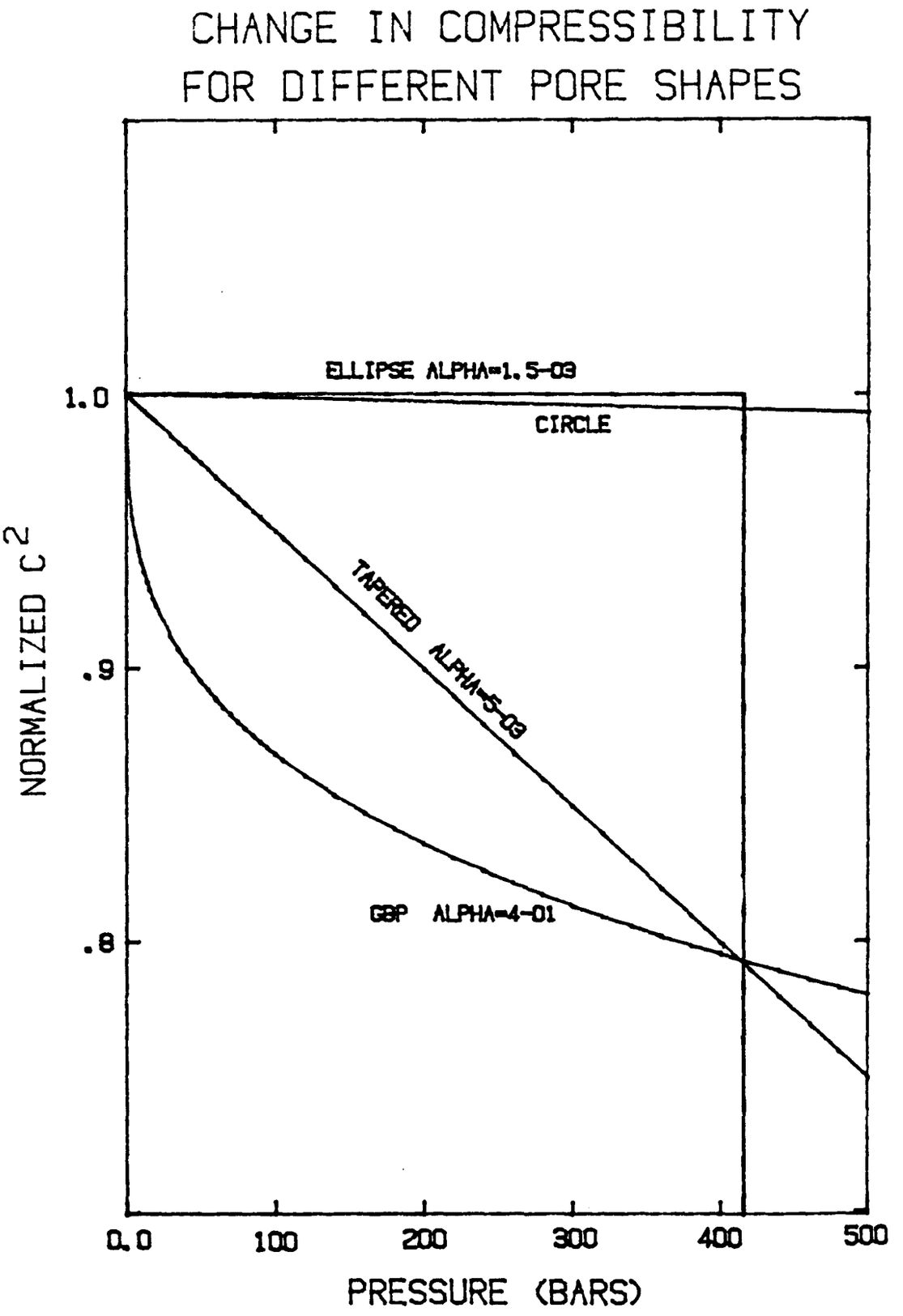

FIGURE 12

Change in pore widt h squared, c^2, with pressure for different pore tube shapes. Compressibility related to c^2

$$c(P)^2 \propto \left[1 - \left(\frac{P}{\alpha^* E}\right)^{1/3}\right]^2 \quad \text{GBP} \qquad (25)$$

The aspect ratios for the thin elliptical and thin tapered shapes are adjusted to match the change in c^2 observed in a GBP shape of aspect ratio .4 (RC=1) at 410 bars. The aspect ratio or α of each GBP shape is defined as b/c as illustrated in figures 10a and b and α^* is defined as 1/RC. Note that we need to use much thinner elliptical and tapered (α =1.5E-3 and 5E-3) shapes to match the high aspect ratio GBP shape. We also note the step function, linear and non-linear behaviors of the elliptical, tapered and GBP curves respectively. Mendoza (personal communication) has found that the GBP pores can correctly model the change in bulk modulus and compressional velocity for several rocks with very narrow distributions of aspect ratios. Table 3 shows the relationships between pore shape and aspect ratio for the GBP and tapered pores.

We start the network approach by analyzing the flow, storage and deformation characteristics of each pore in the network. Network theory gives us a set of simultaneous equations which relate those microscopic pore properties to the macroscopic rock properties of permeability and conductivity. In the following section, we describe the equations which relate the size and shape of the pore to its hydraulic and electrical conductance, its volume and its elastic characteristics.

Flow and Storage Equations for Pores

In order to calculate the hydraulic conductance of a pore tube, the size and shape of the pore must be known. Each pore tube is assumed to have a constant cross-section across its length and each pore is fully characterized by specifying the pore tube length, cross-sectional shape and cross-sectional width. We use three different pore tube shapes in our model; circular cylinders, tapered cross-section pore tubes and pore tubes with the GBP type shape. The simplest pore tube shape is a cylinder of circular cross section a where the hydraulic conductance can be calculated from Hagen-Pouiselle pipe flow:

$$Q = \frac{\Delta P \pi r^4}{8\mu\ell} \tag{26}$$

where Q=volumetric flow rate, ΔP=pressure drop, ℓ=pore length, r=radius of the pore, and μ=viscosity of the pore fluid. The hydraulic conductance is defined as:

$$HCON = \frac{Q}{\Delta P} = \frac{\pi r^4}{8\mu\ell} \tag{27}$$

For pores of tapered cross-section, comparison of numerical and analytical results shows that the equation for flow in elliptical pores is an excellent approximation.

$$HCON \simeq .685 \cdot \frac{\pi b^3 c^3}{(b^2+c^2)\mu\ell} \tag{28}$$

For the GBP shapes, simple analytical solutions for the hydraulic conductance do not exist. In order to calculate the hydraulic conductance, we first solve a dimensionless Poissons equation across a unit cross-section of a pore tube:

$$\frac{\partial^2 u}{\partial x^2} + \frac{\partial^2 u}{\partial y^2} = 1 \qquad (29)$$

where u=fluid velocity due to a unit pressure gradient perpendicular to the cross-section and a no-slip or u=0 boundary condition is imposed along the walls. Because the GBP shapes are hyperbolic, the solution to Poissons equation is most easily solved numerically using a finite difference grid. The solution to the Poisson equation gives the fluid velocity at all points in the cross-section perpendicular to the cross-section. This velocity profile is then integrated to find the flux through the cross-section and by integrating the flux in the direction of the pressure gradient, the hydraulic conductance can be calculated. The flow equation becomes:

$$Q = \frac{\Delta P c^4}{\mu \ell} \cdot FLRT \qquad (30)$$

where FLRT is the dimensionless hydraulic conductance found from integrating the Poisson solution over a unit cross-section and a unit length pore tube (c is the pore tube width). The hydraulic conductance is defined here as:

$$HCON = \frac{Q}{\Delta P} = FLRT \cdot \frac{c^4}{\mu \ell} \qquad (31)$$

The change in hydraulic conductance with stress is found by calculating how each cross-sectional shape changes with pressure (using Hertz contact theory) and then solving for the hydraulic conductance of the new shape (by integrating the Poisson solution for that shape). The change in hydraulic conductances for pores of circular, thin elliptical, thin tapered and GBP cross-section are shown in figure 13. Note that at

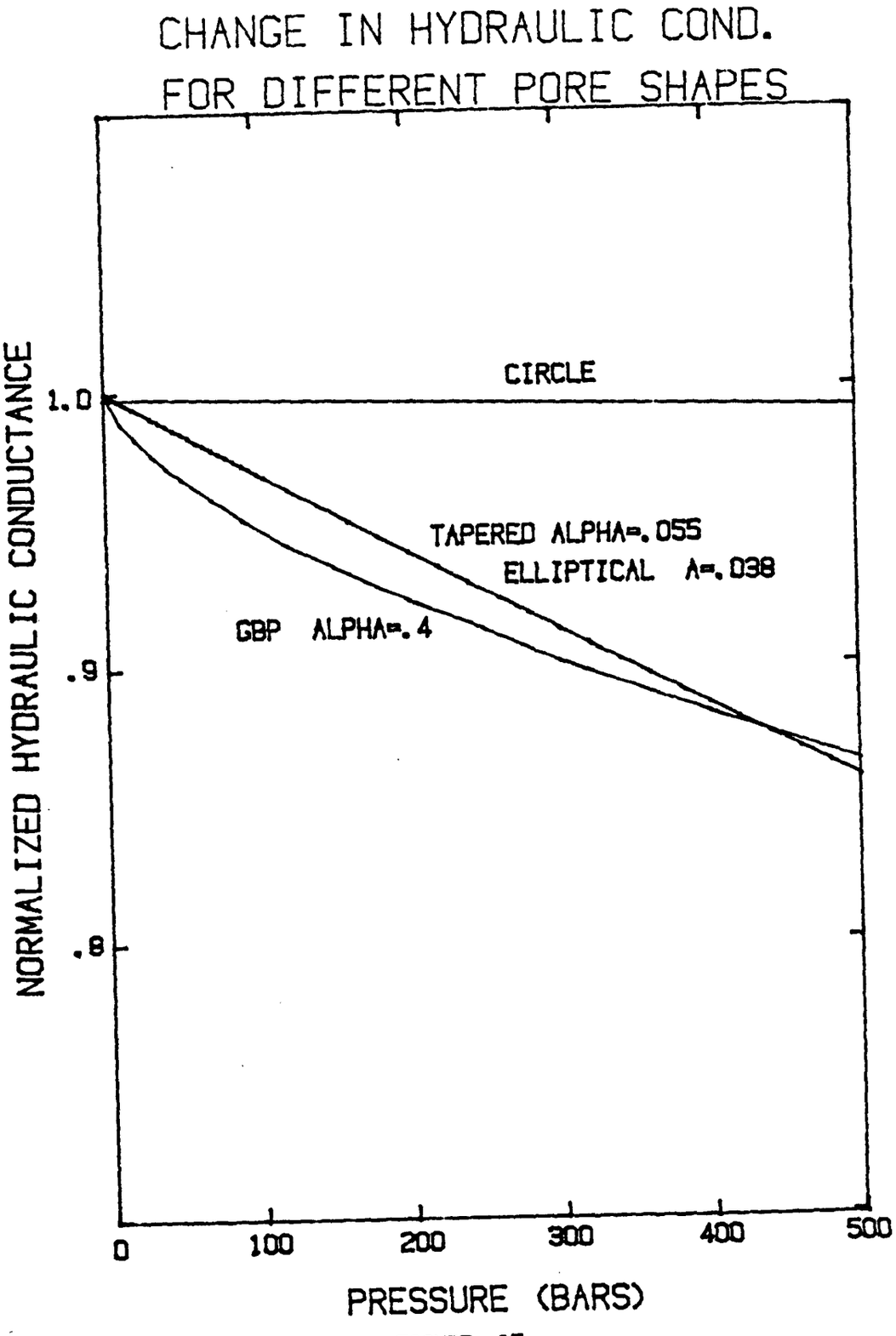

FIGURE 13

Change in hydraulic conductance with pressure for different pore tube shapes. Alpha or A equals aspect ratio of shape

500 bars stress, the percent change in hydraulic conductance is only 0.7% for a pore tube of circular cross-section whereas it is nearly 14% for the GBP shape of aspect ratio 0.4. As with figure 13 on bulk modulus comparisons, we show the elliptical and tapered pores which match the change shown by the GBP shape. Again much thinner elliptical and tapered pores are needed to match the GBP shape and the GBP shape has the highest order curvature of any of the shapes. This high order of curvature in both permeability and bulk modulus is seen experimentally in most sedimentary rocks.

The nodal pores in the model are for the most part taken to be spherical voids. Koplik (1981,1982) found the pressure drop across half a nodal pore due to incoming fluid at rate Q from a pore of hydraulic radius r_h to be:

$$\Delta P = \frac{8Q\mu}{\pi r_h^4} \tag{32}$$

$$HCON = \frac{\pi r_h^4}{8\mu} \tag{33}$$

The hydraulic radius of a pore tube is the radius of a cylinder that has the same hydraulic conductance as the pore tube.

$$r_h = c \cdot \left[\frac{FLRT}{\pi/8}\right]^{1/4} \tag{34}$$

Koplik (1981) has shown that the radius of the nodal pore drops out of equations 32 and 33 due to spherical symmetry. Although the previous equations were valid for any laminar flow (Reynolds number<2000) Koplik's equation is only valid for slow Stokes flow. Our calculations show that the Reynolds number for single pore flow under geologic and

reservoir flow rates is on the order of 1E-1 to 1E-3, well within the bounds of slow Stokes flow.

We have an analogous set of equations governing electrical flow through the pore tubes and nodal pores. The electrical conductance of a pore tube with any cross-section is given by:

$$ECON = \frac{A}{\rho \ell} \tag{35}$$

where ρ=specific resistivity of the pore fluid, ℓ=length of the pore tube and A=area of the cross-section of the pore tube. For the nodal pores, the change in the area of the conductor going from pore tube to nodal pore must be taken into account. The electrical conductance equation for the nodal pore is:

$$ECON = \frac{\pi}{\rho}\left(\frac{1}{1/r_e - 1/S}\right) \tag{36}$$

where S=radius of the spherical nodal pore and r_e=electrical radius of the pore tube connected to the nodal pore. Like the hydraulic radius, the electrical radius is the radius of a pipe which has the same cross-sectional area (and thus the same electrical conductance) as the pore tube. The validity of equation (36) has been shown experimentally by Owen (1952).

Since porosity is defined as the volume of the pore space divided by the volume of the rock, the volumes of both the pore tubes and nodal pores must be calculated. They are simply defined as:

$$VOL = A\ell \quad \text{pore tubes} \tag{37}$$

$$VOL = \frac{4}{3}\cdot\pi S^3 \quad \text{nodal pores} \tag{38}$$

Deformation and Pressure Dependence

In order to calculate the change in permeability, electrical conductivity, and porosity, a set of equations governing the elastic deformation of the pore tubes and nodal pores must be established. The shape of each pore tube and nodal pore explicitly controls its deformation with stress. In two earlier sections we developed the elastic equations governing the deformation of the pore tube shapes we have used. Because the GBP shapes change size and shape as pressure is increased, we can not derive analytical solutions for the hydraulic, electric and pore volume compressibilities for individual pores. We must numerically solve for how the pore tube deforms with stress and then solve for change in hydraulic and electrical conductance and volume of the deformed pore.

Although the pore volume and bulk compressibilities are summations of the single pore effects, the hydraulic and electrical compressibilities must be found by solving for the permeability and electrical conductivity of the entire network at different pressures. In the next section, we analyze the equations necessary to convert a collection of hydraulic and electrical pore conductances into the permeability and electrical conductivity of a network of pores.

Network Equations

As mentioned in chapter 1, the reason for representing the pore space as an interconnected network of pores is to correctly simulate the interconnected flow paths responsible for fluid and electrical transfer across the rock. The reason we project our model onto a cubic lattice

is that in order to calculate the permeability and conductivity of the network, we must simultaneously solve for the fluxes and pressure drops across every pore in the network. The set of network equations which follow allow us to calculate the flow properties of the network from the individual pore properties.

The network equations are a set of simultaneous equations which relate the hydraulic and electrical conductance of the individual pore elements to the permeability and conductivity of the network. Using the electrical analog, the voltage drop, V_j, across any given pore element with resistance R_{jj}, for a current of I_j is:

$$V_j = R_{jj} I_j \tag{39}$$

For the entire network of pore elements, this can be rewritten as a set of matrix equations:

$$\begin{pmatrix} R_1 & 0 & 0 \\ 0 & R_2 & 0 \\ 0 & 0 & R_3 \end{pmatrix} \begin{pmatrix} I_1 \\ I_2 \\ I_3 \end{pmatrix} = \begin{pmatrix} V_1 \\ V_2 \\ V_3 \end{pmatrix} \tag{40}$$

$$\text{or} \quad V = [R]\, I \tag{41}$$

Kirchoff's circuit law (Lobkowicz and Mellosimos 1975) states that there can be no accumulation of charge at any node in the network and the mass balance equation of fluid mechanics (Bird,Stewart and Lightfoot 1969) prohibits the accumulation of mass at any node in the network (for an incompressible fluid). These two laws allow for the construction of a matrix B which has the following properties:

$B_{ij} = 1$ if flow in element j is away from node i (42)

$= -1$ if flow in element j is towards node i (43)

$= 0$ if element j and node i are not connected (44)

If we define a vector J as the current applied to each node and a vector U as the voltage at each node (with respect to the last node) then the following equations are true:

$$V = [R]\ I \tag{45}$$

$$J = [B]\ I \tag{46}$$

$$V = [B^t]\ U \tag{47}$$

These can be combined to yield:

$$[B]\ [R^{-1}]\ [B^t]\ U = J \tag{48}$$

Since R is a diagonal matrix:

$$[R^{-1}] = [1/R] = [ECON] \tag{49}$$

$$[B]\ [ECON]\ [B^t]\ \Delta V = I \tag{50}$$

where [ECON] is a diagonal matrix of all the electrical conductances of the network elements. The hydraulic equivalent of equation 40 is:

$$[B]\ [HCON]\ [B^t]\ \Delta P = Q \tag{51}$$

where [HCON] is a diagonal matrix of all the hydraulic conductances of the network elements.

The permeability and conductivity are found by specifying the flow rate or current, J(1), into the first node of the network, then solving equations 50 and 51 for the pressure drop or voltage drop across the network, U(1). The matrix [B CON B^t] is a septdiagonal banded symmetric matrix (for a three-dimensional cubic network). If the network is cubic with width, length and height of nXnXn nodes then the bandwidth of the matrix is n^2 and the rank is n^3. Because the matrix is extremely sparse, we have found that an over-relaxed iterative solution (Young 1971) is both faster and requires less storage than the direct solution especially for matrices representing three-dimensional networks. The

iterative solution starts must start with a "best guess" of the solution and then converge from that to the final solution. Because the equations are solved through a sequence of pressures, the solution at the previous pressure turns out to be an excellent guess for the solution and the iterative scheme converges much more quickly than the pass at pressure 0 where the "best guess" is a vector of all zeros.

Two major reasons for using the iterative approach for solving these matrices are 1) even though the matrices are positive definite symmetric, they turn out to be algorithmically singular for most commercially available direct (Gaussian elimination or Cholesky method) solvers and 2) there can be up to nine orders of magnitude difference in the values of different matrix elements. The iterative algorithm we use converges for matrices which are very nearly singular and the iterative process does away with most of the truncation and roundoff error that would hamper a direct solution due to the large variations between matrix elements.

The iterative method used here is a variation of the standard Gauss-Seidel iterative approach (Atkinson 1978) called SOR (Young 1971, Dahlquist and Bjorck 1974). We first decompose the matrix A from the equation Ax=b into three matrices:

$$[D] = \text{main diagonal of } [A] \tag{52}$$

$$[L] = \text{lower triangular part of } [A] - [D] \tag{53}$$

$$[U] = \text{upper triangular part of } [A] - [D] \tag{54}$$

Convergence of the solution is accelerated considerably (up to 500 times faster) by including an overrelaxation factor, w, which is between 0 and 2 in general but for our matrices turns out to be limited to between 1.7 and 2.0. The basic iterative equation is then:

$$x^{(n+1)} = (b - [L]x^{(n+1)} - [U]x^{(n)})[D^{-1}]w + (1-w)x^{(n)} \qquad (55)$$

The iterative process is continued until the normalized change in any x(n) from the previous step is less than 1E-4. The number of iterations need for convergence depends on the variability of elemental conductances which depends upon the width of the distributions. For networks in which the variables are chosen from narrow distributions the method converges in 20 to 50 iterations at optimal w and for wider distribution the number of iterations can increase to between 100 and 300 but rarely above that.

NETWORK SIMULATIONS

The previous section described how the network model developed here can calculate the permeability, formation factor, porosity and their changes with pressure, provided that the size and shape of all the pores in the network is known. In the rest of this chapter we show the results of preliminary simulations in order to 1) test the numerical and statistical artifacts of the model and 2) test the effect of how changes in pore parameters effect the petrophysical properties, i.e a forward model. This forward modelling helps us greatly in the next chapter when we invert the experimental petrophysical data to yield information about the pore space.

The pore parameters which are variables in the simulations are:

1) pore tube width, c
2) pore tube length, ℓ
3) nodal pore radius, S
4) pore tube cross-sectional shape

The pore tube width, c is the length of the semi-major axis of the pore tube cross-section. Each of these variables is randomly assigned to each pore in the network from some distribution of values. From the equations specified in the earlier section, we can then calculate the individual pore's hydraulic and electrical conductance and its volume at each of eight confining pressures and then a set of network equations calculates the permeability, formation factor and porosity of the simulated network at each of the eight pressures.

Numerical and Statistical Considerations

The first three pore parameters are assigned to each pore tube and nodal pore in the network from either single valued, uniform, Gausssian or discrete distributions. Because of the calculations required for the hydraulic and electrical conductance of the pore shapes, the pore tube cross-sectional shapes are assigned from a discrete distribution of values. Each pore is assigned several random numbers which are generated from a standard pseudo-random number generator. The value of each pore parameter is assigned to a given pore depending on where the random number falls within the distribution of values for that parameter. This method is statistically identical for large networks to randomly placing pores of a specific value in the network. Our method has the advantages that it honors discrete distributions more closely in finite networks and is much simpler to manipulate.

Correct calculation of transport properties using a Monte Carlo simulation necessitates a trade-off between statistically random distributions and computation times. Even in the smaller three-dimensional networks of 5X5X5 nodes, the number of pore elements, 400, is large enough to get statistically valid distributions. The network model, however, requires that these distributions must be randomly placed within the network. In other words, the network must be large enough so that a string of largest pores is not connected through the network, giving an anomalously high permeability or that a set of smallest pores does not occupy a large portion of a given plane perpendicular to flow, giving an anomalously low permeability. At the same time we want to keep the size of the network small, because the computer time increases greatly with the number of nodes in the network.

We have studied these problems for five sizes of networks. These being 5X5X5, 8X8X8, 10X10X10, 5X5X10 and 5X5X20. The number of nodes and number of pore elements for the 5X5X5 and 10X10X10 case are 126 and 1001 nodes and 400 and 3100 elements respectively. We ran 15 simulations on each of the above 5 network sizes using the same pore parameter distributions but changing only the pseudo random number seed. Different random number seeds generate different sequences of pseudo random numbers on the computer. Although the distribution of pore parameters remains the same with different seeds, the placement of pores of a particular value is different. The variability in permeability, etc. due to different seeds gives a measure of the non-randomness of the network due to less than infinite size. The 10X10X10 case gave the most consistent results with only a 3.8% standard deviation in permeability among the runs. The deviations in conductivity, porosity and compressibility were substantially smaller. The 5X5X5 case had the largest standard deviation at 22% in permeability; however, the mean of the runs was only 2.5% higher than in the 10X10X10 case. All the other sizes fell in between the two extremes. The average run time for the 10X10X10 case was 200 seconds on an IBM 3081 and only 20 seconds for the 5X5X5 case. Although the 5X5X20 network showed similar statistics as the 8X8X8 case (both have about 500 nodes and 1500 elements), the 5X5X20 case needed three times as many iterations to converge. In general, we have found it easier to average a few 5X5X5 cases using random number seeds which give reliable distributions than to run the 10X10X10 network. In matching experimental data, we generally test 5X5X5 simulations until we are fairly close and then we go to the 10X10X10 case for the final matching.

There have been questions raised as to network edge effects and simulations of infinite networks (Koplik 1982, Nicholson and Petropoulus 1971). Two possible network configurations are 1) no flow out of the network, perpendicular to the average pressure gradient and 2) periodic boundary conditions on the edges perpendicular to the average pressure gradient. The periodic boundary condition is similar to assuming that there are similar networks on the four boundaries perpendicular to the average flow direction. We have found that this condition is superior to the no-flow boundary condition and eliminates edge effects and greatly reduces variations due to network size (using the periodic boundary condition we found only a 2.5% difference in permeability between the 5X5X5 networks and the 10X10X10 networks).

The one other computational problem that we have run into is the determination of the optimal over-relaxation parameter, w. We have found that w depends upon the width of the pore parameter distributions when that width covers more than one order of magnitude. It also depends a great deal on the size of the network. For the 5X5X5 network the optimal w (i.e. the w which allows convergence of the solution in the least number of iterations) is about 1.85 to 1.88. For the 10X10X10 networks, the optimal w is between 1.90 to 1.94. For pore shape distributions using log uniform distributions in aspect ratio (used only for tapered cross-sections to model tight gas sands and granites), the w for 5X5X5 networks needs to be as high as 1.92. The optimal w is very important in that using a w that is 10% below the optimal w will require about 4 to 10 times more iterations than the optimal w. Over-relaxation factors that are too far above the optimal w generally cause the

solution to diverge. As mentioned previously, without the over-relaxation factor, the number of iterations to reach convergence is 50 to 500 times larger than with the factor. Although Young (1971) has derived a way to find the optimal w before trying to solve the equations, he even suggests that trial and error is a faster method for finding the optimal w. For most of our simulations the optimal w is within a narrow enough band that we can use a constant value that we have found from our past simulations.

Pore Parameter Effects

We consider here the forward model in an effort to understand how the variables effect the properties we are modelling. This is a first step in both determining how the pore space controls various properties and in inverting the model to yield information about the pore space. As mentioned in the previous section the four pore parameters are pore tube width, nodal pore radius, pore tube length and pore tube cross-sectional shape. In the following section we go through each parameter and how it effects each property and then see how the four properties are coupled together.

The basic equations relating pore tube width, c, to each property are:

$$\text{hydraulic conductance (permeability)} \propto c^4 \tag{56}$$

$$\text{electrical conductance (CF)} \propto c^2 \tag{57}$$

$$\text{pore tube volume (porosity)} \propto c^2 \tag{58}$$

This means that a 10% increase in the average c should increase the permeability by 46% and the electrical conductivity and porosity by 21%.

Calculations from network simulations with no nodal pores and all pore tubes of the same shape and size (single valued distributions) show exactly this behavior. Therefore, as long as all the pores in the network have the same size and shape, the effect of c on permeability, electrical conductivity and porosity of the network is the same as the effect of c on hydraulic conductance, electrical conductance and volume of the individual pore tubes. In a real pore space, however, the pore sizes are distributed over some range and therefore the width, shape, and mean of the distributions become important.

We have run several sets of simulation to test the effect of the width of a distribution of pore sizes on permeability, conductivity and porosity and the results are summarized in Table 2. This table lists seven continuous uniform distributions of pore widths, all with an arithmetic mean of 50 um. Uniform distributions are used as a worst case estimate of the effect of a wide distributions of pore widths. Tests with Gaussian distributions show much smaller effects on the width of the pore width distribution. The permeability, formation factor and porosity of network simulations with pore widths assigned from these uniform distributions are list in the "ACTUAL" columns of Table 2.

Because of the c^4 and c^2 dependence of hydraulic and electrical conductances on pore width, we predict that the mean hydraulic and mean electric widths should depend upon the width of the distribution. We define the mean hydraulic width as the 4th root of the 4th moment of the distribution of pore sizes:

$$c_h = \sqrt[4]{E(c^4)} = \left[\frac{c_1^4 + c_2^4 + \ldots + c_i^4}{i}\right]^{1/4} \qquad (59)$$

TABLE 2

Effect of a Wide Distribution of Pore Widths

c Dist. (um)	ACTUAL perm (mD)	ff	poro	2nd M (um)	4th M (um)	PREDICTED perm (mD)	ff	poro	Hydr. tortuosity	Elec. tortuosity
50	2162.	27.73	.1174	50	50	2162.	27.73	.1174	1.0	1.0
45-55	2137.	27.96	.1176	50.11	50.28	2210.	27.61	.1176	1.03	1.01
40-60	2134.	28.21	.1183	50.39	51.06	2347.	27.31	.1183	1.10	1.03
25-75	2291.	28.95	.1225	52.24	55.79	3319.	25.48	.1226	1.45	1.14
10-90	2766.	29.44	.1303	55.45	62.64	5214.	22.66	.1304	1.89	1.30
5-95	2992.	29.38	.1337	56.79	65.16	6079.	21.63	.1338	2.03	1.36
1-99	3195.	29.17	.1367	57.94	67.22	6862.	20.79	.1368	2.05	1.40

Notes : "ACTUAL" permeabilities, formation factors and porosities are for networks with the given distribution of pore widths.

"2nd M" is a mean weighted to r2.

"4th M" is a mean weighted to r4.

"PREDICTED" permeabilities are found by calculating the permeability of a network where all pores have width c="4th M". "PREDICTED" formation factors and porosities are calculated from networks where all the pores have widths of c="2nd M".

"Tortuosity" is found by dividing predicted permeabilities and conductivity formation factors by the actual values.

The mean electrical pore width is defined as the square root of the second moment of the distribution:

$$c_e = \sqrt{E(c^2)} = \left(\frac{c_1^2 + c_2^2 + \ldots + c_i^2}{i} \right)^{1/2} \qquad (60)$$

where $E(c^j)$ is the jth moment or the expected value of c^j (Bouker and Lieberman 1972), c_i are the pore widths and i is the number of values in the distribution.

The permeabilities of networks where all the pores have a pore width equal to the mean hydraulic pore width are listed in Table 2 in the "PREDICTED" column. The formation factors and porosities of simulations where all the pores have pore widths equal to the mean electrical pore width are shown in the "PREDICTED" columns also (the porosity is related to c^2 and therefore to the mean electrical width). Because the hydraulic and electrical mean pore widths are weighted towards the large pore widths, they both increase with increased distribution width which leads to increases in the "PREDICTED" permeabilities and porosities and decreases in the formation factors.

The "ACTUAL" petrophysical properties show a different behavior altogether. The "ACTUAL" permeability decreases for small increases in distribution width and then only increases 48% when the width of the distribution spans two orders of magnitude in pore widths. This is compared to a "PREDICTED" increase of over 300% between the single valued and widest distributions. The formation factor was predicted to decrease 25% over the span of distributions yet it actually increased 5%. Only the porosity followed the predictions.

Comparison of the network model with the bundle of capillary tubes model (Archie 1942, Carmen 1937, Kozeny 1927)(see Morgan 1984 for a review of capillary tube models) illustrates the reason why the "ACTUAL" values are so different from the "PREDICTED" values in Table 2. In the capillary models the pore space is represented as a bundle of capillary tubes which run the length of the sample, i.e. there are no connections between adjacent tubes. We set up such a model where the pore length, ℓ, equalled the sample length (i.e. tortuosity=1) and assigned pore widths (or radii in this case) according to the distributions in Table 2. We found that the "PREDICTED" values from Table 2 exactly matched the values calculated from the capillary model. We infer that differences between the two models will yield information on the discrepancy between "PREDICTED" and "ACTUAL" values in Table 2.

The main difference between the two models is the interconnectedness of the pore space. In the capillary model fluid is constrained to flow the entire length of the sample within a single capillary. Therefore, the large pores carry the largest part of the total flow through the sample. In the network model, fluid enters different pores at each nodal pore depending upon the hydraulic conductance of each adjoining pore and the pressure drop across it. Because the pore tube widths are randomly placed within the network lattice, there is little chance that a string of large pores will connect through the sample to allow for a capillary tube effect. This means that the "path of least resistance" for a fluid particle (or electric particle) will be larger than the sample length for a network with distributed pore widths. It also means that the ratio of "ACTUAL" to "PREDICTED" values is a measure of the fluid path length or tortuosity of the network.

These tortuosities are listed in Table 2 for the hydraulic and electrical flow paths. Because there is a larger variation in hydraulic conductance than electrical conductance for the same pore width distribution (c^4 versus c^2 dependence), we find that the hydraulic tortuosity is always greater than the electric tortuosity. Also note that both tortuosities increase with an increase in the width of the distribution. The difference in hydraulic and electrical tortuosities suggests that the hydraulic flow paths are different from the electric flow paths and that one should not attempt to correlate permeability and formation factor for networks or rocks where there is a very wide distribution of pore widths. The porosities are the same in the two models because the porosity does not depend on the connectedness of model, only on the total pore volume over sample volume. One interesting observation is that the increase in mean hydraulic and electric widths is nearly balanced by the increase in tortuosity for networks where the variation in pore widths is an order of magnitude or less, which suggests that the width of the pore tube distribution is not significant in changing the permeability or formation factor unless it spans more than an order of magnitude.

Equations 26, 33, and 35 show that the hydraulic and electrical conductances of the pore tubes are related to the inverse of the pore tube length and that the pore volume is directly related to pore tube length. Because permeability and conductivity are normalized to the length of the sample over the area of the sample, an extra factor of ℓ^{-1} is added to the conductance equations provided the network is cubic and all the pore tubes have the same length. Porosity is pore volume over sample

volume so that porosity is also related to ℓ^{-2} for a cubic network. An increase in pore length decreases all three properties according to the square of the increase. Simulations on cubic networks with no nodal pores yield these relationships.

Assigning pore tube length from a distribution of lengths is found to be unrealistic unless extreme precautions are taken. Increasing the width of a distribution of pore lengths while keeping the arithmetic mean constant, removes the dependence of permeability conductivity and porosity on network size because the average ℓ is constant and the overall size of the network depends only on the average ℓ. This means that permeability and conductivity are dependent on ℓ^{-1} for constant mean distributions and porosity is dependent on ℓ. As these relationships are first order, we expect permeability, conductivity and porosity to be related to the first moment or arithmetic mean of the distribution. Since we are holding the mean constant, the width of the distribution should have no effect. Simulations run using a capillary model and network model show the properties of the capillary model to be unaffected by the width of the distribution of pore lengths but in the network model only the porosity is unaffected by the distribution width. Permeability and conductivity both increase 20% when the distribution spans two orders of magnitude in values. Analysis shows that these increases are due to fluid and electrical flow path lengths that are less than sample length, i.e. tortuosities less than 1. This is unrealistic and is due to the lack of a placement algorithm which requires all flow paths to be of realistic length. Because of the predicted lack of dependence of permeability, conductivity and porosity on the

distribution of pore lengths, we confine our simulations to those where all the pore tubes have the same length.

For cubic networks of pore tubes with no nodal pores the relationships between properties and pore width and length become:

$$\text{permeability} \propto c^4/\ell^2 \quad (61)$$

$$\text{conductivity} \propto c^2/\ell^2 \quad (62)$$

$$\text{porosity} \propto c^2/\ell^2 \quad (63)$$

Note that the relationships for conductivity and porosity are the same and that both are dependent on the ratio of c to ℓ. We suggested earlier that permeability and conductivity are not related to one another when their flow paths are different. Here we see that if the ratio of pore width to radius is constant in a set of simulations, the porosity and conductivity will remain fixed while the permeability can vary substantially. This illustrates that a knowledge of what the pore parameters are can yield a great deal of insight into the relationships between petrophysical properties.

Another difference between the capillary tubes model and our network model is the presence of nodal pores at the junctions of pore tubes in the network. Nodal pores are an essential part of our network model considering our starting point for pore shapes is a sphere or grain pack. As shown in figure 10b, an equivalent representation of a grain pack is a GBP shaped pore tube connected to a spherical nodal pore connected to another GBP shaped pore tube. The presence of nodal pores also accounts for two experimental observations which have not previously been well explained through past pore space models. Equations 62 and 63 suggest that without nodal pores the network model predicts a one

to one relationship between porosity and conductivity which translates to an Archie's exponent of 1. Empirical evidence shows that Archie's exponent is rarely below 1.6 and rarely above 3. Capillary tube models have accounted for this by making the pore tubes very tortuous (see equation 2). However, tortuosities as high as 10 to 70 are needed to model rocks with high Archie's exponents. With nodal pores accounting for 30% to 90% of the pore volume, the network model exhibits Archie's exponents between 1.6 and 3.0 with tortuosities of 1.

A second observation is that conductivity always decreases more with pressure than porosity, yet the no nodal pore network model predicts both conductivity and porosity to change the same with pressure. The capillary tube model assumes that the change in conductivity is equal to the change in porosity to the power m (Archie's exponent). Experimental data (Fatt 1957, Chierici 1967, Yale 1984a) all show that this last assumption underestimates the conductivity at pressure by between 20% and 60%. Only by allowing a large part of the pore space to be taken up by spherical (and thus "stiffer") nodal pores, can the relationships between the change in conductivity and change in porosity be correctly reproduced.

Nodal pores, however, make it more difficult to analyze the relationships between rock properties and pore parameters. Equations 38 and 36 show that:

pore volume of nodes $\propto S^3$

conductance of nodes $\propto 1/(1/r_e - 1/S)$

Doubling the nodal pore radius does not increase the porosity eight fold because:

$$\Phi = \frac{\text{nodal volume + pore tube volume}}{\text{sample volume}} \tag{64}$$

or

$$\Phi \propto \frac{S^3 \text{ and } c^2\ell}{(\ell+S)^3} \tag{65}$$

The relationships for permeability and conductivity are:

$$k \propto \frac{c^4/\ell \text{ and } c^3}{(\ell+S)} \tag{66}$$

$$CF \propto \frac{c^2/\ell \text{ and } 1/(1/r_e-1/S)}{(\ell+S)} \tag{67}$$

We see that all three properties are related to all three pore parameters. It is this non-linear coupling between properties and parameters that makes it very difficult to construct a true inverse model. The three properties and three parameters do insure that a forward model that fits some experimental data will be unique for a constant set of pore shapes. Simulation tests of nodal pore size distributions show that the width of the distributions has no effect on permeability or porosity and the effect on conductivity is less than 5% even when the distribution varies over two orders of magnitude. Therefore, we let all nodal pores have the same radius.

The last pore parameter we mentioned earlier was pore tube cross-sectional shape. Table 3 shows the full set of pore tube shapes used in our model along with their aspect ratios, effective hydraulic and electric radii and their hydraulic and electrical conductance. The conductances are normalized to the conductance of a pore tube of circular cross-section, with unit radius and unit length. Note that the

TABLE 3

List of Aspect Ratios and Conductances for Various Pore Shapes

shape	alpha	Rh	Re	HCON	ECON
CIRCLE	1	1	1	1	1
GBP-RC1	.414	.471	.523	4.92E-2	2.73E-1
GBP-RC2	.251	.319	.402	1.03E-2	1.62E-1
GBP-RC3	.183	.247	.341	3.72E-3	1.16E-1
GBP-RC4	.144	.203	.301	1.70E-3	0.91E-1
GBP-RC5	.120	.174	.273	9.17E-4	7.45E-2
GBP-RC6	.100	.152	.252	5.34E-4	6.35E-2
GBP-RC8	.079	.123	.221	2.29E-4	4.88E-2
GBP-RC10	.065	.105	.199	1.22E-4	3.96E-2
GBP-RC15	.044	.077	.165	3.52E-5	2.72E-2
GBP-RC20	.034	.062	.144	1.48E-5	2.07E-2
TAPα5E-2	.050	.105	.223	1.22E-4	4.97E-2
TAPα1E-2	.010	.032	.100	1.05E-6	1.00E-2
TAPα5E-3	.005	.019	.071	1.30E-7	5.00E-3
TAPα2.5E-3	.0025	.0112	.050	1.56E-8	2.50E-3
TAPα1E-3	.001	.0056	.032	1.00E-9	1.00E-3
TAPα5E-4	.0005	.0033	.022	1.00E-10	5.00E-4
TAPα1E-4	.0001	.0010	.010	1.00E-12	1.00E-4

Note : alpha = aspect ratio of the cross-sectional shape

Rh = effective hydraulic radius of pore shape i.e. radius of circular pore tube with same hydraulic conductance

Re = effective electrical radius of pore shape i.e. radius of circular pore tube with same area and electrical conductance

HCON = hydraulic conductance of pore tube of this shape with unit width and length relative to a pore tube of circular cross-section with unit width and unit length

ECON = electrical conductance of pore tube of this shape relative to pore tube of circular cross-section

hydraulic conductances vary over twelve orders of magnitude but the electrical conductances vary over only four orders of magnitude. For thin pores, the effective electrical radius is always greater than the effective hydraulic radius so that the hydraulic conductance is less than the electrical conductance squared. The thinner the pore the larger this discrepancy between effective hydraulic and electrical radii.

One of the major differences between this model and past network models is the inclusion of realistic pore shapes whose deformation with pressure allows for the calculation of the changes in permeability, conductivity and porosity with pressure. The variation of the change in hydraulic conductance with pore shape is illustrated in figure 14a for several different pore shapes. These curves are equivalent to the change in permeability for network simulations where all the pores have the same pore shape. Note that the change in hydraulic conductance at 500 bars is only 0.7% for pores of circular cross-section (see figure 13) but over 90% for pores with very thin (α=2.5E-4) tapered cross-sections. The TAP or tapered pore shapes introduced by Mavko and Nur (1979) are used for modelling rocks with very thin pores because of the numerical difficulties in calculating the hydraulic and electrical conductance of very thin GBP shape pore tubes. The nearly linear behavior of the conductance curve and the need for low aspect ratio pores, makes the TAP pores undesirable in the regime spanned by the GBP shaped pores.

Figure 14b shows the change in electrical conductance with pressure for a variety of pore shapes. Note the percent decrease is less for the same shape at the same pressure than in the hydraulic case. This is

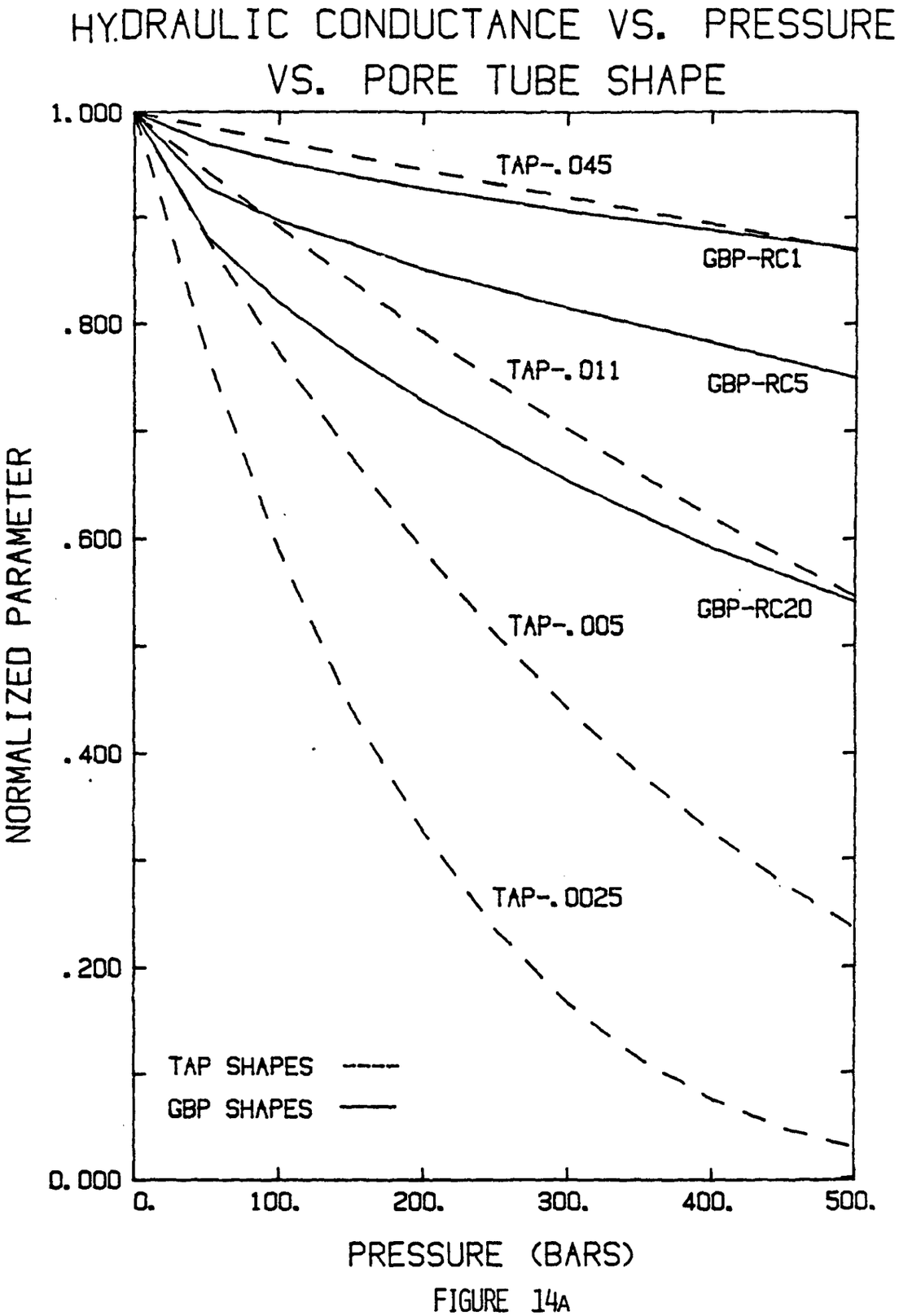

FIGURE 14A

Change in hydraulic conductance with pressure for different GBP and TAP pore shapes. Number after TAP- refers to aspect ratio

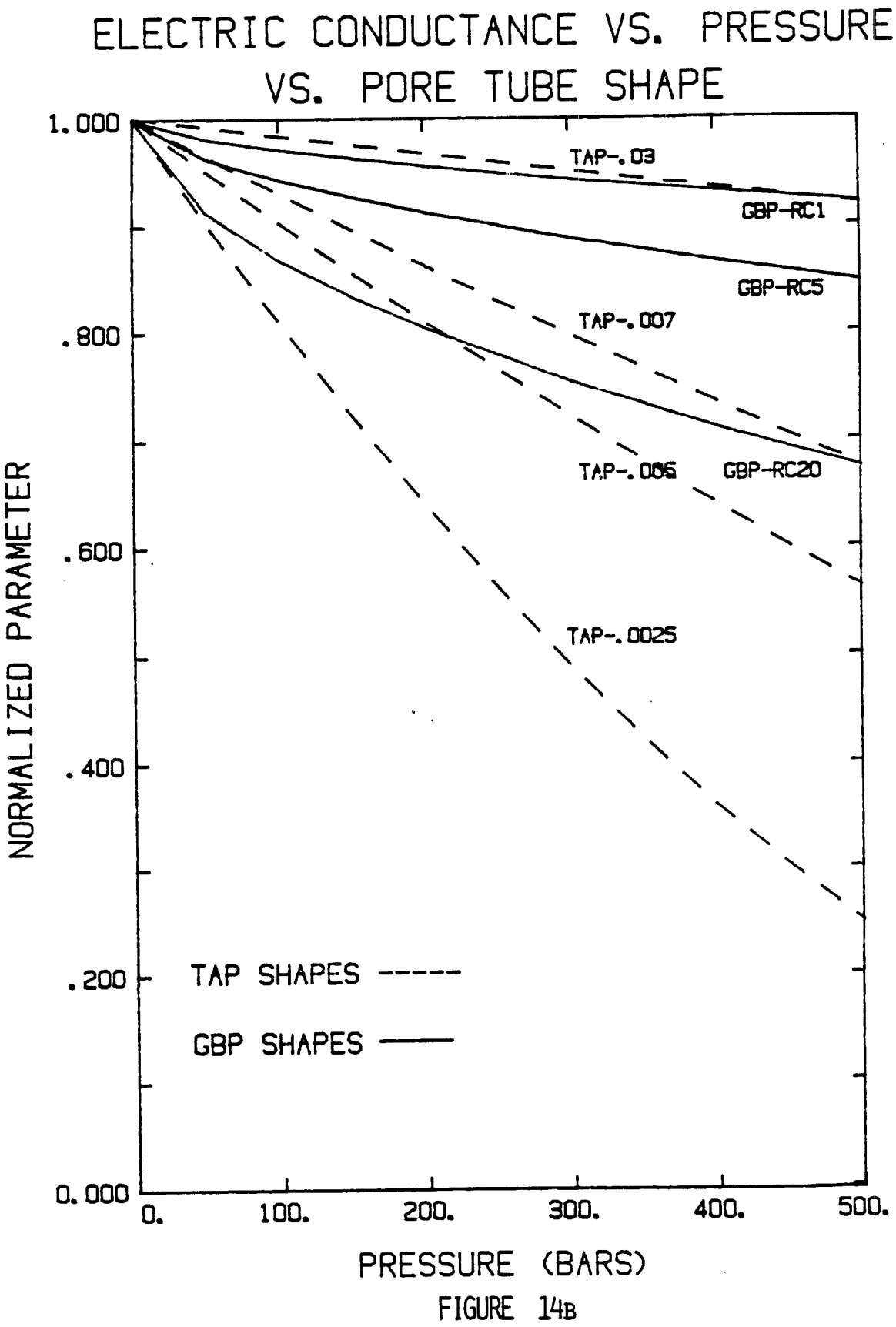

FIGURE 14B

Change in electrical conductance with pressure for different GBP and TAP pore tube shapes.

expected since for a given decrease in effective radius the hydraulic conductance should change more than the electrical conductance because of their respective c^4 and c^2 dependences. Empirical evidence also suggests that conductivity tends to decrease only 5% to 60% at 500 bars compared to 8% to 90% changes in permeability at the same pressure.

The changes in permeability, conductivity and porosity are dependent to a large extent exclusively on pore shape. If all the pores in the network have the same shape then the percent change in permeability is equal to the change in hydraulic conductance for that pore tube shape. Similarly the change in conductivity is due for the most part to the change in the electrical conductance of the pore tubes. The (1/r-1/S) relationship for the resistance of the nodal pores can change the conductivity decrease with pressure between 1% and 15% but rarely more than that. Because the nodes are assumed to be spheres whose volume changes very slowly with pressure, the change in porosity is related to :

$$\Phi(P) \propto \begin{matrix}\text{fraction of pore space} \\ \text{occupied by pore tubes}\end{matrix} \times \begin{matrix}\text{change in pore tube} \\ \text{volume with pressure}\end{matrix} \qquad (68)$$

Unlike pore tube width, pore tube length and nodal pore radius, the cross-sectional shape of the pore tubes are assigned from various discrete distributions of values. Discrete rather than continuous distributions are used because of the lengthy numerical calculations required to find the hydraulic and electrical conductance of each pore tube shape. Because the changes in permeability, conductivity and porosity are all controlled by a single distribution of pore tube shapes, we have no lack of data to fix the mean, width and shape of the pore tube shape distribution. This is the reverse of the situation for pore tube width,

length and nodal pore radius where we have three parameters to fit just three properties. We discuss the effect of distributions of pore shapes on petrophysical properties in the next chapter.

CHAPTER THREE

Inversion of Experimental Data for a Quantitative Representation of the Pore Space

INTRODUCTION

Few pore space models have been rigorously compared with experimental data (Dullien 1979, Cheng and Toksoz 1979) . Many models have simply been representations of the pore space which reproduce general trends observed in the data (Fatt 1956a,b,c, Greenberg and Brace 1969, Haring and Greenkorn 1970, Harris 1965, Koplik 1981a, Korringa et al 1979, Larson et al 1977, Mavko and Nur 1979, O'Connel and Budiansky 1974, Seeburger 1984). As shown in chapter one, matching general trends can help discriminate between various pore shapes, but exact comparison with experimental data yields much more information about the pore space and usefulness of the model.

Pore space modelling can be done from two approaches, one being the method used by Dullien and his coworkers (Dullien 1979, Dullien el al. 1976, Dullien and Dhawan 1974,1975). In their approach photomicrographs and mercury injection data are used to calculate pore size distributions for various sandstones and then these distributions are the input data for their network pore space model. In other words they try to predict properties such as permeability and formation factor from the pore size distributions in the real rock. The other approach, taken by Cheng and

Toksoz (1979), is to invert specific petrophysical data through a pore space model to get a representative (but model dependent) pore shape distribution. Analysis of how these predicted distributions vary from rock to rock yields information about the differences between the rocks.

In our model we adopt the latter approach because the goals of this project are to use the network pore space model developed here to gain a better understanding of how the pore space controls various properties, how the properties are interrelated and what differences in model simulations between rock types tell us about the differences between rocks. One ultimate goal of the project is to accurately model n properties with (n-1) or (n-2) variables so that (n-1) or (n-2) experimentally measured properties can be used to predict one or two other properties that may be difficult or impossible to measure in the field. We will concentrate in this study on analyzing the distributions of pore size and shape which we obtain from 'inverting' the experimental petrophysical properties, to better understand how the pore space controls these properties.

The model is only pseudo-inverse in that many simulations are run with different pore size and shape distributions until the experimental data is matched. The model pore space is simple enough so that we can analyze how those distributions effect the various properties and from there infer how the real pore space may be effecting or controlling the properties in the real rock.

Experimental Petrophysical Database

The petrophysical properties we simulate are permeability, porosity, formation factor, and their variations with isotropic confining stress. Although there are many studies concerning one or two of these properties (Brace and Orange 1968, Chierici et al. 1976, Dobrynin 1963, Fatt 1953,1957,1958b,c, Fatt and Davis 1952, Ferrell et al. 1962, Gray et al. 1963, Handin et al. 1963, Jennings et al. 1981, Jones and Owens 1979, Jones 1978, McLatchie 1958, Murphy 1982, Walls 1978,1979, Wyble 1958, Zoback 1975), there are very few which show results for permeability, formation factor, porosity and their variations with stress (Dobrynin 1963, Chierici et al. 1967, Gray et al. 1963, Wyble 1958) and none which have also measure bulk modulus or Vp and Vs along with the flow properties of permeability and formation factor. Because of this, we will concentrate on simulating permeability, formation factor, and porosity at various pressures. The lack of a full range of petrophysical properties versus pressure, the lack of microscopic analysis, and the lack of sufficient data density (pressure interval between data points in Chierici et al. 1967 is large) have prompted us to undertake our own experiments. In this way we have been able to measure all of the petrophysical properties we wish to measure (permeability, formation factor, porosity, and bulk modulus versus pressure) under more controlled conditions and since we have the rock samples we can perform detailed microscopic analysis to make sure pore shapes and sizes are realistic and we can perform other experiments on the same sample if we wish to add properties to the model.

EXPERIMENTAL SETUP AND PROCEDURE

We have constructed an experimental system (shown in figures 15 and 16) to measure steady state fluid permeability, electrical resistance, and pore volume change at confining pressures between 0 and 700 bars and pore pressures of between 0 and 50 bars. The system includes a heavy duty stepping motor (680 oz/inches torque) which drives a dual cylinder/ single piston flow system. The stepping motor rotates a threaded piston which forces fluid out of cylinder A, past a differential pressure transducer (0-10 psi) through the rock sample in the pressure vessel, and then into cylinder B (see figure 15). The total volume of fluid in the system remains constant (at about 45 cc) so that driving the piston at a steady rate induces a very steady flow rate. The constant volume of the system also allows flow at elevated pore pressures (up to about 50 bars). Valves 1 and 4 are open and valves 2 and 3 closed when flow is from cylinder A to B and valves 2 and 3 are open and 1 and 4 closed when flow is from cylinder B to A. This allows us to maintain a constant flow direction within the sample (see figure 15).

Pulses from an HP8116a signal generator are amplified by a Superior Electric translator which drives the stepping motor at a constant rate. For different rocks the motor can be run at rates from .00025 to 2.5 revolutions per second yielding flow rates of between .00221 to 22.1 cc/minute. Pressure drops across the sample of between 1 and 10 psi can be accurately measured with a Sensotec differential transducer allowing us to measure permeabilities between 30 microDaries and 3 Darcies. A HP3497a Data Aquisition unit provides an HP85 computer with the driving

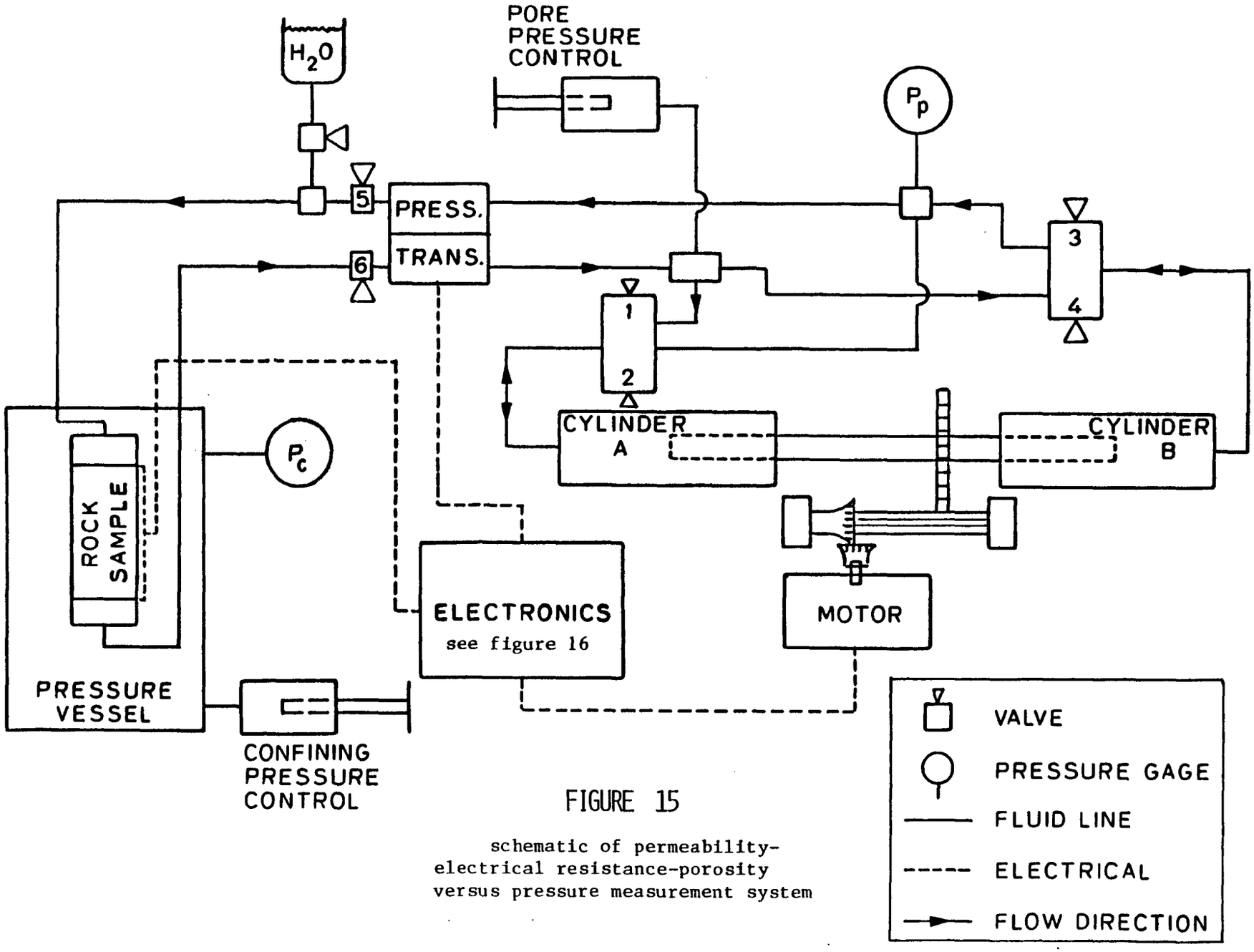

FIGURE 15

schematic of permeability-electrical resistance-porosity versus pressure measurement system

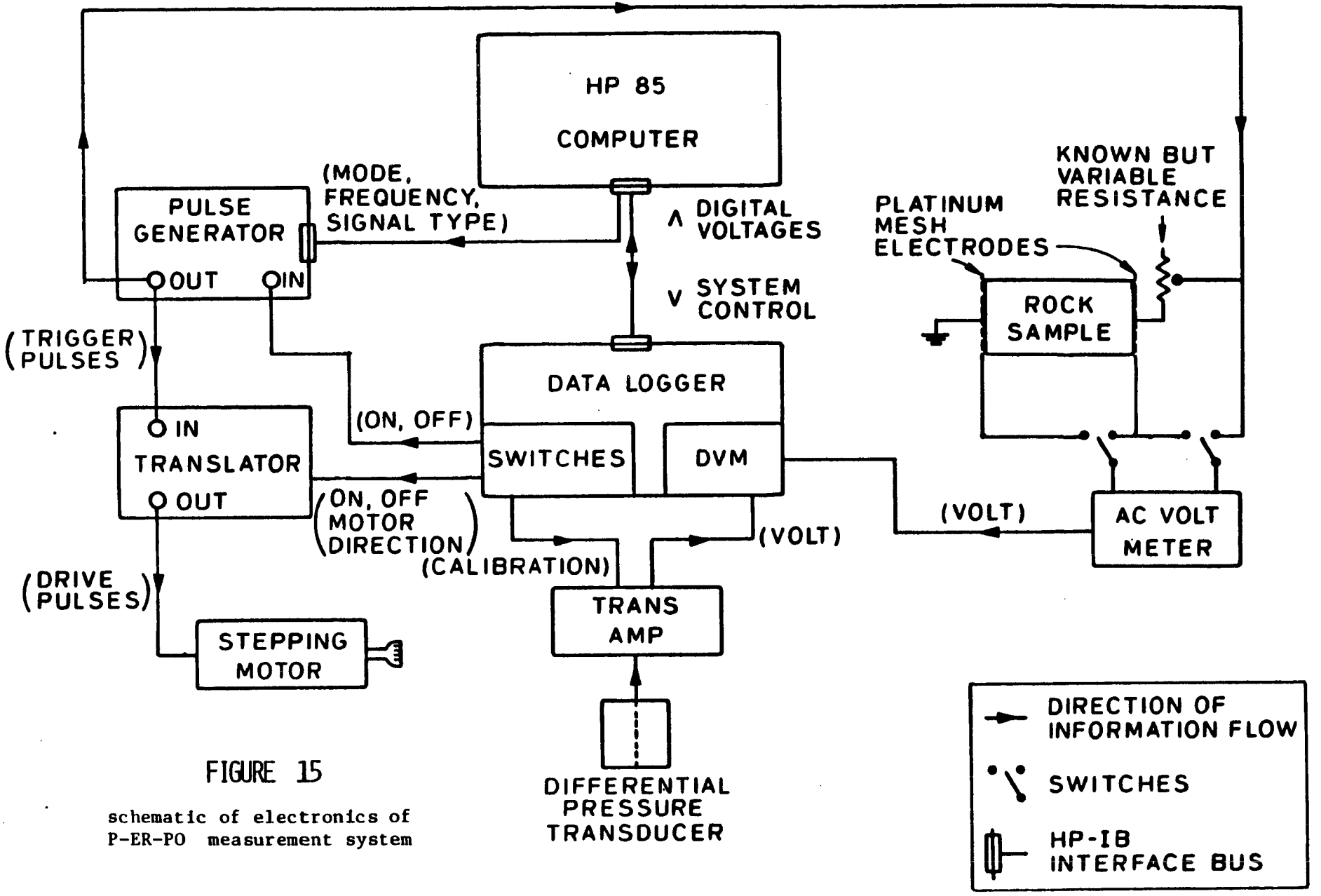

FIGURE 15

schematic of electronics of P-ER-PO measurement system

frequency of the motor and the pressure drop across the sample (see figure 16).

The permeability, k, of the sample can then be calculated from the flow rate, Q, pressure drop, ΔP, sample cross-sectional area and length, A and ℓ, and fluid visicosity, μ. Darcy's law states that:

$$k = \frac{Q\mu}{A\ \Delta P/\ell} \tag{69}$$

Flow rate, Q, is related to motor driving frequency by:

$$Q = \text{frequency (Hz)} / 271.5\ \text{(Hz/cc/sec)} \tag{70}$$

The differential pressure across the sample is corrected for gravitational flow (-0.0383*ℓ psi) and flow resistance of the tubing leading into and out of the pressure vessel (-0.651*Q psi). Dimensional analysis shows that even at the highest flow rates (0.5 cc/sec), the Reynolds number is between 1E-3 and 1E-1 for pores with radii between 5 and 50 um. This is not only within the limits of laminar flow, but also within the regime of slow Stokes flow.

Porosities are measured at atmospheric pressure with a helium (Boyles law) porosimeter. The change in porosity with pressure is calculated by measuring the volume of fluid expelled as the confining pressure on the sample is increased. The A cylinder and positive side of the pressure transducer are sealed off from each other and from the rest of the system. The confining pressure is increased on the saturated sample within the pressure vessel which raises the pore pressure and the pressure on the negative side of the pressure transducer. The piston is then stepped out of cylinder B until the pore pressure returns to its original value. The number of steps required to accomplish this

translates into the volume of fluid that was 'squeezed' out of the sample due to the pressure increase and is equal to the decrease in pore volume. The change in pore volume is measured to within 1/1000 cc or to within 0.1% of the pore volume change.

The electrical resistance of the sample is measured using an AC resistance technique with two electrodes at frequencies between 1000 and 5000 Hz. As shown in figure 16 the pulse generator provides a constant frequency and constant amplitude sinusoidal voltage. A know but variable resistance is put in series with the sample. The AC voltage across the known resistor and the sample are compared to calculate the resistance of the sample. Since the two resistances are in series the current across each is the same and the resistance of the sample can be calculated from:

$$R_{sam} = \frac{\Delta V \text{ sample}}{\Delta V \text{ resistor}} R_{res} \qquad (71)$$

Platinum mesh electrodes are used on either end of the samples and the samples are saturated with a 0.505 M NaCl (2.9% by weight) brine which has a resistivity of 0.2347 ohm-m. Sample resistance is divided by sample length over sample area to yield sample resistivity which was divided by brine resistivity to yield resistivity formation factor, FF. Conductivity formation factor is calculated from 1/FF.

All three measurements are taken at various pressures as the confining pressure is increased. All curves of permeability, conductivity and porosity versus confining pressure presented in this report by "Yale (1984)" (see figures 17 through 23) are the average of two or three pressure cycles. In all the measurements, pore pressure is kept

constant at between 10 and 40 bars except the Fahler samples for which the pore pressure was maintained at 140 bars.

The system is run through a HP3497a Data Aquisition unit which is in turn controlled by a HP85 micro-computer across a HP-IB interface bus (see figure 16). The 8116a pulse generator is also computer controlled and allows the computer to select the driving frequency of the stepping motor, mode and type of signal (constant frequency pulse for permeability, burst pulse for porosity, and constant frequency sine wave for formation factor), and allows the computer to count the number of pulses output by the 8116a during porosity versus pressure measurements. A set of mercury relays within the 3497a controls various switching functions for the translator and pulse generator and the 3497a's high resolution A/D voltmeter allows transducer voltages to be output to the computer.

The permeability of the Fahler samples (see Table 4) was measured using a transient pulse technique (Brace et al., 1978). Permeability is measured by applying a 1 bar gas pore pressure differential across the sample and measuring its decay as gas flows through the sample. The rate of decay is related to the permeability and a complete description of the technique is found in Walls et al. (1982) and Walls (1982). Formation factors and porosity versus pressure for the Fahler samples are measured using the same techniques as the rest of the sample

All samples used are two inch diameter core plugs, drilled either from quarry blocks or larger drill cores. The cores were cut to between 1 and 3 inches in length and then their faces surface ground parallel to within 0.002 inches. Samples were then flushed with 5 to 10 pores volumes of deionized water to remove any salts and loose particles. No

organics were present in the samples so that a Soxlex extraction was not performed. To preserve the clays in the samples, they were never dried above 70°C. All Fahler samples and the Tertiary 807 sample were from drill cores and the rest of the samples were obtained from building stone quarries by Leslie Yale. Detailed petrographic descriptions of these rocks can be found in the SRP Rock Catalog, volumes 1 and 2 (L.Yale 1984a,b) and in Appendix B of this report.

Experimental Data Analysis

We have collected and compiled experimental data on permeability, formation factor and porosity and their changes with pressure for twenty-eight sandstones. The data is presented in figures 17 through 23 and is summarized in Table 4. In each of the figures, permeability, conductivity formation factor and porosity are plotted against isotropic confining pressure to 500 bars. The data as plotted are normalized to the values of permeability, conductivity and porosity at 10 bars pressure and these values are given in the lower left corner of the plots and are also listed in Table 4. Resistivity formation factor is used for comparison purposes in Table 4 but conductivity formation factor versus pressure is plotted in all the figures. Table 4 also lists the rock name, group type and source of data. The rock name is either a formation name or its geologic age followed by a reference number or letter. The "group type" classifies the rock according to the relationship between the permeability and conductivity changes with pressure.

As shown in Table 4, the experimental data sets are divided into four main groups as designated by the first letter of their group type. The first eleven rocks in Table 4 are classified as part of the "N" or "normal" group because they all exhibit changes in permeability with pressure that are related to the 1.5 to 2 power of the change in conductivity with pressure (see figures 17a through 19c). Fatt (1957,1958a) suggested that permeability should change with pressure roughly as the square of the conductivity change with pressure due to the c^3 and c^2 dependence of permeability and conductivity on pore width. Rocks within the "N" group follow this general trend.

Table 4

Absolute Values of Petrophysical Properties for Experimental Data Sets

Rock name	Perm.	FF	Poros.	Type	Reference
Indiana D	30.3	12.1	.267	NH	Yale (1984a)
Torpedo	45.0	42.4	.202	NM	Dobrynin (1962)
Branford	2.5	95.1	.109	NM	Wyble (1958)
Fahler 162	0.270	293.	.030	NL	Yale (1984a)
Triassic 41	42.4	144.	.212	NM	Chierici (1967)
Cambrian 16	9.5	308.	.137	NM	Chierici (1967)
Fahler 154	0.009	128.	.044	NL	Yale (1984a)
Fahler 192	0.007	282.	.046	NL	Yale (1984a)
Pliocene 35	36.9	157.	.201	NM	Chierici (1967)
Triassic 26	67.7	17.3	.180	NH	Chierici (1967)
Triassic 27	72.3	20.1	.181	NH	Chierici (1967)
Tensleep	163.	19.0	.297	SH	Fatt (1957)
Massillon DV	6.90	27.4	.190	SM	Yale (1984a)
Kirkwood	12.3	40.5	.152	SL	Wyble (1958)
Fahler 142	0.018	165.	.076	SL	Yale (1984a)
Fahler 189	0.019	739.	.019	SL	Yale (1984a)
Massillon DH	129.	23.8	.161	CH	Yale (1984a)
Berea 100H	49.0	17.2	.165	CH	Yale (1984a)
Miocene 7	4.40	383.	.083	CM	Chierici (1967)
Falher 161	0.010	424.	.023	CL	Yale (1984a)
Boise	901.	12.0	.258	LH	Yale (1984a)
Triassic 38	400.	12.7	.205	LH	Chierici (1967)
Tertiary 807	152.	14.9	.218	LH	Yale (1984a)
Cambrian 6	23.0	89.2	.081	LH	Chierici (1967)
Berea 500	494.	20.1	.197	LM	Yale (1984a)
Cambrian 14	31.9	51.9	.109	LH	Chierici (1967)
Triassic 34	352.	13.8	.199	LH	Chierici (1967)
Beaver	10.0	90.0	.070	LM	Yale (1984a)

Notes: Permeability (Perm.), Formation factor (FF) and Porosity (Poros.) are all measured between 0 and 10 bars pressure. These values are referred to as the "absolute values" of permeability, formation factor and porosity. formation factor and porosity.

Type refers to the "group type" of the rock with:
First letter N, S, C, or L refering to the relationship between permeability and conductivity versus pressure
Second letter H, M, L refers to the percent change in permeability at 400 bars confining pressure

The petrology of all Yale (1984a) sample is found in Appendix B and in the SRP Rock Catalog vol.1 (L. Yale 1984a,b)

Figures 17-23 show the changes in permeability, conductivity and porosity with pressure and Appendix C contains the plotted information in tabular form for all these rocks.

The twenty-eight rocks in this study are classified into subgroups according to the percent decrease in permeability over 400 bars of confining pressure. The "H" designation in the second letter of the group type means the rock exhibits less than a 20% change in permeability when confining pressure is increased from 10 to 400 bars. Rocks in the "M" subgroup show decreases in permeability of between 20% and 60% and rocks in the "L" subgroup have permeabilities at 400 bars that are less than 40% of their original permeability.

Figures 17a through 17d show that the change in permeability, conductivity and porosity with pressure varies greatly from rock to rock. The decrease in permeability varies between 8% and 90% at 400 bars pressure, the decrease in conductivity is between 5% and 60% and the decrease in porosity ranges from 2% to 25%. We also see no correlation between the absolute value of permeability, conductivity, or porosity and the inclusion of rocks in the "N" group. Permeability varies between 7 microDarcies and 72 milliDarcies and porosity between 3% and 27% among the rocks in the "N" group.

Figures 19d through 20d show a wide "split" between the permeability versus pressure curve and the conductivity versus pressure curve. The rocks represented in these figures have permeability versus pressure curves which are equal to the 2 to 3.5 power of the conductivity change with pressure and are classified as part of the "S" or "split" group. As with the "N" group, rocks with a wide range of petrophysical properties fall into this group as permeabilities vary between 20 microDarcies and 161 milliDarcies and the percent change in permeability varies between 20% and 90% at 400 bars confining pressure.

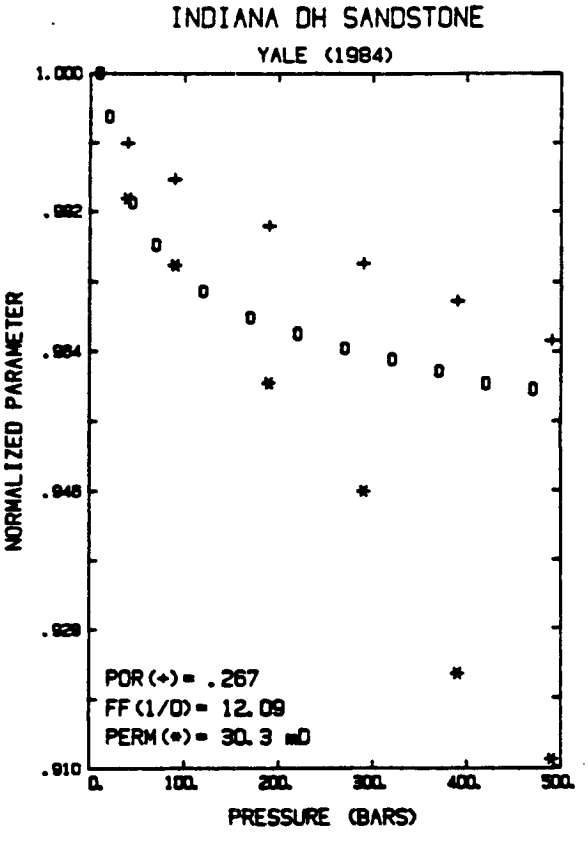

FIGURE 17A

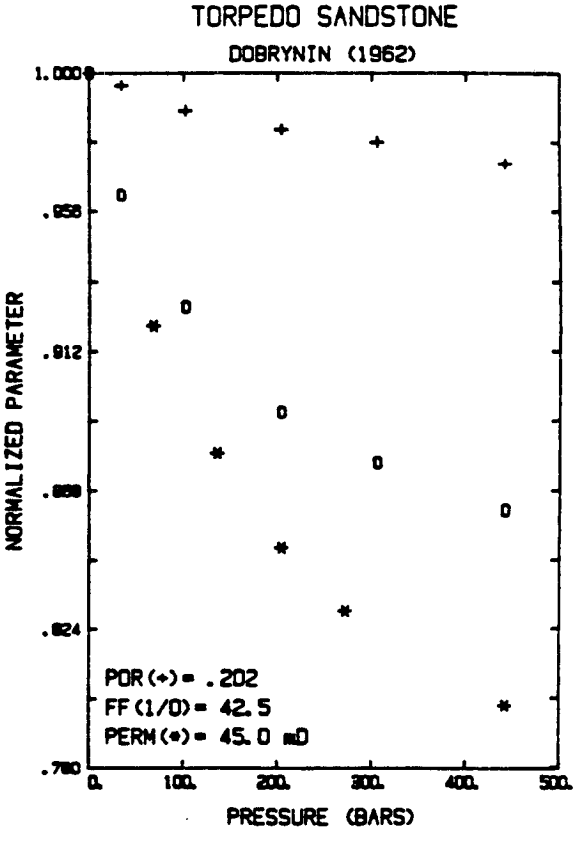

FIGURE 17B

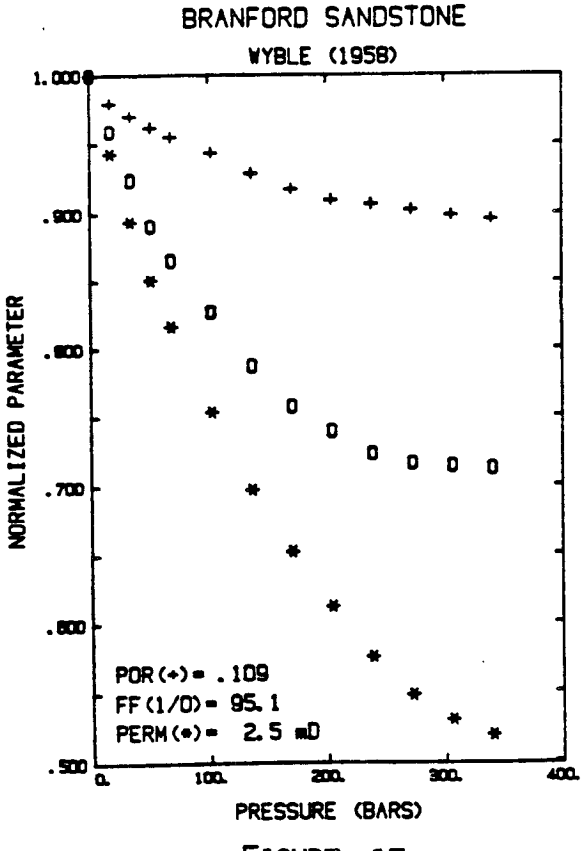

FIGURE 17c

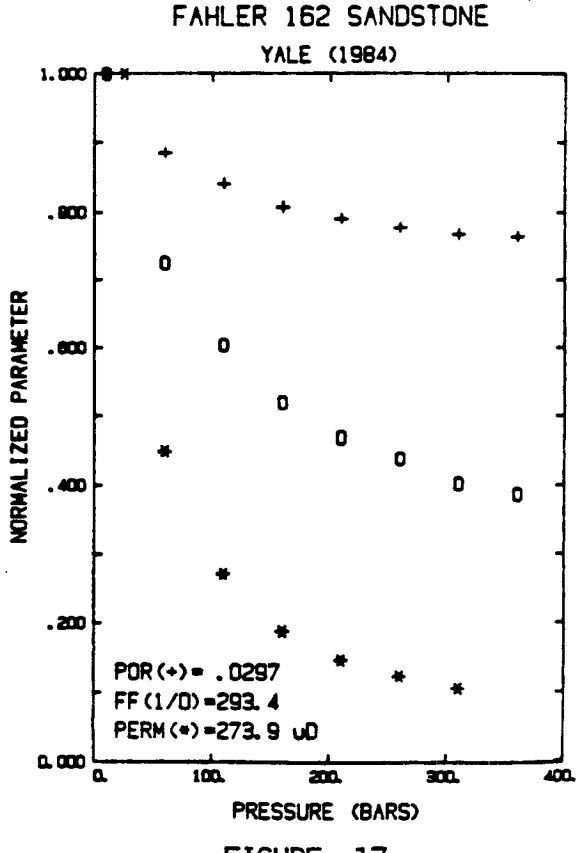

FIGURE 17D

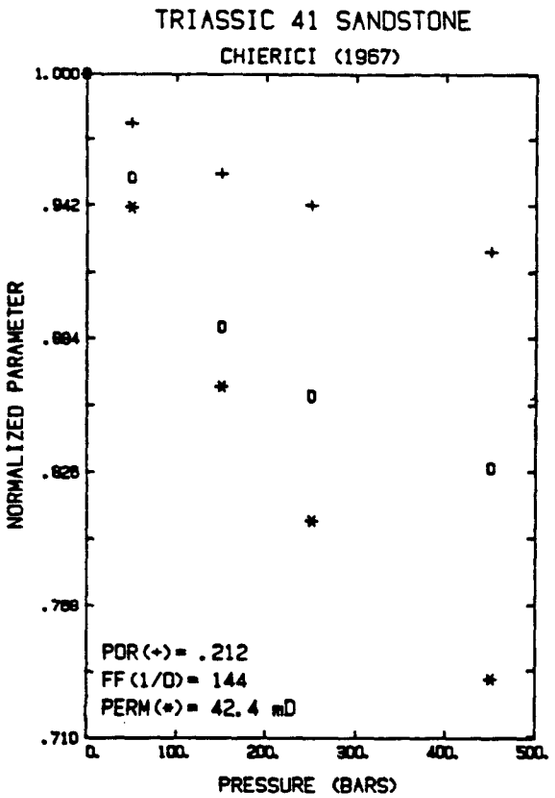

FIGURE 18A

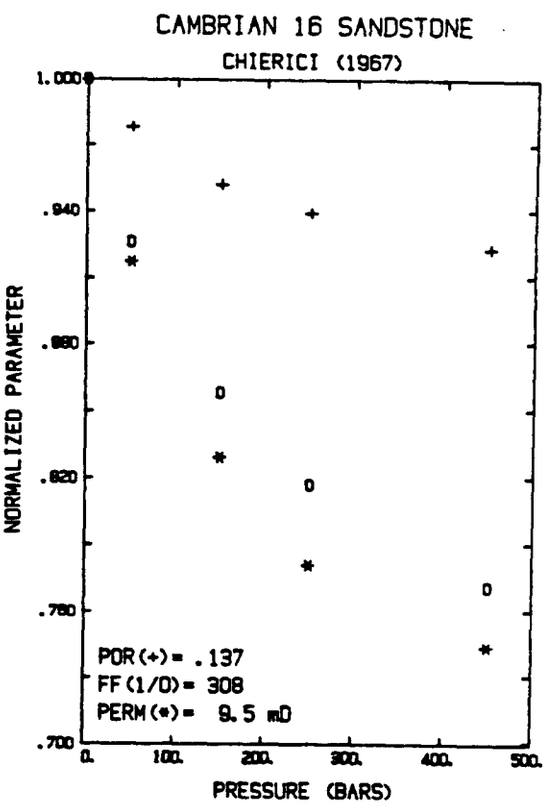

FIGURE 18B

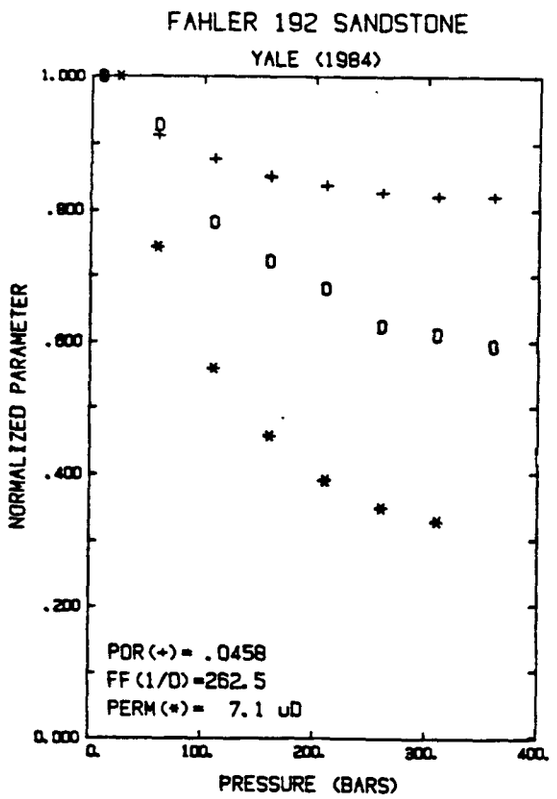

FIGURE 18c

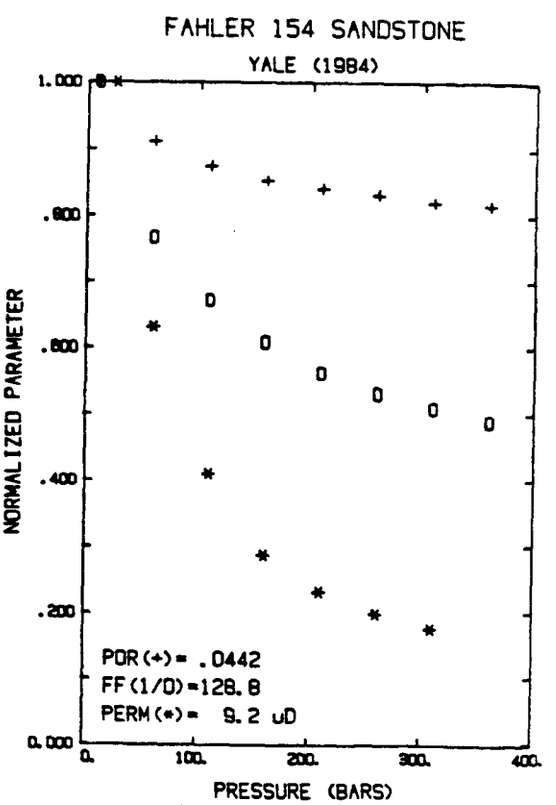

FIGURE 18D

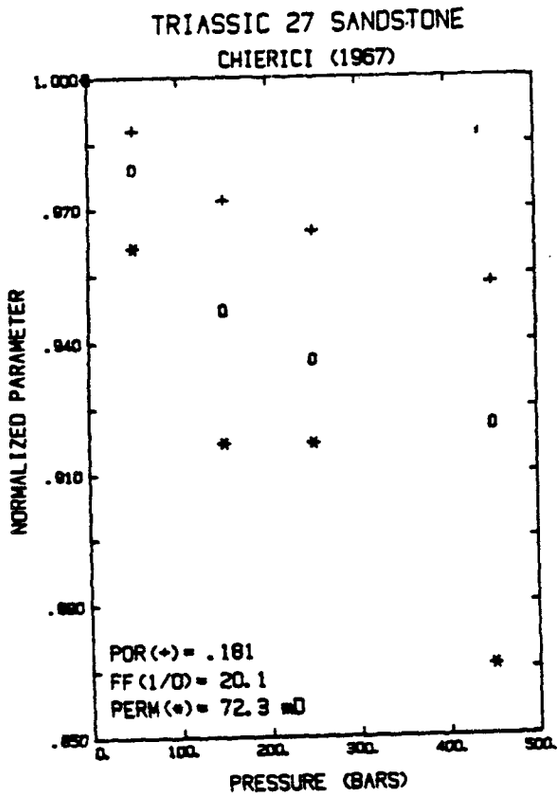

FIGURE 19A

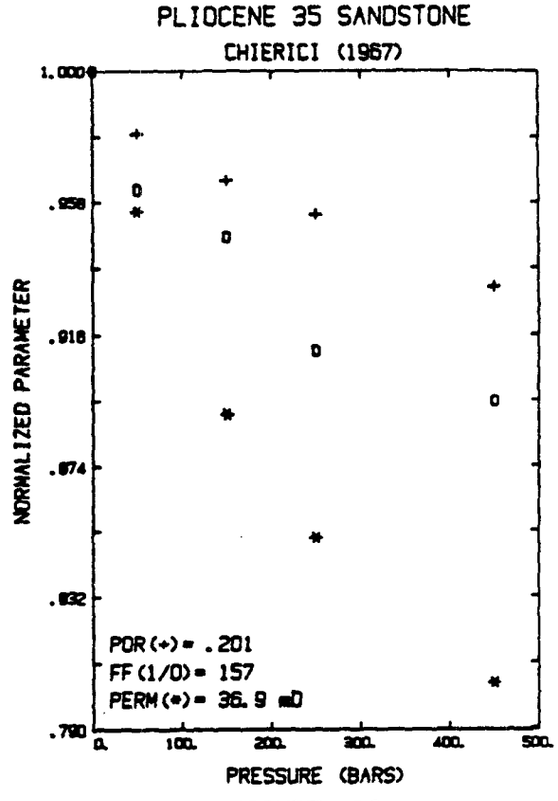

FIGURE 19B

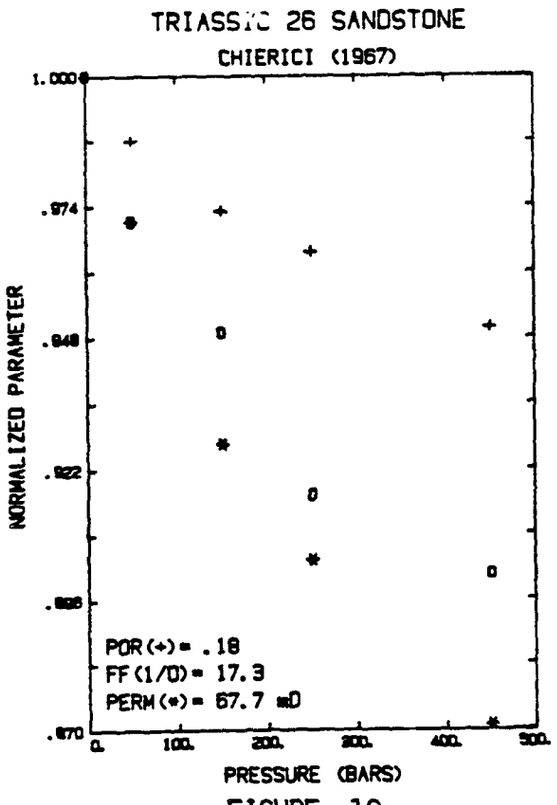

FIGURE 19C

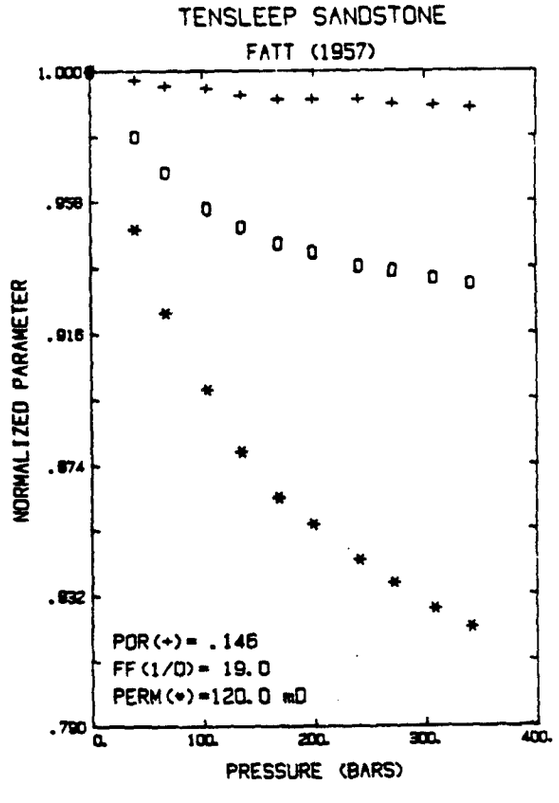

FIGURE 19D

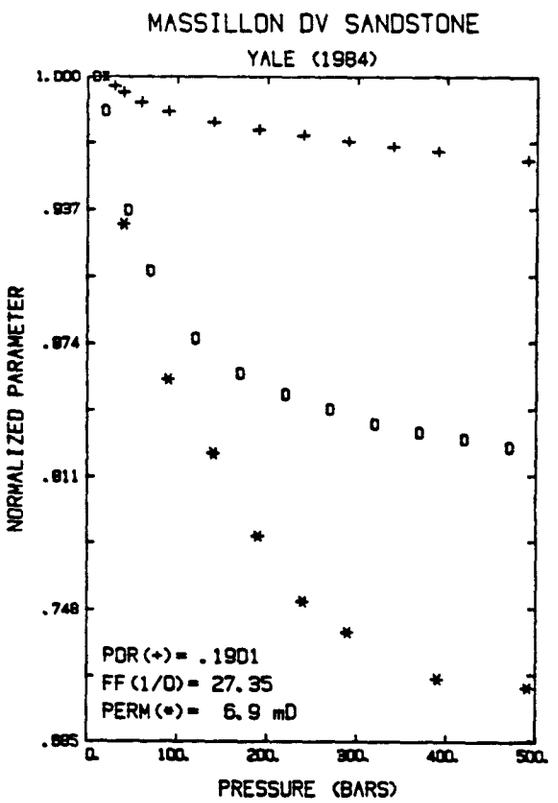

FIGURE 20A

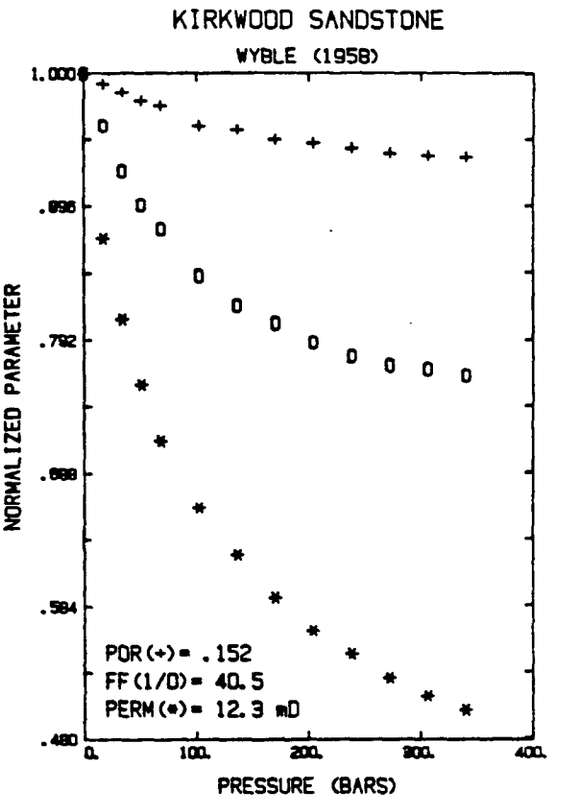

FIGURE 20B

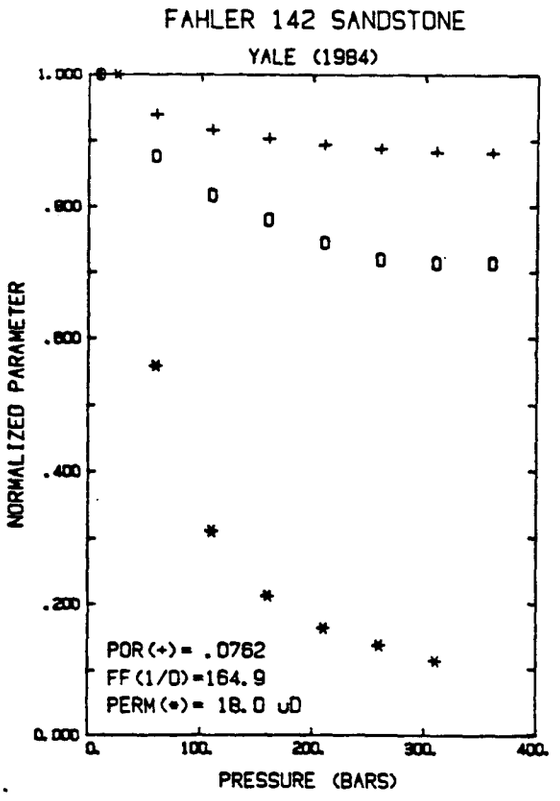

FIGURE 20c

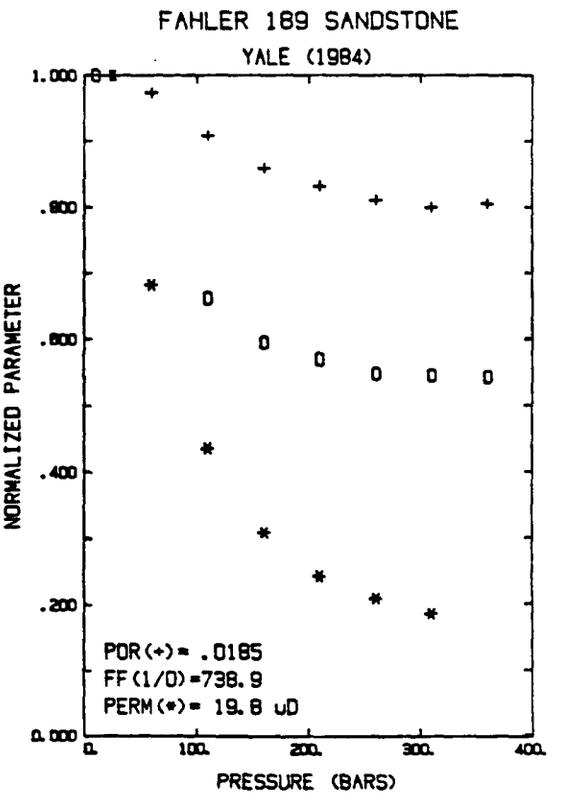

FIGURE 20D

The next four figures (Figures 21a through 21d) represent rocks which are designated in Table 4 as belonging to the "C" or "cross-over" group. They exhibit changes in permeability and conductivity with pressure that are nearly equal. The conductivity versus pressure curve is more concave than the permeability versus pressure curve and that the former cross-over the latter at high pressure. Again a wide range of absolute values and percent changes with pressure of petrophysical properties are represented by rocks in this group.

Figure 22a through 23d represent eight rocks in the "L" group and they show the conductivity versus pressure curve "lower" than the permeability versus pressure curve. There are more rocks with high permeabilities in this group than in the other groups as permeability varies between 12 milliDarcies and 900 milliDarcies among the rocks in the "L" group.

Analysis of these twenty-eight experimental data sets yields the following relationships.

1) There is a continuous variation in the relationship between the permeability versus pressure curve and the conductivity versus pressure curve as we go from rocks in the "S" group and "N" group where permeability decrease with pressure as the 3 to 1.5 power of the conductivity to the "C" and "L" groups where the conductivity decreases as the first to second power of the permeability change with pressure. Our groups are arbitrary divisions on a continuous range of effects.

2) Although there does not appear to be any correlation between the values of petrophysical properties and the inclusion of rocks in the "N" and "C" groups, we do note that rocks in the "S" group tend to have

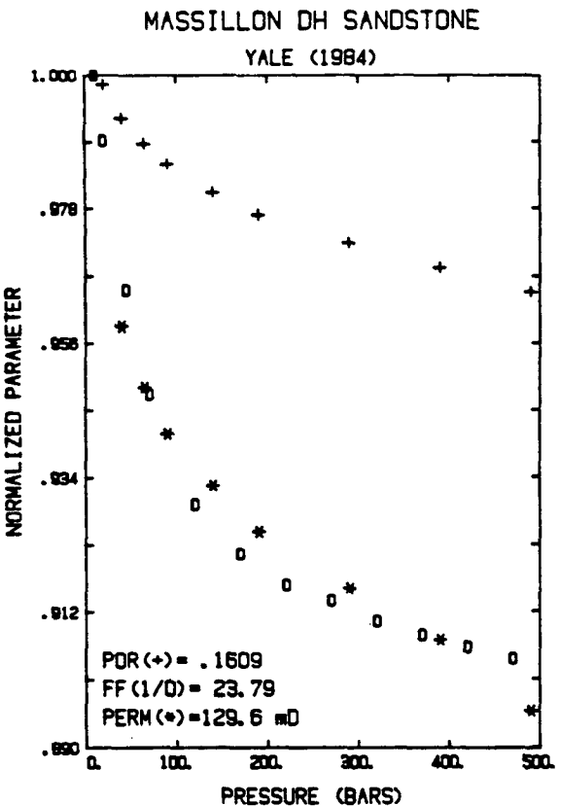

FIGURE 21A

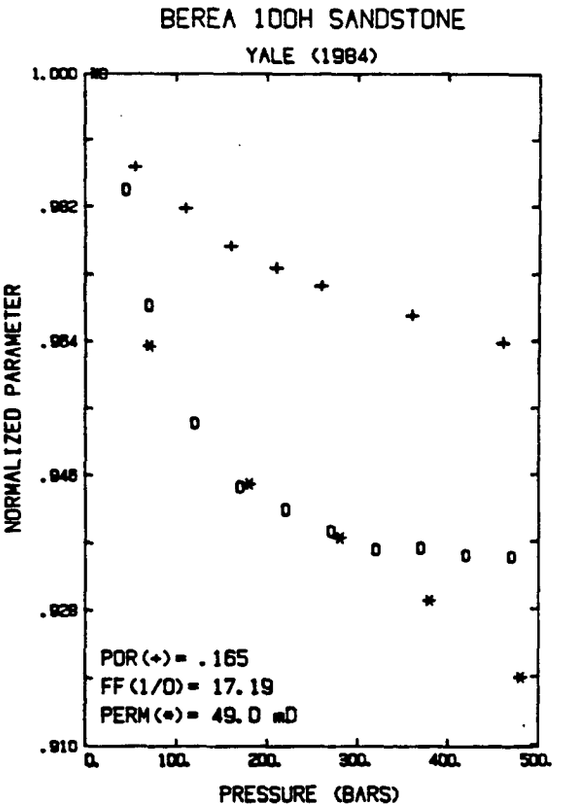

FIGURE 21B

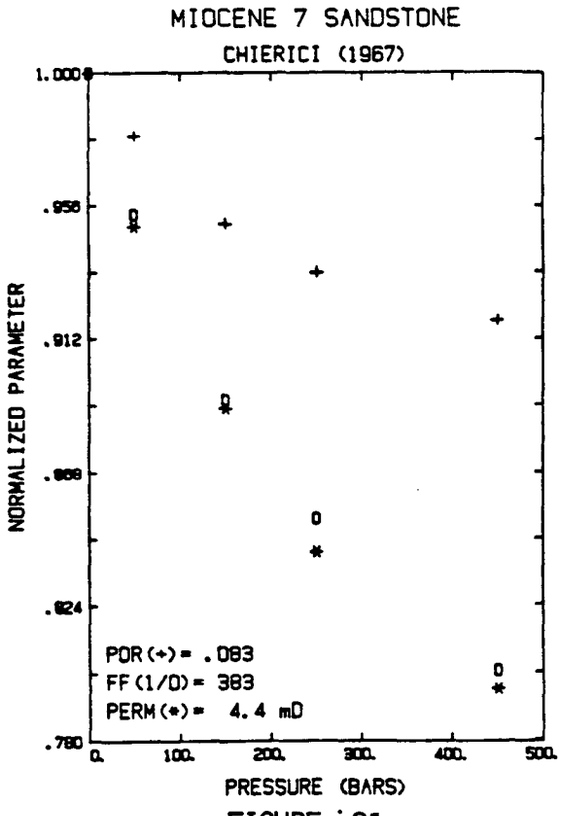

FIGURE 21C

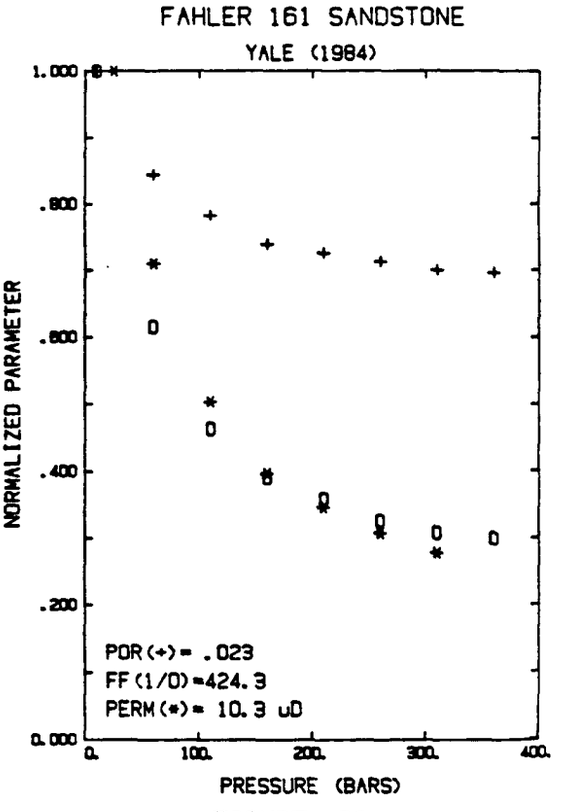

FIGURE 21D

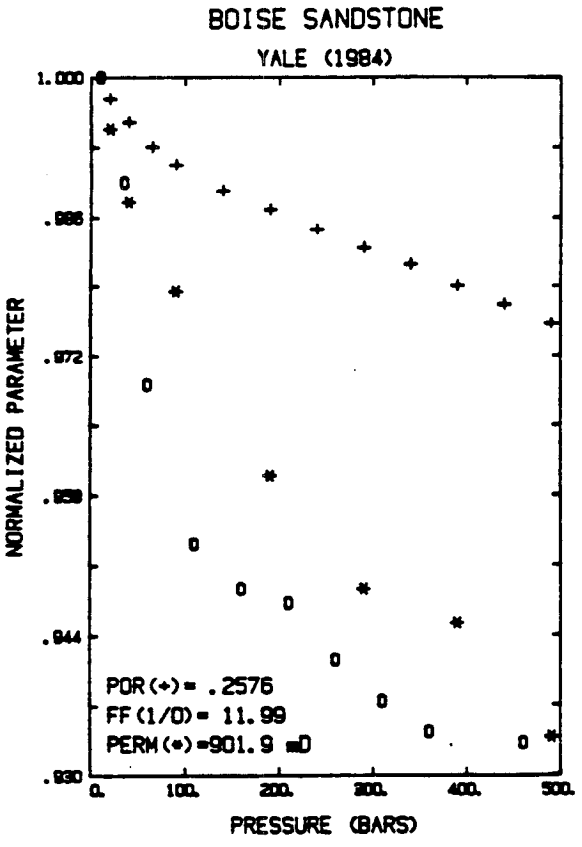

FIGURE 22A

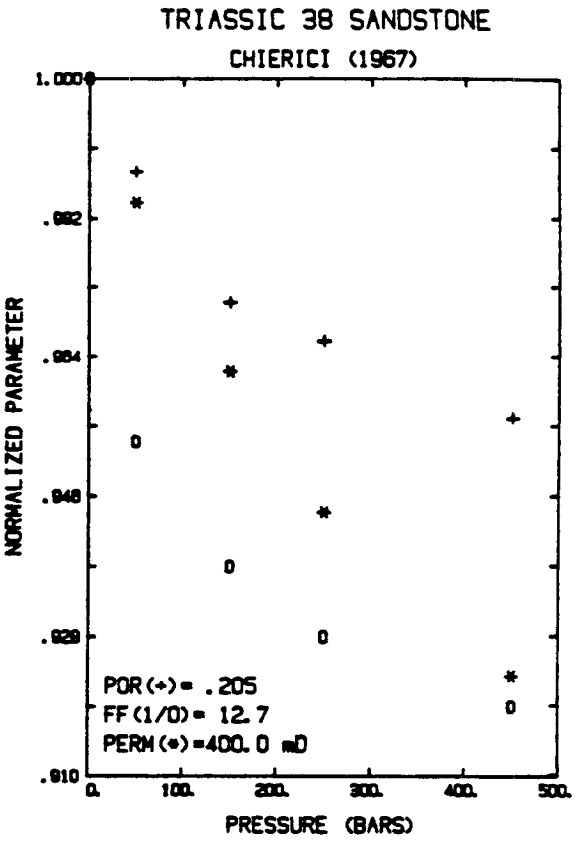

FIGURE 22B

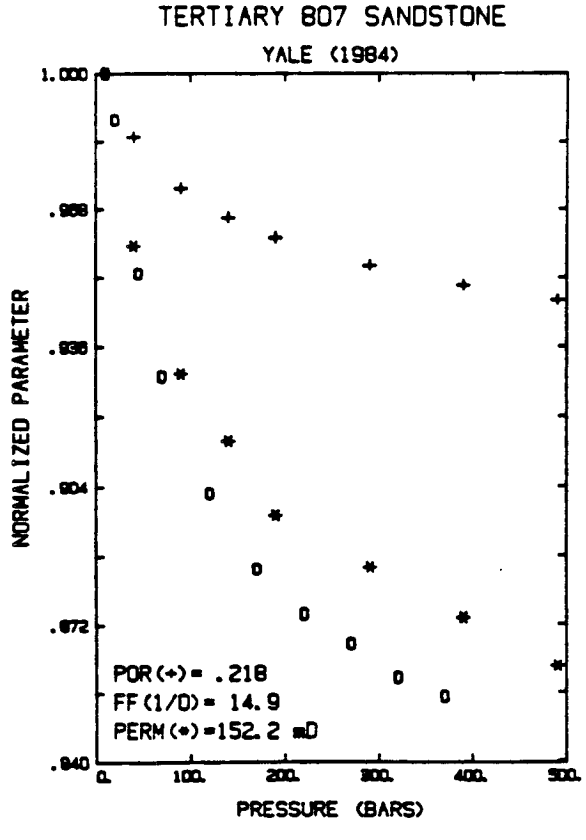

FIGURE 22C

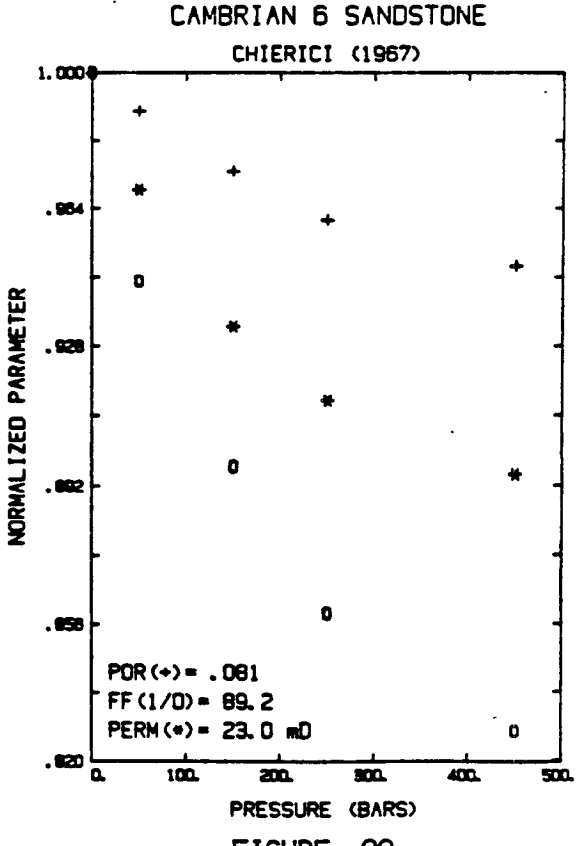

FIGURE 22D

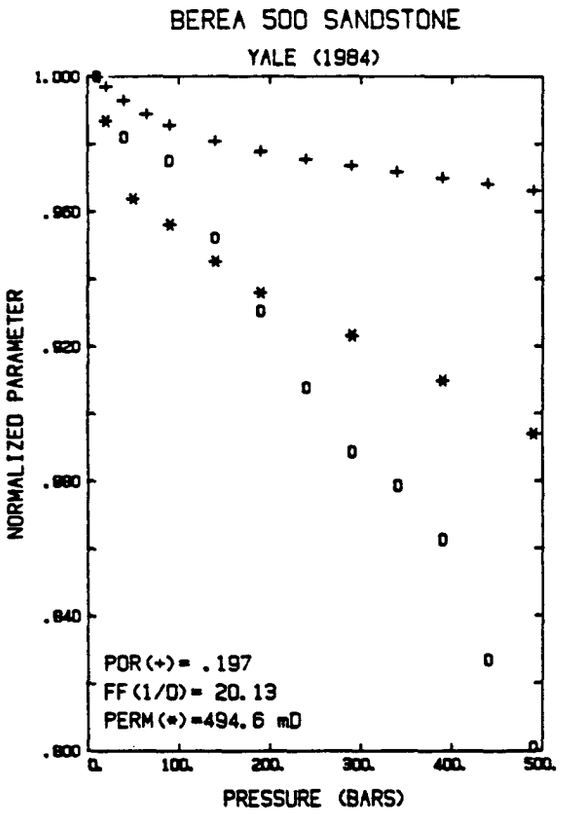

FIGURE 23A

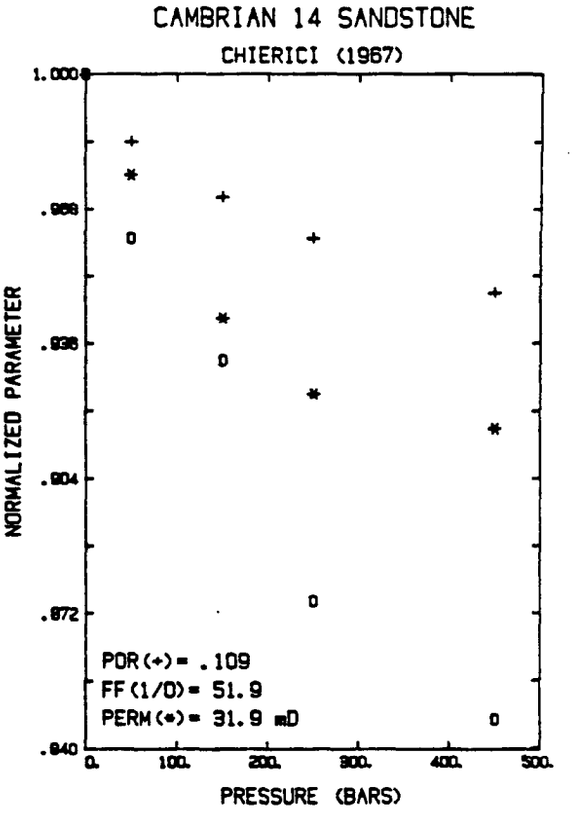

FIGURE 23B

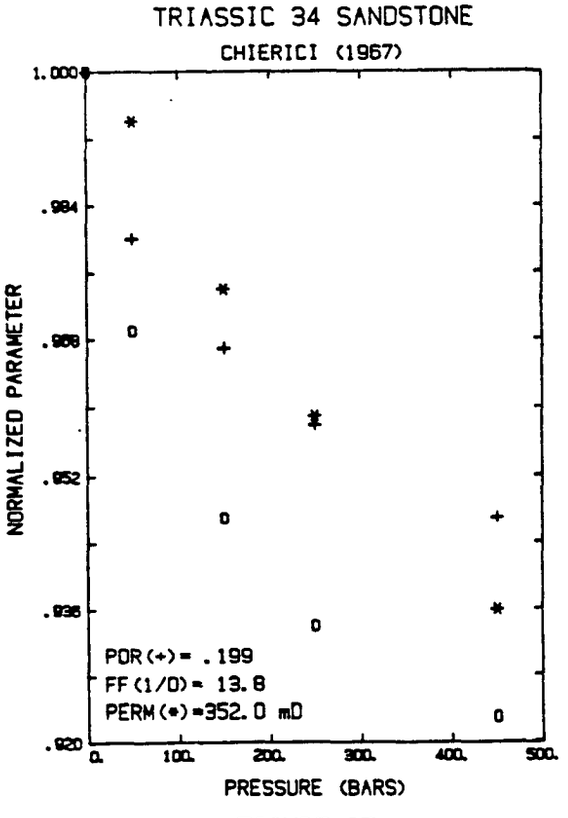

FIGURE 23c

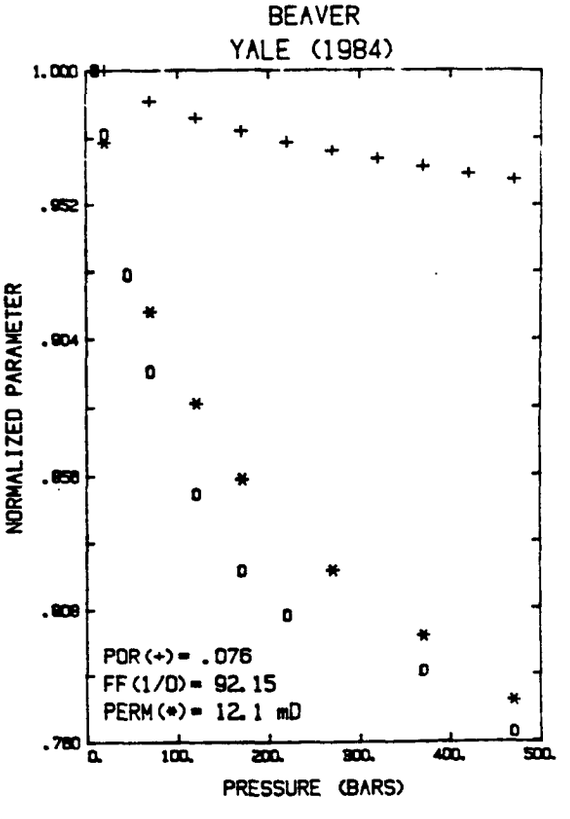

FIGURE 23D

lower permeabilities than rocks in the other groups and that rocks in the "L" group tend to have much higher permeabilities than rocks in the other three groups (see Table 4).

3) Porosity and porosity change with pressure appear to be independent of the group type and the change in porosity with pressure appears only weakly related to the absolute value of porosity. Our only observation is that rocks with porosities less than 8% tend to show decreases in porosity of more than 10% at 400 bars confining pressure and rocks with porosities greater than 8% tend to have changes in porosity with pressure of less than 8% at 400 bars pressure. The change in porosity does appear to almost always be less than the changes in permeability and conductivity with pressure.

4) The experimental data do show a strong correlation between the absolute value of the permeability and the percent decrease in permeability with pressure. Specifically, rocks in this study with permeabilities of less than 1 milliDarcy all showed decreases in permeability of more than 70% at 400 bars confining pressure, those with permeabilities between 1 and 10 milliDarcies had changes in permeability between 30% and 60% at 400 bars, most rocks with permeabilities between 10 and 100 milliDarcies showed changes less than 30% at 400 bars and those with permeabilities greater than 100 milliDarcies showed less than a 10% change in permeability at 400 bars confining pressure. Interestingly, we did not see this sort of correlation between the absolute value of conductivity or formation factor and the change in conductivity with pressure as the two values appeared to be fairly independent of one another.

In order to understand these relationships, we next simulate nine of the twenty-eight data sets with our model in order to investigate the influence of the pore space on the petrophysical properties of the rocks studied.

DATA SIMULATION

In this section we attempt to determine how well specific experimental data can be fitted with the network model and whether various features observed in the experimental data can be simulated and explained. The main thrust of this section is to analyze the pore space simulation parameters to determine how the pore space controls the variety of rock property patterns and how the various petrophysical properties are interrelated. Because the actual pore space of rocks is too complex to be described fully, we search for a model representation which contains the salient features of the pore space so that the petrophysical properties are reproduced, yet is simple enough to reveal how the pore space parameters and their distributions control the physical properties of rocks.

As discussed in chapter two, the four pore parameters are:

1) pore tube width, c
2) pore tube length, ℓ
3) nodal pore radius, S
4) pore tube shape

The values of c and ℓ are the same for all pore tubes, S is the same for all nodal pores and the pore tube shapes are randomly assigned from a distribution. Even though c, ℓ and S in a rock may be distributed over some range of values, the petrophysical data we use at present only allows use to simulate the mean value of c, ℓ, and S. The magnitude and

shape of the permeability, conductivity and porosity versus pressure curves allow us to more rigorously specify the distribution of pore shapes within the rock. There are five variables then in our simulations, three to describe the mean pore width, mean pore length and mean nodal radius and two to describe the distribution of pore tube shapes.

The simulation of experimental data involves two to three steps. The first step is to match the normalized permeability, conductivity and porosity versus pressure curves without regard to the absolute values of the properties. As mentioned in chapter 2, these curves are almost exclusively controlled by the distribution of pore shapes in the model. The distribution of pore shapes is adjusted until all three simulated curves (permeability, conductivity and porosity versus pressure) match the experimental curves to within 2%

The second step is to adjust the pore tube width, pore tube length and nodal pore radius to bring the absolute values of the permeability, conductivity and porosity to within 10% of the experimental values. Because nodal pore size does effect the change in conductivity and porosity with pressure, small changes in the pore shape distribution are often necessary at this point to bring all six properties close to the experimental values. The first two steps require between 15 and 25 simulations to accomplish for any one experimental data set. Comparison of the normalized curves (type 1 plots) and absolute values between the model and experiment show the degree of matching (see figures 24a and 24b for example).

For three of the experimental data sets we have extended the matching process to a third step which entails refinement of the

absolute values of the model until they are within 1% of the experiment. This data is then presented in "type 2" plots (see figure 25 for example) where the model data is plotted over the experimental data on an absolute rather than normalized scale. The type 2 plots show the ability of the model to match experimental data very closely. The type 1 graphs represent the changes in permeability, conductivity and porosity better and the type 2 graphs converge very slowly to the final match (10 to 30 additional iterations) because of the strong coupling between pore parameters. The fit of the type 2 graphs is also very dependent on the percent change in a particular property. For instance, a 1% difference in the absolute value or an extra 1% change in porosity appears as a large mismatch because the overall change in porosity is only 5%. But for permeability, a similar 1% difference would appear as a very good match because of the 30% overall change in permeability at 500 bars. The difficulty in getting the type 2 matches suggests that there is a high degree of uniqueness in this model.

Table 5 lists the nine experimental data sets analyzed by rock name and group type as defined in Table 4. It also lists the values of the pore space parameters of the simulation which best matches the experimental data. Archie's exponent, m, and the p/c ratio are calculated from the experimental values of permeability, conductivity and porosity according to the following equations.

$$CF = 1/FF = \Phi^m \quad \text{or} \quad m = \log(CF)/\log(\Phi) \tag{72}$$

$$p/c = \frac{\sqrt{\text{permeability}}}{\text{conductivity}} \tag{73}$$

TABLE 5

Model Simulations of Experimental Data

Rock Name	Type	m	perm/cond	c/ S / l	Pore tube shapes
A)Triassic 27	NH	1.76	5.40	10.4/11.7/26.2	50% 1,4
B)Pliocene 35	NM	3.15	30.2	35 /110 /190	25% 2,3,4,5
C)Triassic 41	NM	3.20	29.7	80 /180 /300	25% 5,6,8,10
D)Massillon DV	SM	1.99	2.28	13.5/12.3/23.5	15%2 70%8 15%10
E)Fahler 189	SL	1.67	3.22	70 / 25 /130	20%1-2 60%2.5-3 20%no pore
F)Miocene 7	CM	2.39	25.4	30 / 70/180	10%2 30%3 60%20
G)Fahler 161	CL	1.60	1.34	45 / 8/ 40	30%5-3 10%2.5-3,1-3 15%5-4 35%1-4
H)Tertiary 807	LH	1.77	5.81	15.85/10.7/26.2	40%1 60%15
I)Cambrian 6	LH	1.79	13.5	15 / 12 /60	10%CIR 25%1 30%15 35%20

Note: c=pore tube width (in um), S=nodal pore radius (in um)
L=pore tube length (in um)

Fraction of pore tubes with a given shape is given in the third column.
GBP pores listed by RC value 1,2,3,4,6,8,10,15,20
TAP pores listed by aspect ratio 1-2,5-3,2.5-3,1-3,5-4,1-4
CIR stands for pore tubes of circular cross-section
"no pore" means pore tube site not occupied by a pore

Group type for experimental data same as Table 4

m=Archies exponent for experimental data where
$m = \log (CF)/\log (porosity)$

p/c = (permeability)$^{1/2}$ * formation factor
with permeability in Darcies this ratio has units of microns (Darcy = .987 micron^2)

Permeability has units of (microns)^2 in equation 73, so that p/c has units of microns. The p/c ratio and exponent m characterize the relationships between permeability and conductivity and between conductivity and porosity for the rock sample.

A) Triassic 27 sandstone (Chierici 1967)

Figure 24a shows the permeability, conductivity and porosity versus pressure for this sample and is flanked by figure 24b which displays the same curves for the network simulation which best matches the experimental data. We note that the curves match very well and the absolute values of permeability, formation factor and porosity (as shown in the lower left corner of the plots) are within 1% of each other. The high degree of correlation between the simulation and experimental data is shown in figure 25 (a type 2 plot) where both model and experimental data are plotted together.

The simulation has pore parameters of c=10.4 um, λ=26.2 um, S=11.7 um and pore tube shapes divided evenly between the GBP-RC1 shape and the GBP-RC4 shape. The experimental data set is classified as belonging to the "N" group and "H" subgroup (see Table 4 and 5). This signifies that the experimental data show the permeability decreasing with pressure as the 1.5th to 2nd power of the conductivity change with pressure ("N" group) and that the overall decrease in permeability at 400 bars pressure is less than 20% ("H" subgroup). Analysis of over 800 simulations has shown that simulations where the distribution of pore shapes is narrow (width of distribution equal to +-50% of the mean aspect ratio) and uniform, fall into the "N" group. Fatt (1957, 1958a) suggested that permeability should change as the square of the conductivity change if the fluid and electricity were conducted through the same cylindrical pore tubes. For our pore shapes, we find that if the hydraulic and electrical flow paths are the same, the permeability should be related to the 1.7th to 1.9th power of the conductivity versus pressure. This

suggests that rocks which fall in the "N" group and can be simulated with narrow uniform distributions of pore shapes which have hydraulic and electrical flow paths which are the same. We show in some later simulations that rocks which fall into the "S", "C" and "L" groups tend to have different hydraulic and electrical flow paths. The similarity of flow paths is important in finding relationships betwen permeability and conductivity. For instance, a small change in mean pore width or mean aspect ratio for rocks with similar hydraulic and electrical flow paths means that permeability is related to the square of the conductivity.

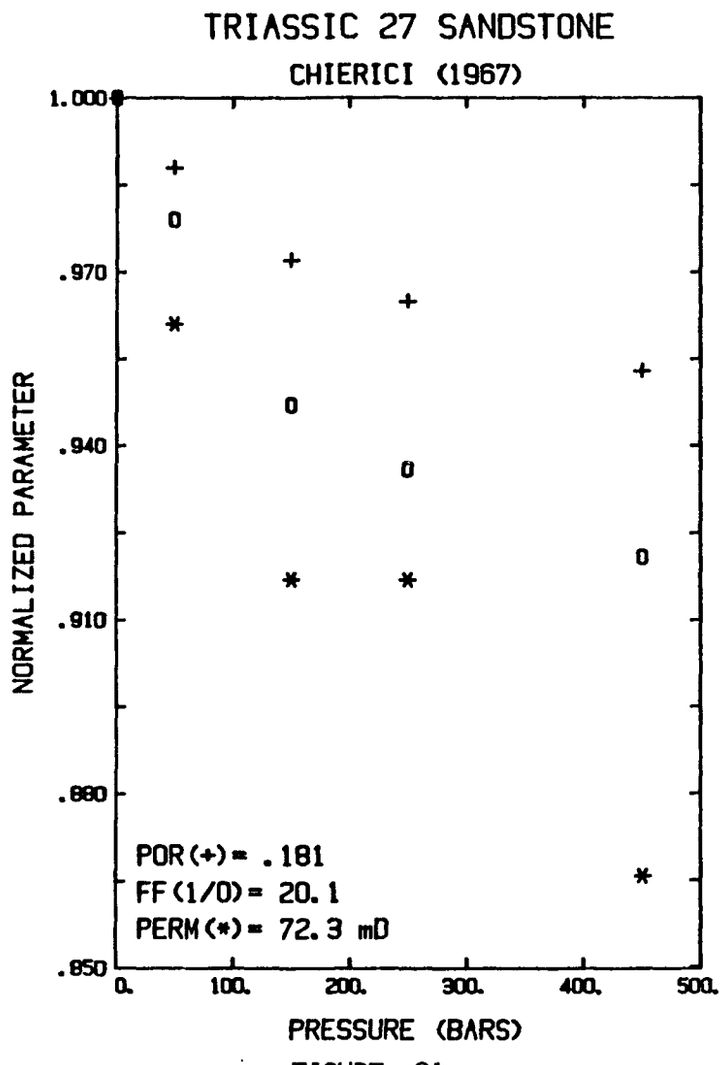

FIGURE 24A

Experimental data

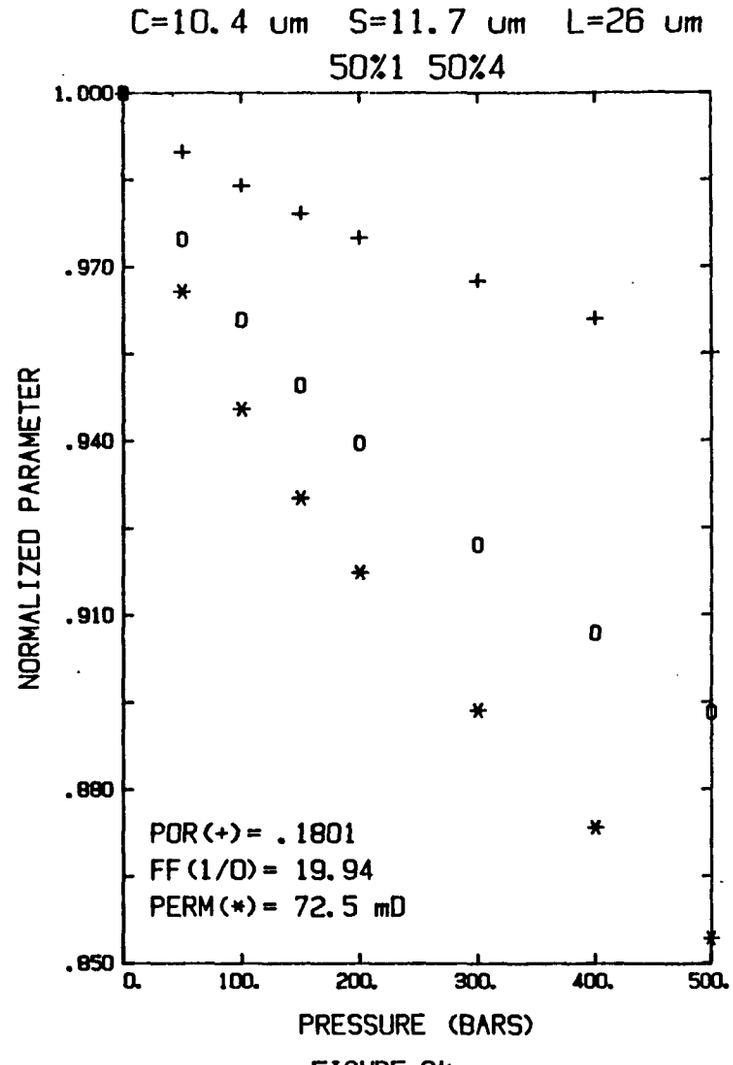

FIGURE 24B

Model simulation

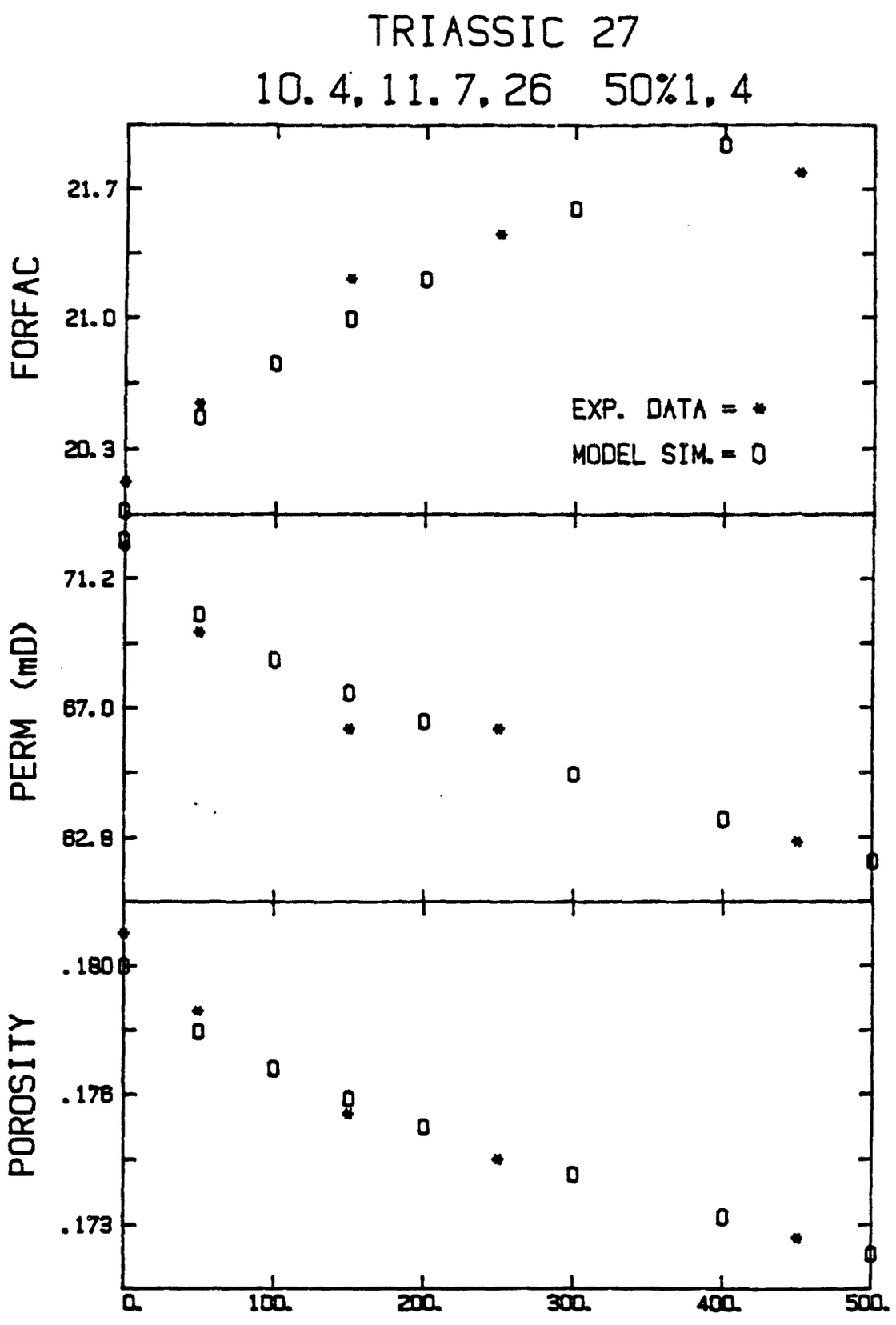

FIGURE 25

Comparison of experimental data (*) and model simulation (0) for Triassic 27 sandstone (Chierici 1967) Type 2 plot

B) Pliocene 35 sandstone (Chierici 1967)

Figures 26a and 26b show the experimental data and the network simulation of that data. Note that the permeability, conductivity and porosity versus pressure curves are very similar in the two plots and that the absolute values of the petrophysical properties are within 10% The differences and similarities between the Pliocene 35 data and the Triassic 27 data are reflected in the pore space parameters used in their respective simulations.

The Pliocene 35 data set falls into the "NH" category as did the Triassic 27 data, however, the permeability decrease in the former at 500 bars is nearly 21% compared to only 15% in the latter. The fact that both rocks fall into the "N" group is explained by their narrow and uniform distributions of pore shapes (see Table 5) and the larger decrease in permeability for the Pliocene 35 data is due to the presence of thinner (lower aspect ratio and higher RC values) pores in the Pliocene 35 simulation. Figure 14a shows that the thinner the pore shape, the larger the change in hydraulic conductance with pressure. The mean aspect ratio for pore shapes in the Pliocene 35 simulation is .175 as compared to .279 for the Triassic 27 simulation (see Table 3 for the aspect ratios of different pore shapes). Because the hydraulic and electrical flow paths are similar we note a corresponding increase in the percent change of conductivity with pressure between the Triassic 27 and Pliocene 35 simulations due to the thinner pores.

The major difference between the Pliocene 35 data and the Triassic 27 data is the nearly 8 fold increase in formation factor (from 20 in the Triassic 27 to 157 in the Pliocene 35 data). The porosities are

very similar and the permeabilities vary only by a factor of 2. The high electrical resistivity of the Pliocene 35 sample accounts for the high m=3.15 and the high p/c ratio=30.2 um as compared with the values of m=1.76 and p/c=5.4 um for the Triassic 27 sample. In chapter 2 we showed that the conductivity was strongly related to the ratio of pore width to pore length (c/ℓ) which means that formation factor should be related to ℓ/c. The ℓ/c ratio for the Pliocene 35 simulation is 5.43 compared with a value of only 2.5 for the Triassic 27 simulation. The very large nodal pores are related to the very large Archies exponent of 3.15.

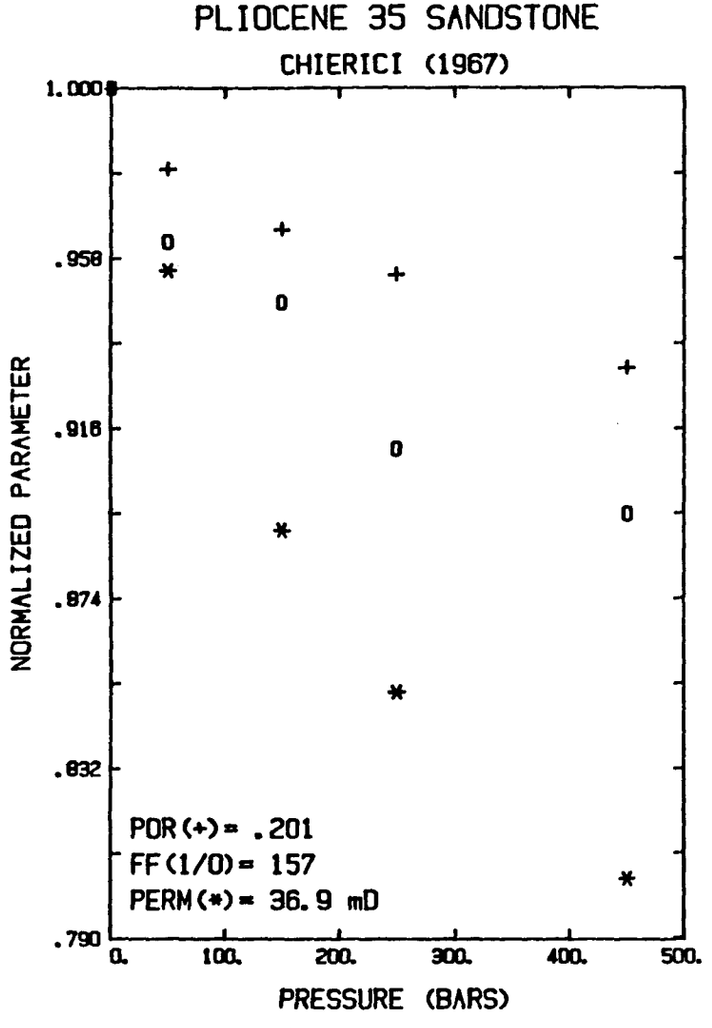

FIGURE 26A

Experimental data

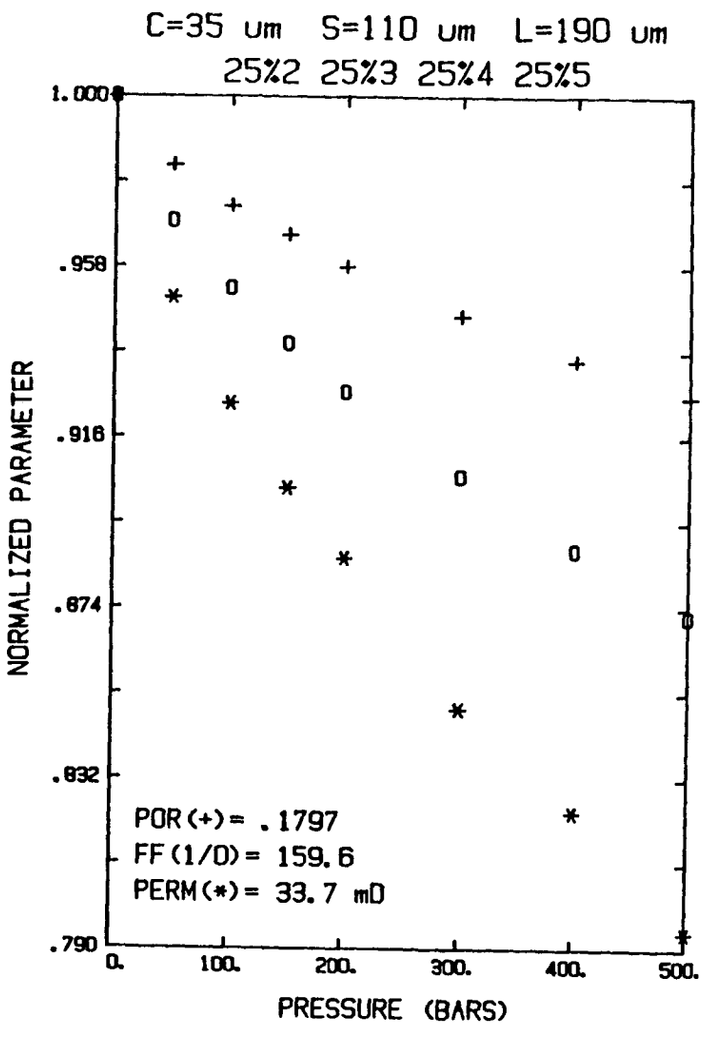

FIGURE 26B

Model simulation

C) Triassic 41 sandstone (Chierici 1967)

We see from figures 27a and 26a that the Triassic 41 and Pliocene 35 data sets are very similar except that the permeability and conductivity of the Triassic 41 change approximately 8 percentage points more than in the Pliocene 35 sample. This is again reflected by the thinner pore shapes in the Triassic 41 simulation in figure 27b. The mean aspect ratio of the pore shapes in the Triassic 41 simulation is .091 compared with an α=.175 in the Pliocene 35 simulation. The Triassic 41 data still fall into the "N" group as shown in figure 27a and the simulation in figure 27b shows a uniform and narrow distribution of pore shapes. The data also fall into the "M" subgroup which is explained by the lower mean aspect ratio of the simulated pore shapes.

Despite the similarities in their petrophysical properties (perm=42.4 versus 36.9, FF=144 versus 157, porosity=.212 versus .201 for the Triassic 41 and Pliocene 35 samples), the pore parameters in their respective simulations are widely different (c=80 versus 30, ℓ=300 versus 190, S=180 versus 110). Analysis of why these parameters are different demonstrates how the complex relationships between pore parameters and petrophysical properites affects the simulations.

Because the mean pore shape has an aspect ratio of .091 in the Triassic 41 simulations, its effective hydraulic radius is only .138 (see Table 3) as compared with the effective hydraulic radius = .238 for the mean pore shape in the Pliocene 35 simulation. This means that the pore width, c, in the Triassic 41 simulation must be 75% greater than the c for the Pliocene simulation if both are to have the same absolute permeability. The Triassic 41 data and simulation do have a slightly

higher permeability than the Pliocene 35 but this results in only a 0.7% further increase in c. Because formation factor is related to ℓ/c, we must increase the pore length to maintain a formation factor of 150 in the Triassic 41 simulation. Increasing the pore length then necessitates a further increase in pore width to maintain the correct value of permeability. Increasing the pore length increases the total volume of the network and therefore decreases the porosity. Nodal pore radius must also be increased to maintain the same porosity.

In the end we need a 58% increase in pore length which leads to an additional 30% increase in pore width (above the 78% needed to compensate for the thinner pores in the Triassic 41 simulation) and a 64% increase in nodal pore radius. The ℓ/c ratio of the Triassic 41 simulation is 3.75 as compared with $\ell/c=5.43$ for the Pliocene 35 simulation. This difference is due to the relatively small 39% difference in effective electrical radii of the mean pore shapes between the two simulations.

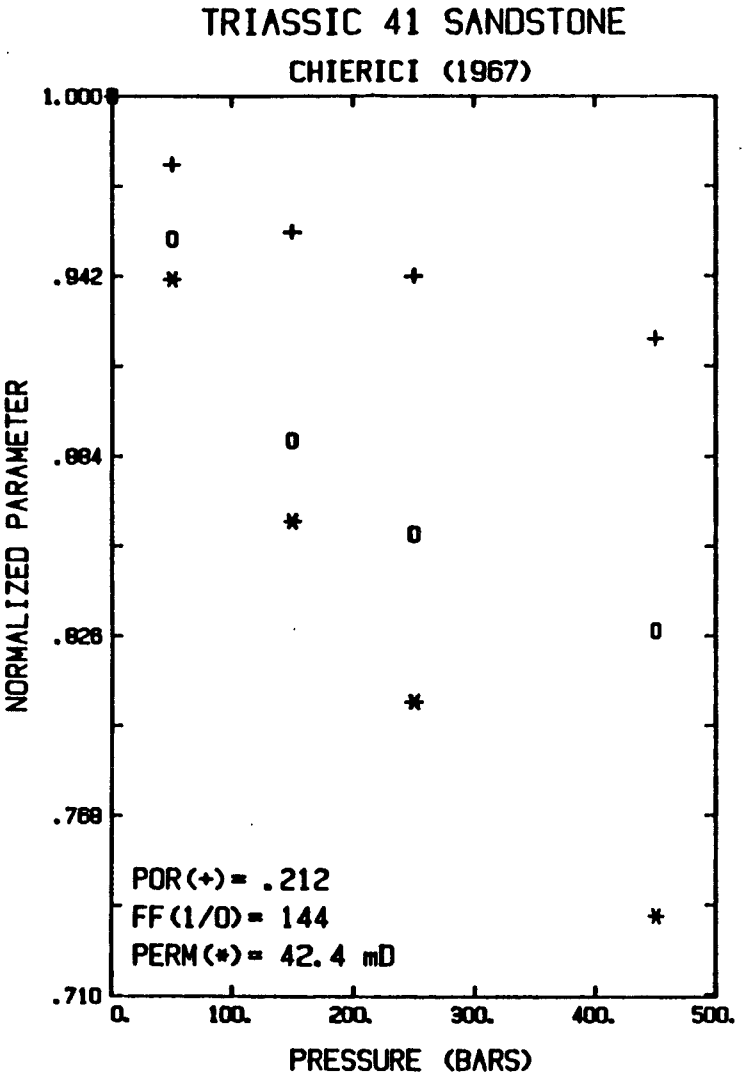

FIGURE 27A

Experimental data

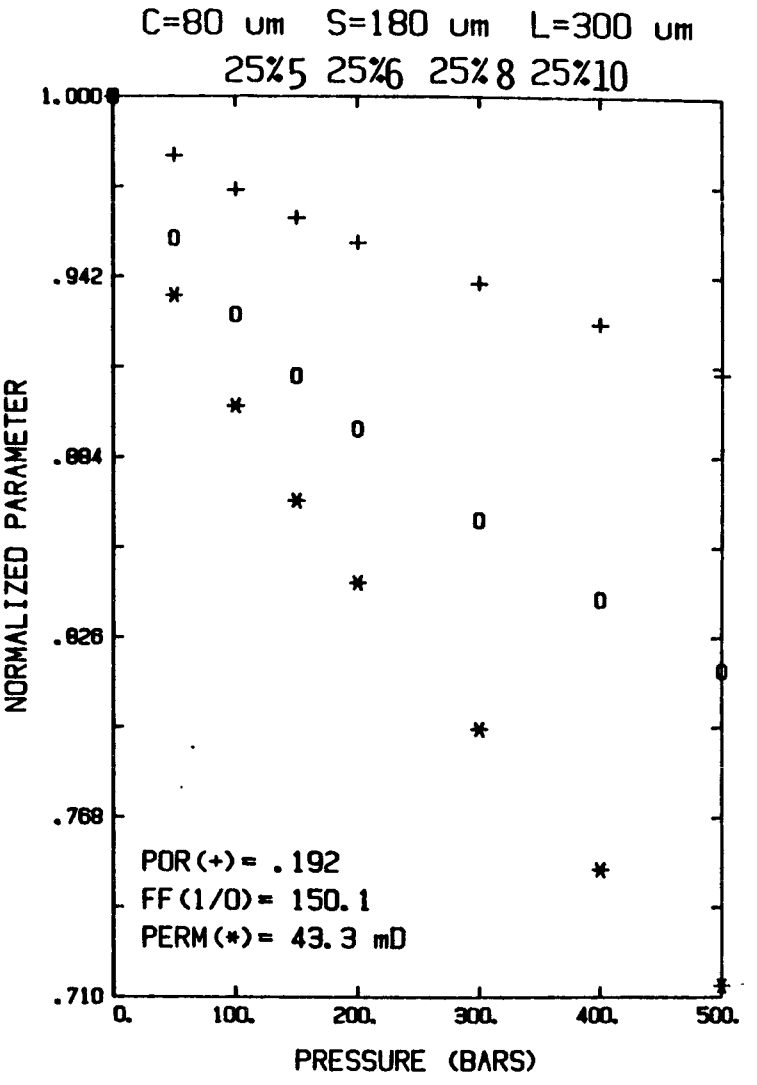

FIGURE 27B

Model simulation

D) Massillon DV sandstone (Yale 1984a)

The Massillon DV sandstone is classified in the "S" group because of the split between the permeability and conductivity versus pressure curves (see figure 28a). The simulation of this data in figure 28b shows that the absolute values of permeability, formation factor and porosity as well as their percent decreases at 500 bars are well matched but the experimental curves are more concave than the simulation curves. Figure 29 shows a type 2 plot of both simulation and experimental data and suggests that the lack of a better fit in the type 1 plots is due to large decreases in permeability and conductivity at pressures less than 50 bars confining pressure. The experimental and simulated curves above 50 bars pressure are similar in figure 29.

Table 5 shows that the values of c, ℓ, and S for the Massillon DV simulation are similar to the pore parameters in the Triassic 27 simulation yet the absolute permeability and change in permeability with pressure are very different between the two simulations (6.6 mD versus 72 mD and 38% versus 15% change at 500 bars for the Massillon DV and Triassic 27 samples respectively). The distribution of pore shapes in the Massillon DV simulations explains these differences and all suggests a fundamental difference between rocks in the "N" group and rocks in the "S" group.

In the Massillon DV simulation 15% of the pore tubes have a GBP-RC2 shape (α=.251) and 85% have GPB-RC8 and RC10 (α=.077) shapes. In chapter 1 we discussed the role of percolation theory on network with a wide distribution of pore shapes. For a cubic network, percolation theory (Shante and Kirkpatrick 1971, Kirkpatrick 1973) has shown that if the

pores of a given shape occupy less than 25% of the lattice, there will not be a continuous path of pore of that shape across the lattice. This means that in the Massillon DV simulation there is not a continuous path of RC2 shaped pores across the network and therefore all fluid and electricity must pass through RC8 shaped pores in order for there to be conduction across the network. Because permeability is related to the effective hydraulic radius to the fourth power, it is controlled by the smallest or thinnest pore the fluid must pass through. The RC8 shaped pores control the permeability which results in the low permeability and a large decrease in permeability with pressure for the Massillon DV simulation.

The decrease in permeability at 500 bars pressure for the Massillon DV simulation is only 0.7% less than a simulation where all the pores have RC8 shape. However, the conductivity change at 500 bars is more than 6% less in the Massillon DV simulation than it is in a simulation with all RC8 shaped pores. In other words, the RC2 shaped pores "pull up" the conductivity versus pressure curve more than they pull up the permeability versus pressure curve. The difference in electrical conductance between pores of RC2 and RC8 shaped pores is only a factor of 3.3 compared to the factor of 45 difference in their hydraulic conductances. This allows the RC2 shaped pores to contribute more to the overall electrical conductance than they contribute to the overall hydraulic conductance of the network and explains the low formation factor and smaller than expected change in conductivity with pressure. It is the "pull up" of the conductivity curve that gives the "S" group rocks the split in the permeability and conductivity versus pressure

curves. The low p/c ratio = 2.28 for the Massillon DV sample as compared with the p/c ratio = 5.4 for the Triassic 27 sample is due to the fact that the RC2 pores contribute to conductivity but not to permeability.

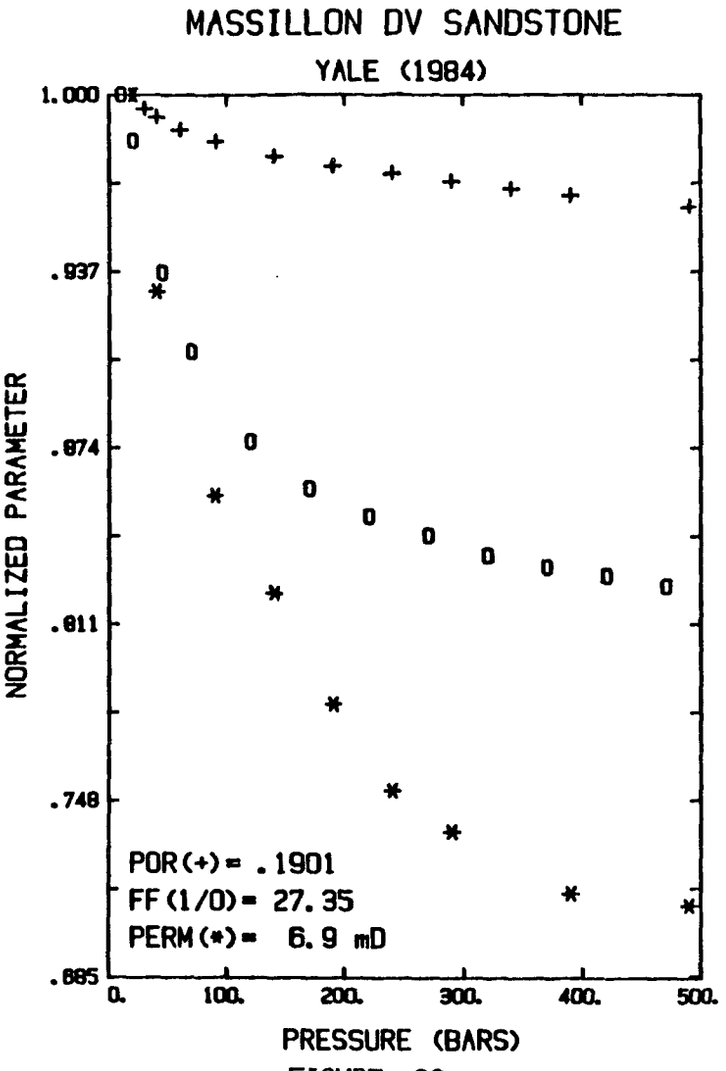

FIGURE 28A

Experimental data

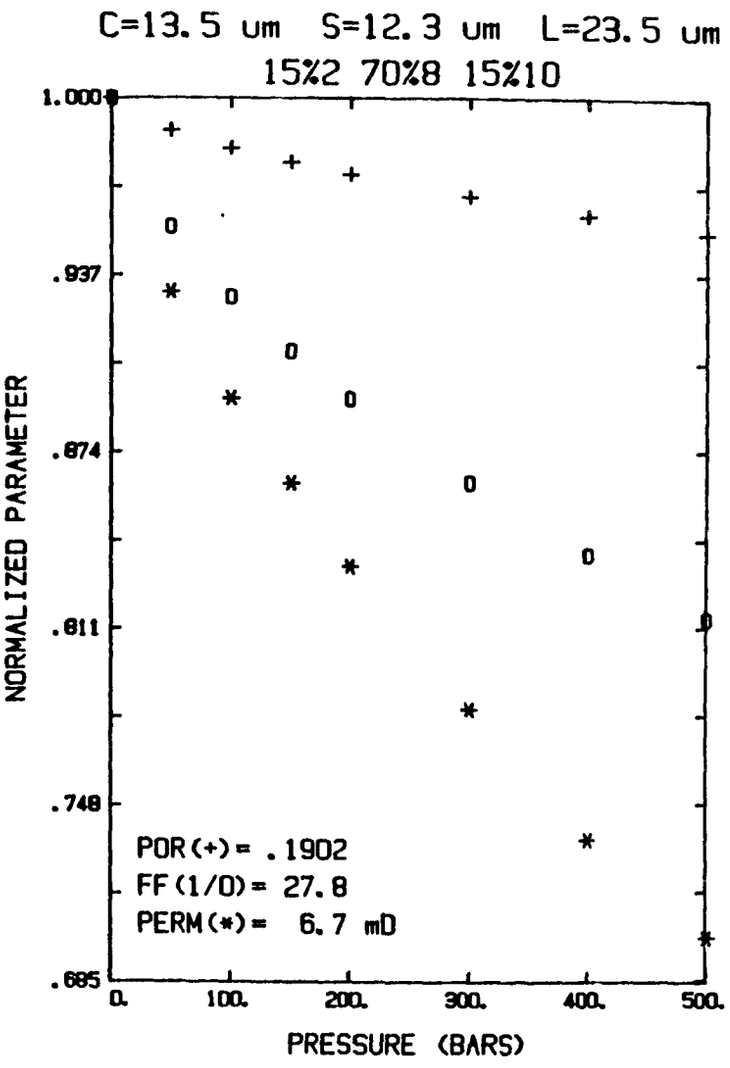

FIGURE 28B

Model simulation

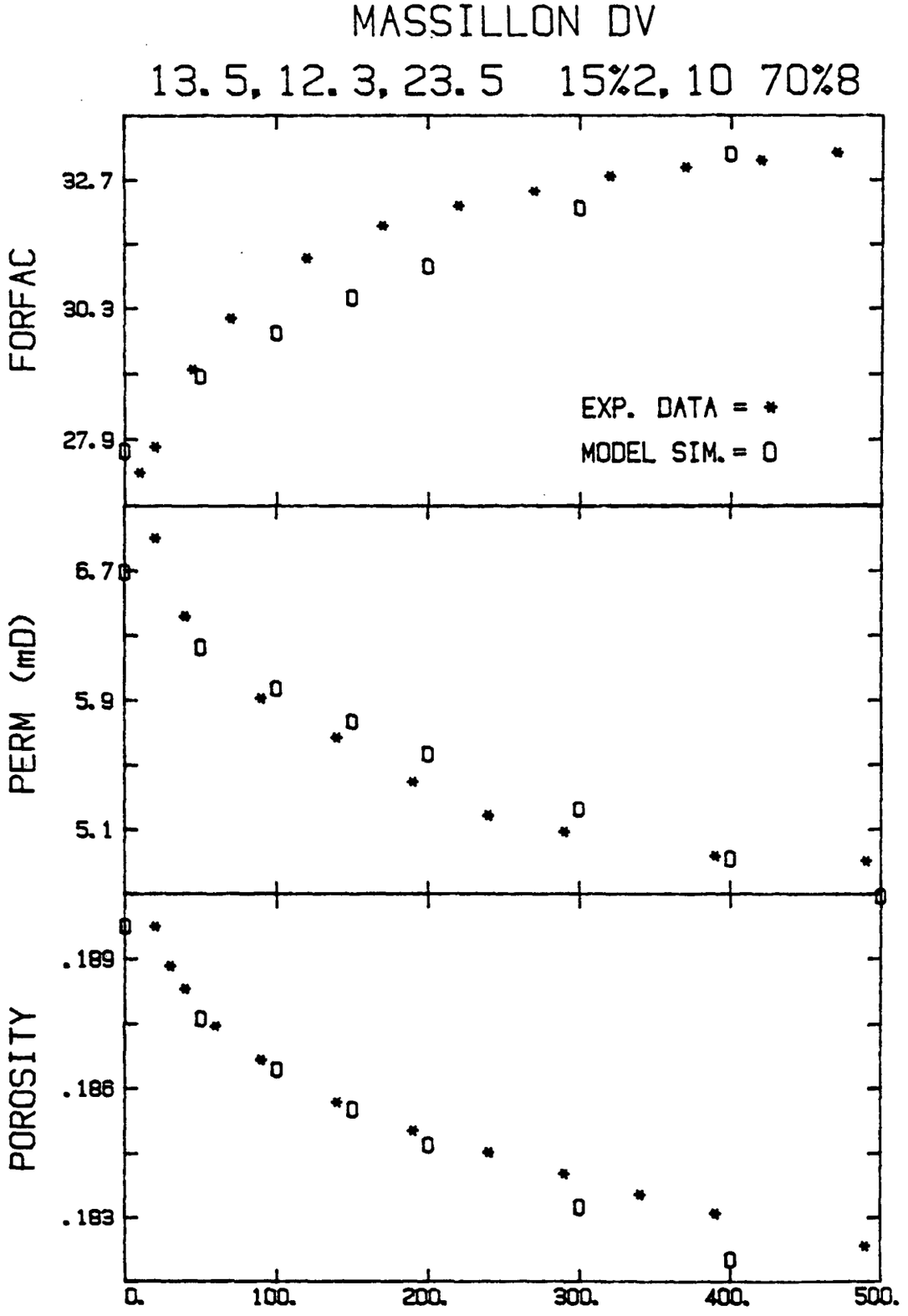

FIGURE 29

Comparison of experimental data (*) and model simulation (0) for Massillon DV sandstone (Yale 1984). Type 2 plot

E) Fahler 189 tight gas sandstone (Yale 1984)

The Fahler 189 data in figure 30a also belongs in the "S" group. Unlike the other four rocks simulated thus far, the Fahler 189 exhibits very large changes in permeability, conductivity and porosity with confining pressure and it falls into the "L" subgroup because of its 80% decrease in permeability at 400 bars. In order to simulate these large changes with pressure, we use tapered shaped pores (Mavko and Nur, 1978 also see figures 5a,b) with very low aspect ratios. The simulation in figure 30b shows that there is nearly an order of magnitude spread in the aspect ratios of the pores, with 20% of the pores having TAPα1E-2 shapes and 60% with TAPα2.5E-3 shapes. The other 20% of the pores are assumed to be closed at all pressures.

The α=1E-2 pores account for less than 25% of the network and therefore the α=2.5E-3 shaped pores control the permeability and its change with pressure. The split, which is very evident in figure 30b, is again due to the contribution of the α=1E-2 to electrical conduction whereas they do not contribute to hydraulic conduction. The conductivity versus pressure curve has been "pulled up" by 13% compared to a simulation where all the pores have α=2.5E-3 shape. The permeability versus pressure curve on the other hand is only 1.5% different from a simulation where all pores have α=2.5E-3 shape.

Interestingly, the pore width, c, in the Fahler 189 simulation is close to the pore width in the Triassic 41 simulation (70 versus 80 um) yet their permeabilities are more than 3 orders of magnitude apart (20 microDarcies versus 43 milliDarcies). Considering just pore width and pore length, we would predict the Fahler 189 simulation to have a

permeability 3 times larger than the Triassic 41 simulation. This comparison illustrates the very large effect pore shape has on permeability in the model. The mean aspect ratio of the Triassic 41 simulation is α=.091 compared to the α=.0025 for the controlling pores in the Fahler 189 simulation. Table 3 shows that there is more than a factor of 10,000 difference in hydraulic conductivities between pores of these two shapes which totally accounts for the difference in permeability between the two samples and their simulations.

We also find that the p/c ratio for the Fahler 189 sample is very close to that of the Massillon DV sample (2.28 versus 3.22 um) and that both are lower than average. The median p/c ratio for the 28 data sets in Table 4 is 7.2 but the median and mean p/c ratio for the 5 "S" group data sets is 3 um. The split in the permeability and conductivity versus pressure curves and the difference in the mean p/c ratios both suggest that there are some electrical flow paths which do not contribute greatly to the hydraulic flow, i.e. a decoupling between permeability and conductivity occurs for rocks which fall into the "S" group.

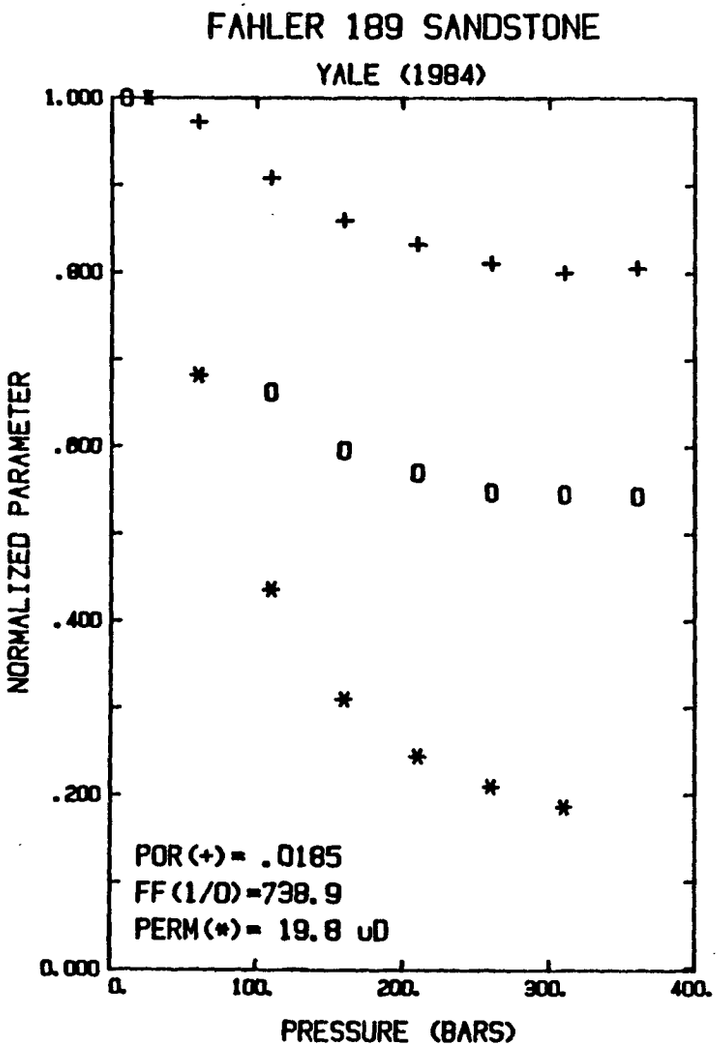

FIGURE 30A

Experimental data

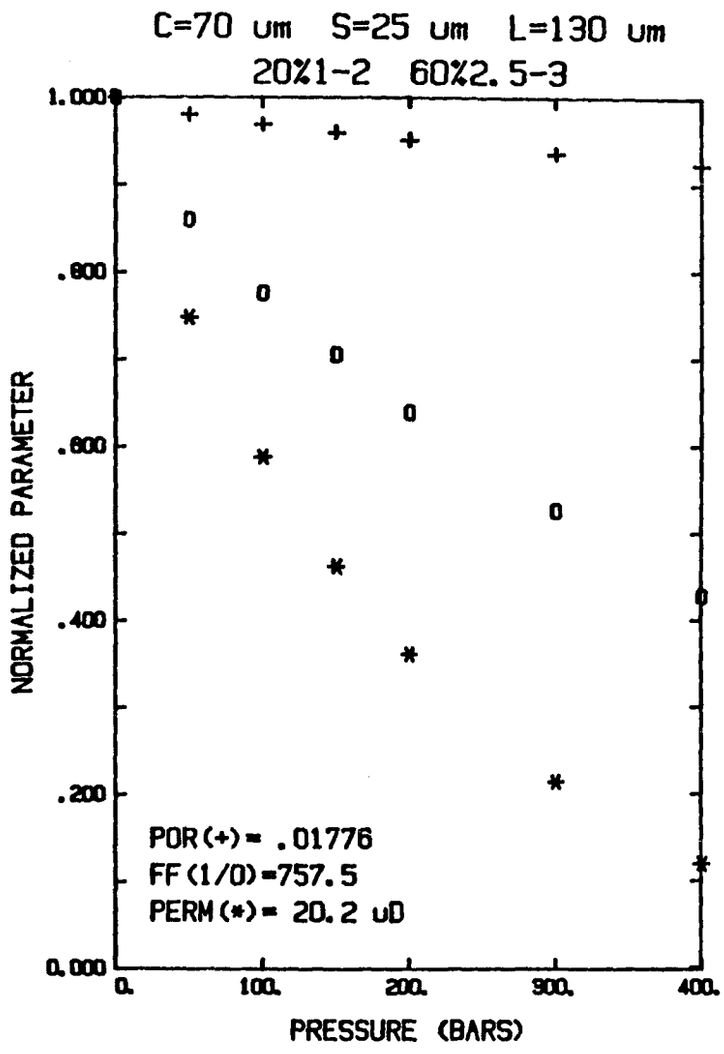

FIGURE 30B

Model simulation

F) Miocene 7 sandstone (Chierici 1967)

Figures 31a and 31b show the permeability, conductivity and porosity versus pressure for the Miocene 7 sandstone and the model simulation which best fits the experimental data. The Miocene 7 data set is classified as "CM" as the conductivity change with pressure nearly equals the permeability change with pressure. The simulation for the Miocene 7 data shows the conductivity curve crossing over the permeability curve at 150 bars. The match between model and experimental plots is excellent in both curve shape and overall change in properties with pressure. The absolute values of permeability, conductivity and porosity match within 5%.

The distribution of pore tube shapes again explains the relationship between the permeability versus pressure and the conductivity versus pressure curves. The simulation in figure 31b shows that 40% of the pore tubes have GBP-RC2 or RC3 shapes while the other 60% have GBP-RC20 shape. The difference in aspect ratios of α=.20 for the RC2 and RC3 and α=.034 for the RC20 shapes leads to a 230 fold decrease in hydraulic conductance for the RC20 versus RC2-3 shaped pores.

In this simulation, the α=.20 shaped pores occupy 40% of the lattice and therefore there is a continuous path of pores of this shape across the network (according to percolation theory). Because of the large difference in hydraulic conductance, the RC20 shaped pores contribute less than 0.5% of the total fluid flow across the network and the decrease in permeability with pressure is only 10% more at 500 bars than in a simulation where all the pores have RC3 shaped pores.

However, because the electrical conductance of the RC20 pores is only 5.7 times less than the RC2-3 shaped pores, between 15% and 20% of the total electrical flow through the network is carried via RC20 pores. The large contribution of RC20 pores to electrical flow causes the decrease in conductivity with pressure at 500 bars to be 90% more than a network simulation of all RC3 shaped pores.

Because the hydraulic conductance of the pore tube is very sensitive to its size and shape, the largest aspect ratio pores which form a continuous path across the network control the permeability. Electrical conductance on the other hand does not change as much with changes in pore shape (see Table 3) as hydraulic conductance which allows it to "average" more of the pore space. In the "S" group, the low aspect ratio pores control the permeability and the high aspect ratio pores "pull up" the conductivity versus pressure curve. In the "C" group, the high aspect ratio pores occupy more than 25% of the network lattice and therefore control the permeability. The low aspect ratio pores serve to "pull down" the conductivity versus pressure curve.

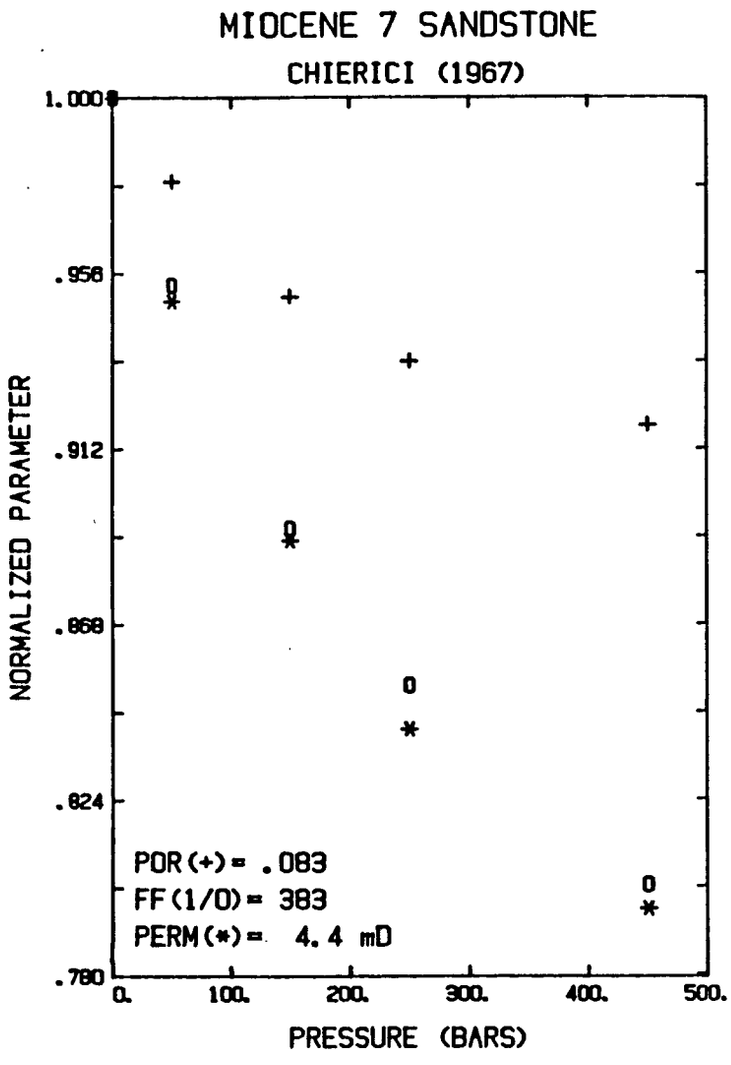

FIGURE 31A

Experimental data

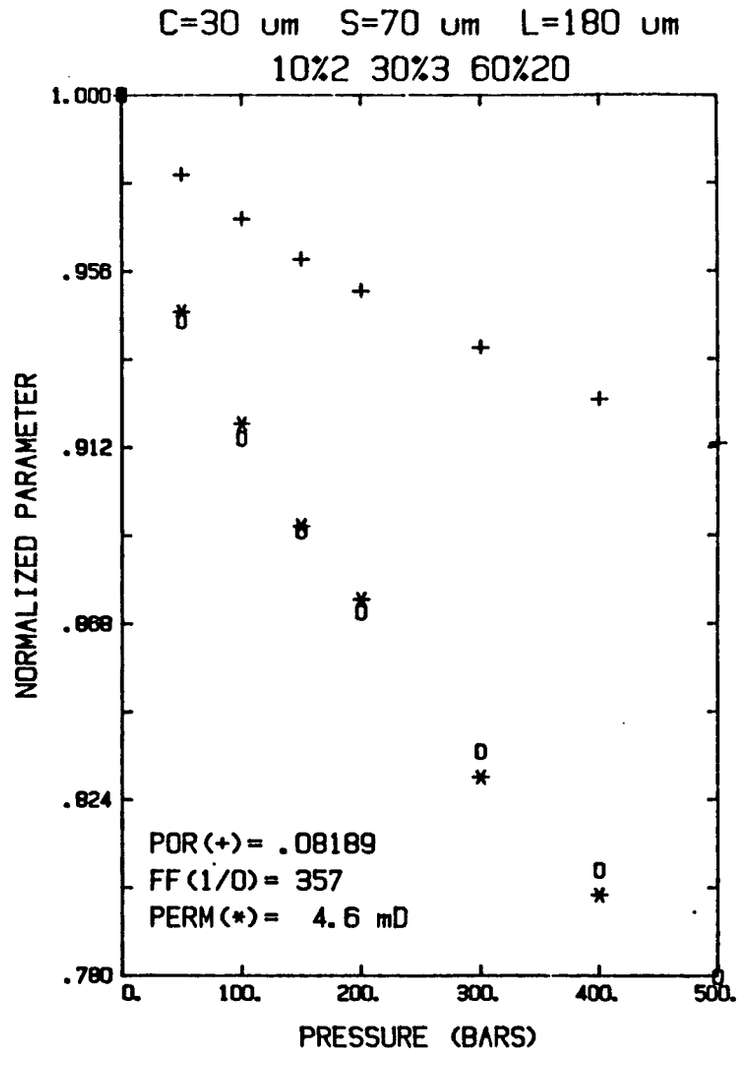

FIGURE 31B

Model simulation

G) Fahler 161 tight gas sandstone (Yale 1984)

The Fahler 161 experimental data is portrayed in figure 32a and falls into our "CL" category. The cross-over is very clear in the data and in the simulation in figure 32b. As with the Falher 189 simulation, the shapes of the permeability, conductivity and porosity versus pressure curves in this simulation are not as concave as the experimental data. We mentioned in chapter 2 that thin tapered pore shapes are used when very low aspect ratio shapes are needed (for large changes in petrophysical properties with pressure) because numerical problems make it impossible to calculate the deformation of GBP-RC30 to GBP-RC100 shaped pores. Figures 14a and 14b demonstrate that in general the GBP shaped pores show more concave permeability and conductivity versus pressure curves than the TAP tapered shaped pores. We suggest that a better fit to these curves can be done with very thin GBP shaped pores once we have improved our numerical calculations.

As in the Miocene 7 simulation, there are enough pores of high aspect ration (α=5E-3) to form a continuous path across the network yet there are a considerable number of pores of much smaller aspect ratios (50% of the pores have α=5E-4 and 1E-4). The hydraulic conductance of the TAPα5E-3 shaped pores is four orders of magnitude higher than the hydraulic conductance of TAPα1E-4 shaped pores and the α=5E-3 and α=2.5E-3 shapes therefore control the permeability. The electrical conductivity of the α=5E-4 pores is 10% that of α=5E-3 pores and figure 14b shows that pore tubes of these shapes yield changes in electrical conductance of 48% and 90% respectively at 500 bars confining pressure. The α=5E-4 and α=1E-4 contribute to a large portion of the electrical

conductance and "pull down" the conductivity versus pressure curve. A network of all TAPα5E-3 pores has a change in conductivity of 35% at 400 bars yet the thinner pores in the Fahler 161 simulation "pull down" the conductivity curve so that we see an 80% decrease in conductivity at 400 bars.

We note that the permeability of the Fahler 161 sample is lower yet the conductivity is higher (formation factor lower) than the Fahler 189 sample. The pore width in the Fahler 161 simulation is lower than c in the Fahler 189 simulation which explains the lower permeability yet this should lead to a higher formation factor also. The increased conductivity is due to the presence of the thin pores which contribute to electrical flow (to bring down the formation factor) but do not contribute to hydraulic flow.

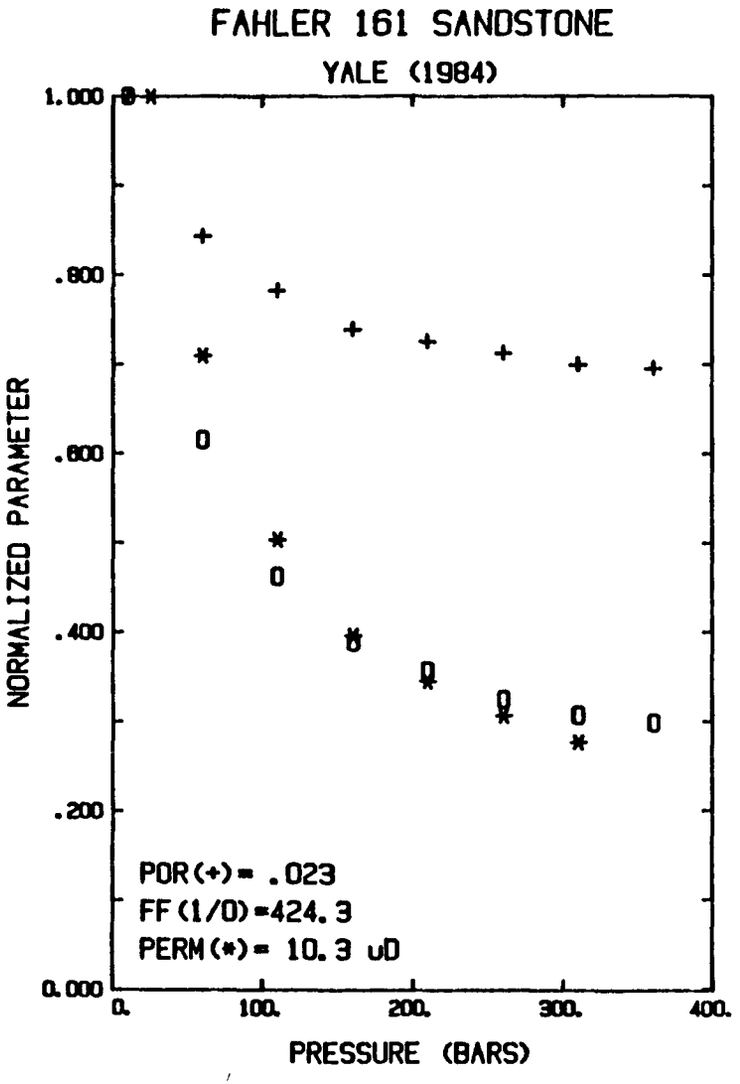

FIGURE 32A

Experimental data

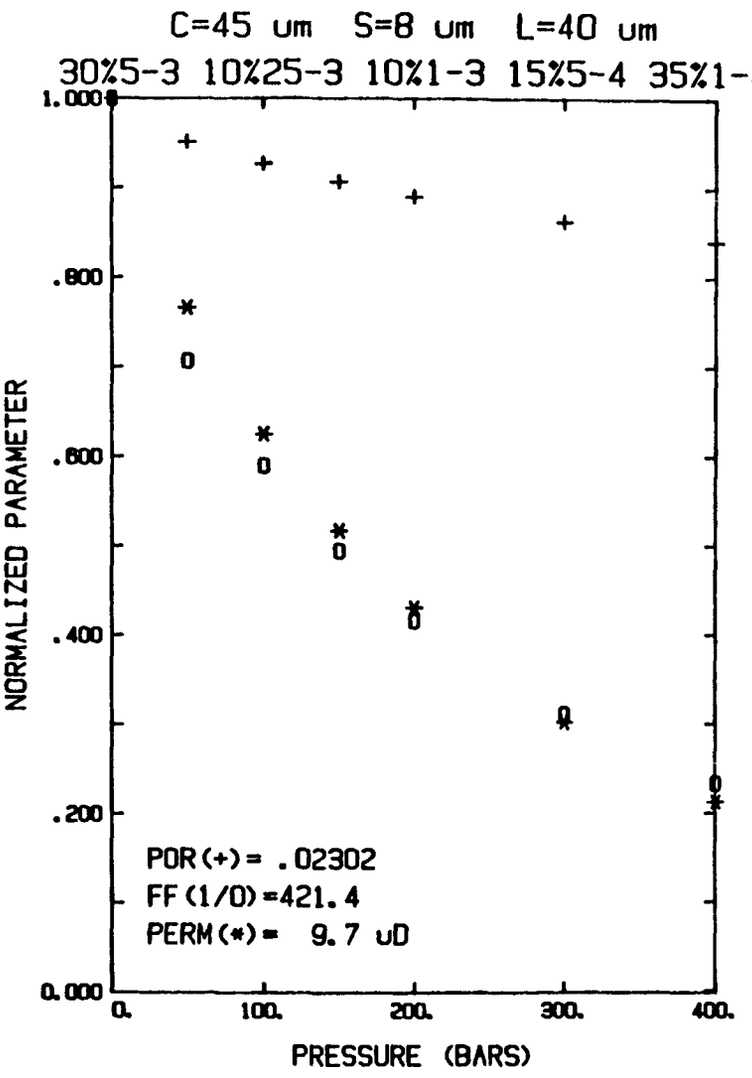

FIGURE 32B

Model simulation

H) Tertiary 807 sandstone (Yale 1984)

Figure 33a shows a sandstone in our "LH" group where the conductivity exhibits a larger decrease with pressure than the permeability. The Tertiary 807 simulation in figure 33b is an excellent match and the absolute values are within 1% of the experimental values (a three step simulation). A type 2 plot is shown in figure 34 for the experimental and simulated data.

A comparison of the Tertiary 807 simulation with the Triassic 27 simulation in figure 24b helps illustrate the effect of the different pore parameters used in the two simulations. In both simulations nearly half the pore tubes have GBP-RC1 shape and this is reflected in the very similar permeability versus pressure curves in the two plots. The pore length and nodal pore sizes are similar and the absolute values of formation factor and porosity are within 25%. The main difference is that half of the pores in the Triassic 27 simulation have RC4 shape and in the Tertiary 807 simulation they have RC15 shape. This difference is reflected in the 50% larger decrease in conductivity of the Tertiary 807 simulation as compared with the Triassic 27 simulation. Again the thin pores in the Tertiary 807 simulation contribute 15% to 20% to the overall electrical flow but nearly nothing to the hydraulic flow. Since the thin pores deform more with pressure than the pores of higher aspect ratio, the conductivity curve is "pulled down" by the thin pores. The conductivity change at 500 bars is 226% higher in the Tertiary 807 simulation than in a network of all RC2 pores. The higher permeability in the Tertiary 807 simulation is due to the small increase in pore width, c, over the Triassic 27 simulation.

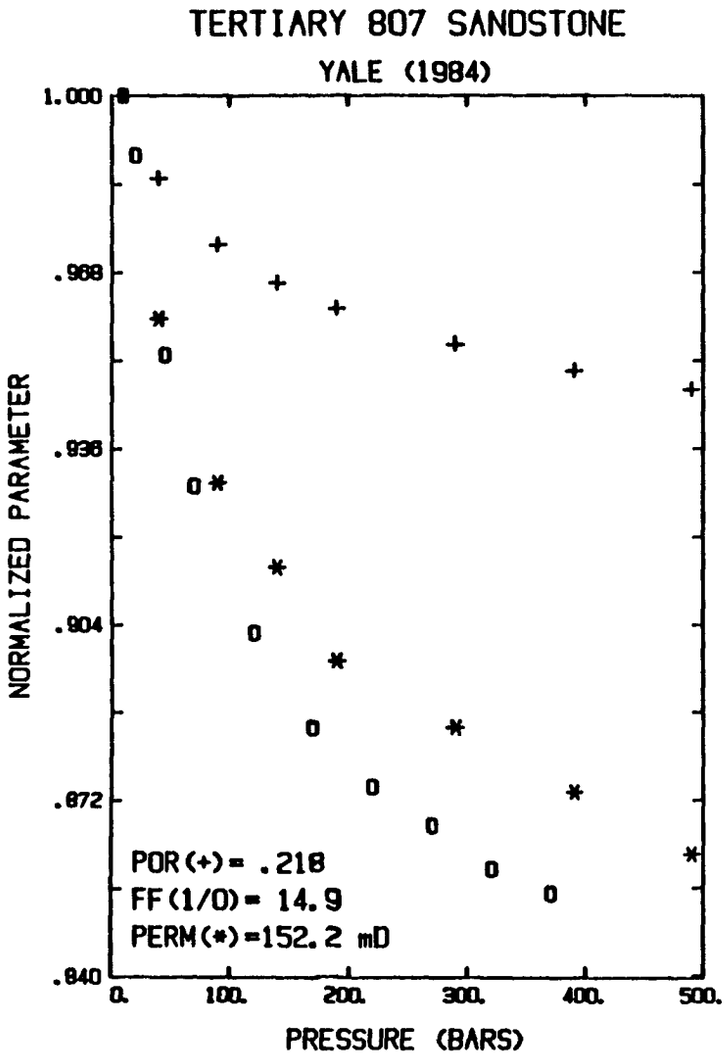

FIGURE 33A

Experimental data

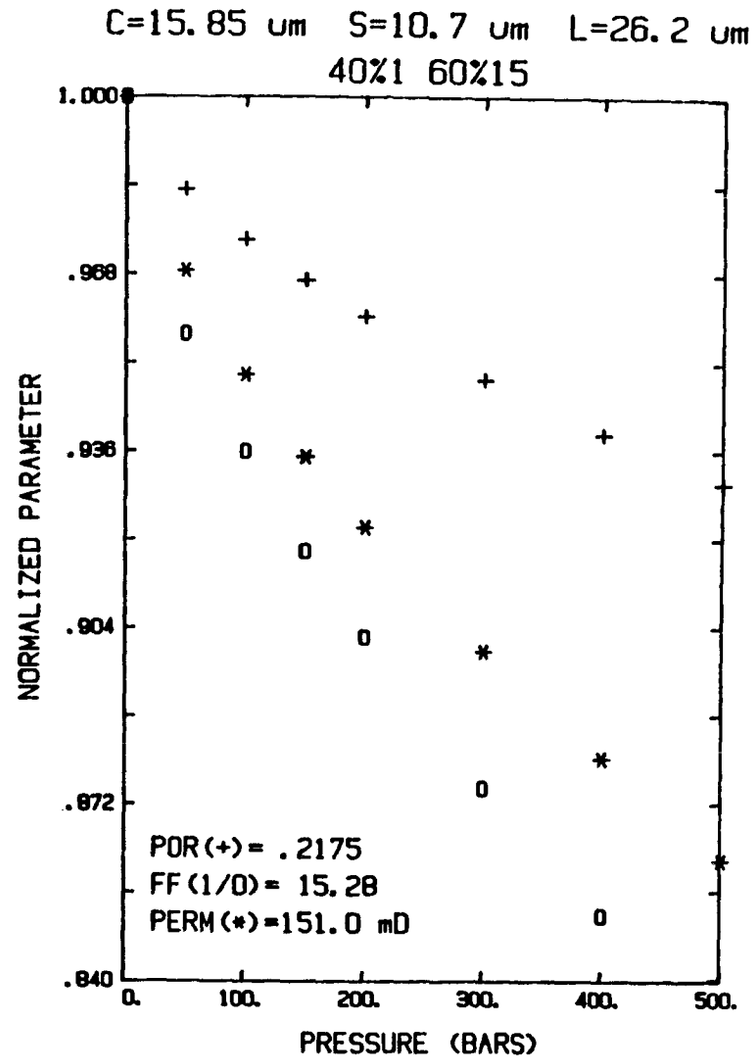

FIGURE 33B

Model simulation

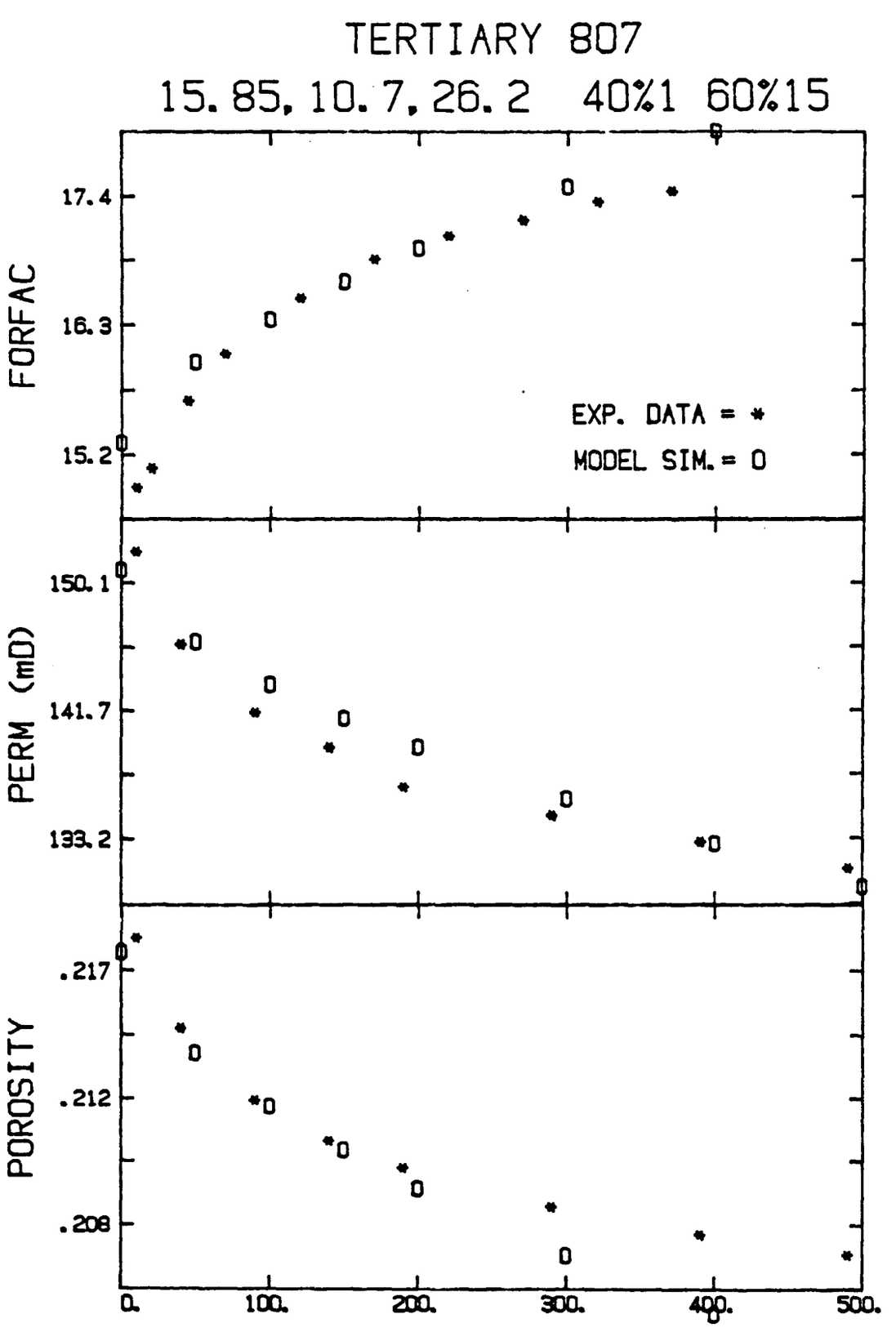

FIGURE 34

Comparison of experimental data (*) and model simulation (0) for Tertiary 807 sandstone (Yale 1984). Type 2 plot

I) Cambrian 6 sandstone (Chierici 1967)

Figures 35a and 35b show the plots for the Cambrian 6 experimental data and its simulation. As with the previous simulation, the conductivity decreases more with pressure than the permeability ("L" group) and we find the pore shapes again widely distributed between CIRCLE and RC20 shapes. The circular (10%CIR pores) and RC1 pores control the permeability (14% change over 500 bars) yet the very thin pores (RC15 and RC20) yield a decrease in conductivity which is even greater than in the Tertiary 807 simulation (19% versus 17% at 500 bars).

Although the pore width and pore shapes are similar the Tertiary 807 simulation, the larger pore length (60 um versus 26 um for the Cambrian 6 and Tertiary 807 simulations respectively) serves to increase the formation factor (80 versus 15), decrease the permeability (25 versus 150) and cut the porosity by nearly two-thirds (.217 versus .074) for the Cambrian 6 simulation.

These last two simulations show that as in the "S" and "C" groups, rocks in the "L" group have electrical flow paths that are different from the hydraulic flow paths. By comparing the differences in electrical and hydraulic conductances for the different pore shapes we can get a rough idea of what percent of the total electrical flow is through which set of pores. We are presently developing a flow analysis algorithm to allow us to analyze exactly how much fluid and electricity flows through each individual pore and how this relates to the overall flow through the network. The 1400 fold difference in hydraulic conductances for the RC1 and RC15 shaped pores (Tertiary 807 simulation) suggest that less than 0.1% of the hydraulic conductance should be along RC15 shaped

pores. Yet analysis of the differences between the Tertiary 807 simulation and a simulation of all RC1 shaped pores suggests that as much as 2% of the flow may be through RC15 shaped pores. For conductivity, differences in electrical conductances between RC1 and RC15 shaped pores suggests that 12% to 15% of the electrical conductance is via the RC15 shaped pores. Analysis of the conductivity versus pressure curves for the Tertiary 807 simulation and a simulation of all RC1 pores shows that as much as 50% of the electricity may have to pass through RC15 shaped pores. Without a doubt there is a decoupling between permeability and formation factor in rocks which exhibit the "L" group behavior.

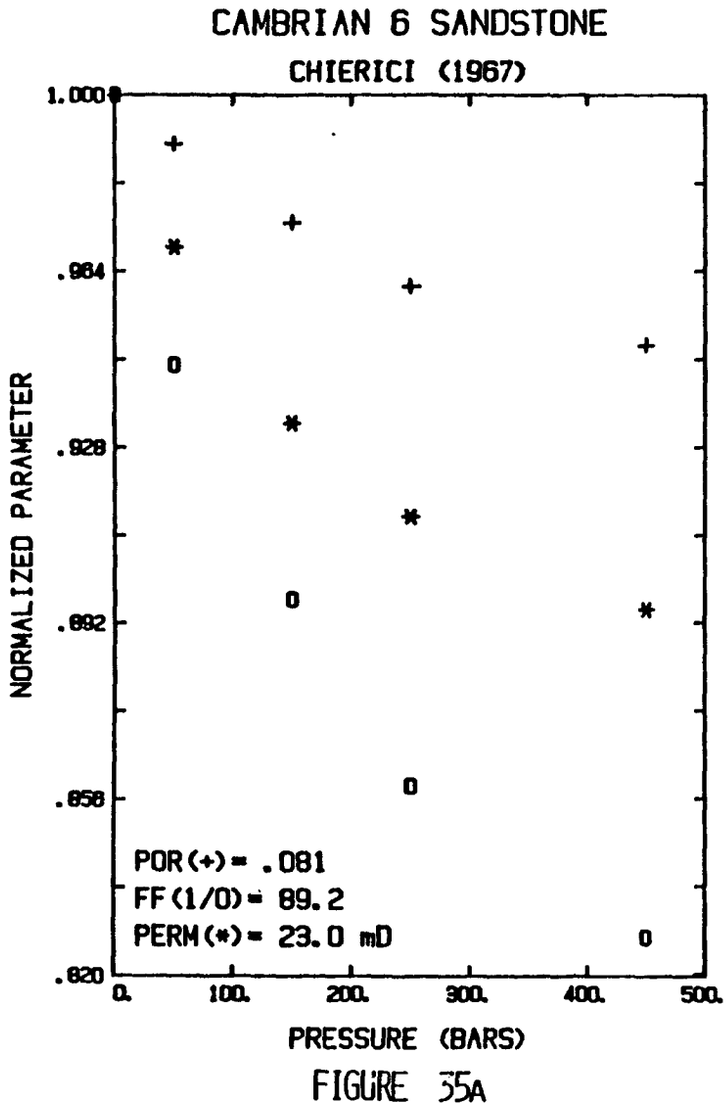

FIGURE 35A

Experimental data

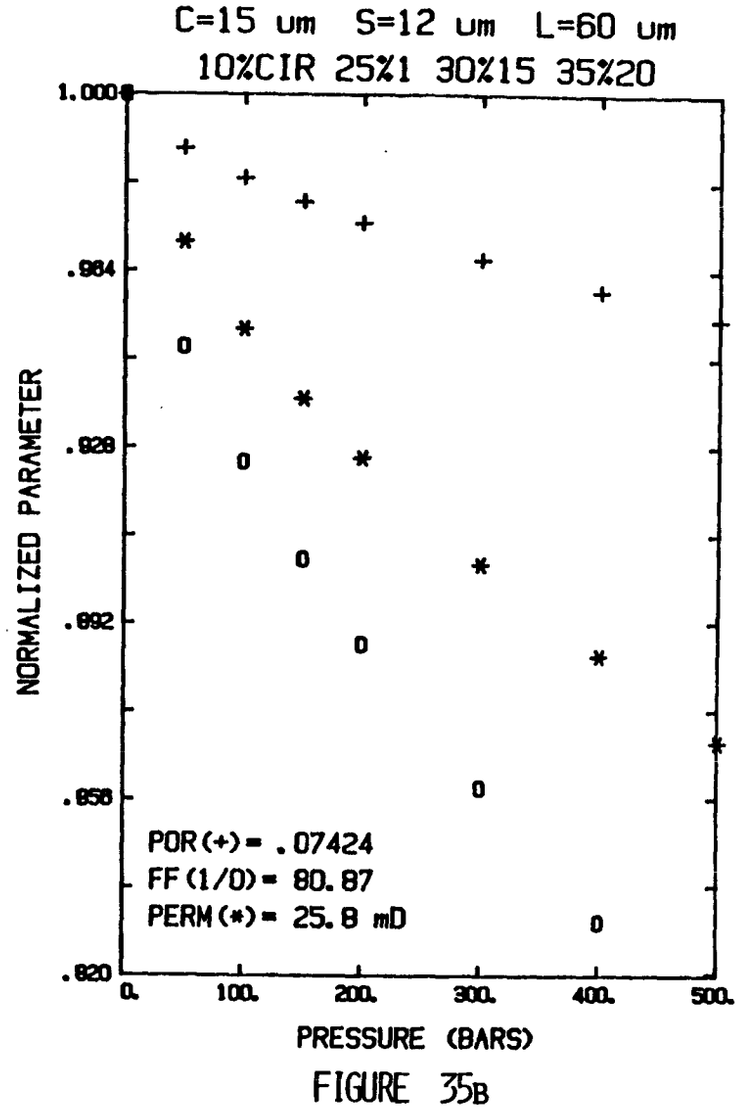

FIGURE 35B

Model simulation

CONCLUSIONS

We have developed in this paper a pore space network model which for the first time unifies six important petrophysical properties into one model. We have shown that the permeability, conductivity, porosity and their changes with confining pressure can be accurately simulated with a single set of pore space parameters. However, any model is only as useful as the information derived from it. We have found that the model advances our understanding of the relationships between petrophysical properties and between petrophysical properties and pore space parameters. Specifically we draw the following conclusions from our analysis of the network simulations.

Relationships between permeability and formation factor are tied to the similarity of hydraulic and electrical flow paths. In Table 4 we divided the experimental data into four groups depending on the relationship between the permeability versus pressure and conductivity versus pressure curves. Our simulations showed that rocks which fall into the "N" group have narrow and uniform distributions of pore shapes suggesting that the hydraulic and electrical flow paths are the same. However, rocks in the other three categories have either larger ("S" group) or thinner ("C" and "L" groups) pores which effect the conductivity without influencing the permeability as much.

Simulations of data sets from the "S", "C" and "L" groups have shown that between 10% and 25% of the current flowed through pores which conducted less than 0.5% of the fluid. One method of analysis (see Cambrian 6 simulation analysis) even suggests that upwards of 50% of the

current may pass through pores which conduct less than 2% of the fluid flow in rocks in the "L" group. This shows that because hydraulic conductance is so sensitive to the pore shape and width (see Table 3), it is controlled by a very narrow distribution of pore shapes; whereas, electrical conductivity is influenced by a wider distribution of pore shapes.

The group type is found to be dependent on the width of the pore shape distribution and the percent of the network occupied by certain pore shapes. The "N" group is characterized by pore shape distributions which are uniform and narrow (aspect ratios within the distribution vary less than +-50% of the mean). The "S" group simulations have a wider distribution of pore shapes with less than 25% of the pores having aspect ratios greater than the mean. The "C" group has distributions with widths similar to the "S" group but with more than 30% of the pores having aspect ratios greater than the mean. The simulations in the "L" group also have 30% or more of the pore aspect ratios higher than the mean but the distributions of pore shapes tend to be wider than in the "C" group. We saw that the behavior of the permeability and conductivity versus pressure curves is related to whether or not the percent of high aspect ratio pores is above the percolation threshold (25% for cubic lattices).

The pores which control the permeability in the "L" group tend to have high aspect ratios and high hydraulic conductances leading to the observed trend of high permeabilities among rocks in the "L" group (see Table 4). We also noted a slight correlation between lower than average permeability and rocks which fell into the "S" group. This is explained

by the effect of the lower aspect ratio pores on permeability in the "S" group rocks.

The permeability change with pressure is shown to be directly related to the aspect ratio of the controlling pore shapes. The thinner the pores the larger the change in permeability with pressure. The subgroups in Table 4 are characterized by pore shapes of aspect ratios greater than .25 for the "H" subgroup, between .05 and .25 for the "M" subgroup and aspect ratios less than .05 for simulations in the "L" subgroup. The three orders of magnitude change in hydraulic conductance for a one order of magnitude change in aspect ratio is responsible for the correlation between absolute value of permeability and pore shape aspect ratio. This in turn explains the correlation between absolute value of permeability and the change in permeability with pressure (see Figures 17 through 23).

The correlation between Archie's exponent and the percent nodal volume is shown in Table 6. Here the exponent, m, is calculated from the simulated values of porosity and conductivity at 10 bars pressure (referred to as absolute values). We see that when the fraction of the pore volume occupied by the nodal pores is high the exponent m is large. This suggests that Archie's exponent is a measure of the decoupling between porosity and formation factor and that a large exponent ($m > 2$) means that most of the pore volume is in pores which do not contribute much to the resistance of the sample. The large resistance of pore tubes as compared to nodal pores and the decoupling of porosity and formation factor was first recognized by Owen (1952).

TABLE 6

Relationship between volume of nodal pores and Archies exponent, m

Rock name	volume in nodes	m
Cambrian 6	36%	1.69
Gulf 807	40%	1.79
Triassic 27	50%	1.75
Fahler 161	60%	1.60
Fahler 189	70%	1.67
Massillon DV	75%	2.00
Miocene 7	81%	2.35
Pliocene 35	97%	2.95
Triassic 41	99%	3.03

Note : volume in nodes is the fraction of the total pore volume that resides in the nodal pores. Rest of pore volume resides in pore tubes. m=Archies exponent for simulated data with m = log (CF)/log (porosity)

Problems with the match between simulations and experiment yields information of possible improvements to the model. The shape of the permeability versus pressure and conductivity versus pressure curves for the Fahler simulations are more linear than the experimental curves suggesting that the thin GBP shaped pores should be used.

The Pliocene 35 and Triassic 41 simulations have very large nodal pore sizes which account for over 90% of the pore volume in these two simulations. Because we normally assume the nodal pores to be spherical these large nodal pores reduce the change in porosity with pressure to less than 1% at 500 bars. Because both the experimental data sets show nearly 8% porosity change at 500 bars we assumed a more compliant nodal pore for these two simulations which matches the experimental data quite well (compliance between that of spherical pore and true sphere pack). The smaller change in simulated porosities than experiments for the Fahler samples suggests that the more compliant nodal pores should also be used here. In order to avoid adding another variable (nodal pore shape), it might be better to use a more compliant shape for all the simulations but then the exact hydraulic and electrical conductances for the new node shape must be solved.

Another problem we have encountered is the very small changes in conductivity with pressure in some rocks above 300 or 400 bars confining pressure. The Fahler 189, Massillon DV, and Pliocene 35 simulations all failed to correctly reproduce the conductivity change between 350 and 500 bars. In the Torpedo sandstone there is very little change in conductivity between 450 and 950 bars (see Appendix C). Success in simulating this behavior may yield additional information about the pore space.

Significance of a Unified Petrophysical Model

The results from any simplified model are model dependent. The aspect ratio spectrum Cheng and Toksoz (1979) calculated with elliptical pores is different from the spectrum calculated using Mavko and Nur's tapered pores for the same rock which is different still from a spectrum calculated using our GBP shaped pores. Mendoza (personal communication) has found that for several sandstones the aspect ratio to match Vp and bulk modulus versus pressure spans less than one order of magnitude in aspect ratio compared to over 4 orders of magnitude spread in Cheng and Toksoz's (1979) spectra for similar rocks. The more realistic the model, the more unique and less model dependent the results should be.

The pore size distributions calculated from mercury injection or capillary displacement porosity are dependent on the assumption that all the pores are tubes of circular cross-section with the capillary pressure linearly dependent on pore width. A thin GBP or tapered shaped pore tube has a much higher capillary pressure than a cylindrical pore tube of the same width. Therefore a distribution of capillary pressure can be translated into a distribution of pore radii using pore tubes of circular cross-section or a distribution of aspect ratios using GBP shaped pores of the same width.

It has recently been suggested that nuclear magnetic resonance may yield the pore size distribution of a rock (Schmidt, personal communication). A distribution of surface area to volume ratios (SA/V) of pores may be translated to a pore radii distribution using either spherical or cylindrical pore tubes. Again the SA/V ratio is linearly related to the

pore radius. However, our calculations show that for constant width pore tubes of GBP, elliptical or tapered shape, the SA/V ratio is linearly dependent upon aspect ratio.

A problem with our present model is the lack of enough petrophysical data to fix the distribution of pore sizes. However, by combining the pore size distribution calculated from mercury injection or NMR measurements with the pore shape distribution from our model, we can eliminate the distribution of capillary pressure or SA/V ratios due to aspect ratio to yield a more realistic pore size distribution. In this way we can remove some of the model dependence of the results as well as erasing the dichotomy of pore shape and pore size that plagues most pore space models.

Just as the addition of realistic pore shapes help unify transport and elastic models in our network model, the addition of other petrophysical properties should help bring the model pore space closer to the true pore space of rocks. The network model is not in and of itself a unified pore space model but simply a framework from which to build a unified model. We have shown that the interconnectedness of the network lattice is important for calculating transport properties and that pore shape is very important in calculating elastic properties. Pore size is probably more important in simulating capillary pressure and SA/V ratio and Knight (1984) has recently suggested that pore geometry and coordination number may be influential in explaining the frequency dependent dielectric constant.

By combining all these petrophysical properties into a single model we hope to gain an even greater understanding of the pore space than we

have done here. The question is whether more properties necessitate more variables. To make the model predictive we must keep the number of variables to less than the number of properties we are simulating. However, as we have already seen, different properties are influenced by different portions of the pore space. Porosity is strongly controlled by the nodal pores which have a second order effect on permeability and conductivity. Simulations of experimental data have shown that in rocks with a wide distribution of pore shapes (or sizes), conductivity is influenced by a much larger range of pore shapes than permeability. The linear dependence of capillary pressure and SA/V ratio on pore radius (or pore aspect ratio) suggests that capillary pressure and SA/V ratio are influenced by an even wider spectrum of pore sizes and shapes. Simulations by Mendoza (personal communication) using the GBP shaped pore tubes, have shown that velocity is influenced in some rocks by thinner pores than are needed to match permeability, conductivity and porosity versus pressure curves.

However, just as we showed that experimental data sets in the "N" group had similar hydraulic and electrical flow paths and that rocks with low Archie's exponents had strong correlations between formation factor and porosity, Mendoza has found that the pore shape distributions used to fit Vp and bulk modulus versus pressure are very close to our pore shape distributions (to fit permeability, conductivity and porosity versus pressure) for a few rocks. It is only by simulating all the petrophysical properties in a single model that we can understand what the relationships are between the petrophsical properties and when they apply.

REFERENCES

Archie,G.E., The Electrical Resistivity Log as an Aid in Determining Some Reservoir Characteristics, Trans. AIME, vol. 146, p. 54, 1942

Atkinson,K.E., An Introduction to Numerical Analysis, John-Wiley and Sons, New York, 1978

Berg,G.A., Deformation of Fine Cracks Under High Pressure and Shear, J. Geophys. Res., vol. 70, p. 3447, 1965

Biot,M.A., General Theory of Three-Dimensional Consolidation, J. Appl. Phys., vol. 12, p. 155, 1941

Birch,F., Compressibility; Elastic Constants, in Handbook of Physical Constants, ed. S.B.Clark, Geol. Soc. Am. Memoir 97, 1966

Bird,R.B., W.E.Stewart, and E.N.Lightfoot, Transport Phenomena, John Wiley ² Sons,Inc., New York, 1960

Bowker, A.H. and G.J.Lieberman, Engineering Statistics, Prentice-Hall, Inc., New Jersey, 1972

Brace,W.F., Permeability from Resistivity and Pore Shape, J. Geophys. Res., vol. 82, p. 3343, 1977

Brace,W.F. and A.S.Orange, Further Studies of the Effects of Pressure on Electrical Resistivity of Rocks, J. Geophys. Res., vol. 73, p. 5407, 1968

Brace,W.F., A.S.Orange and T.R.Madden, The Effect of Pressure on the Electrical Resistivity of Water Saturated Crystalline Rocks, J. Geophys. Res., vol. 77, p. 5669, 1965

Bruner,W.M., Comment on 'Seismic Velocities in Dry and Saturated Cracked Solids' by Richard J. O'Connell and Bernard Budiansky, J. Geophys. Res., vol. 81, p. 2573, 1976

Burdine,N.T., Relative Permeability Calculations from Pore Size Distribution Data, Trans. AIME, vol. 198, p. 71, 1953

Burdine,N.T., L.S.Gournay and P.P.Reichertz, Pore Size Distribution of Petroleum Reservoir Rocks, Trans. AIME, vol. 189, p. 195, 1950

Byrnes,A.P., K.Sampath and P.L.Randolph, Effect of Pressure and Water Saturation on Permeability of Western Tight Sandstones, 1979 DOE Symposium on Enhanced Oil and Gas Recovery and Improved Drilling Technology 1979

Carmen,P.C., Fluid Flow Trough Granular Beds, Trans.Inst.Chem.Eng.

London, vol. 15, p. 150, 1937

Chandler,R., J.Koplik, K.Lerman and J.F.Willensen, Capillary Displacement and Percolation in Porous Media, Schlumberger-Doll preprint, 1981

Chatzis,I. and F.A.L.Dullien, Modelling Pore Structure by 2-D and 3-D Networks with Application to Sandstones, J. Cand. Pet. Tech., vol. 16, p. 97, 1977

Cheng,C.H. and M.N.Toksoz, Inversion of Seismic Velocities for the Pore Aspect Ratio Spectrum of a Rock, J. Geophys. Res., vol. 84, p. 7533, 1979

Chierici,G.L., G.M.Ciucci, F.Eva and G.Long, Effect of the Overburden Pressure on Some Petrophysical Parameters of Reservoir Rocks, Proc. of the 7th World Petroleum Congress, vol. 2, p. 309, 1967

Cleary, M.P., I.W. Chen, and S.H. Lee, Self-consistent Techniques for Heterogeneous Media, J. Eng. Mech. Div., Proc. ASCE, p.861, Oct. 1980

Dahlquist,G. and A.Bjorck, Numerical Methods, Prentice-Hall, New Jersey, 1974

Dengler,L., Pore Structure and Permeability in a Graywacke Sandstone, Stanford Rock Physics report, vol. 5, p. 219, 1978

Delaney,P.T., Magma Flow, Heat Transport and Brecciation, Ph.D. thesis, Stanford University, 1980

Dobrynin,V.M., Effect of Overburden Pressure on Some Properties of Sandstones, Soc. Pet. Eng. J., vol. 2, p. 360, 1963

Dodd,C.G. and O.G.Kiel, Evaluation of Monte Carlo Methods in Studying Fluid-Fluid Displacement and Wettability in Porous Rocks, J.Phys. Chem, vol. 63, p. 1646, 1959

Dodds,J.A. and P.S.Lloyd, A Model for the Void Structure in Multi-Component Sphere Packs Applied to Capillary Pressure Curves, Powder Tech., vol. 5, p. 69, 1971/72

Duffy,J. and R.D.Mindlin, Stress-strain relations of a granular medium, J. Appl. Mech. ASME, vol. 24, p. 585, 1957

Dullien,F.A.L., New Network Permeability Model of Porous Media, AIChE J., vol. 21, p. 299, 1975a

Dullien,F.A.L., Prediction of 'Tortuosity Factors' from Pore Structure Data, AIChE J., vol. 21, p. 820, 1975b

Dullien,F.A.L., Porous Media: Fluid Transport and Pore Structure, Academic Press, New York, 1979

Dullien,F.A.L., I.Chatizis and M.S.El-Sayed, Modelling Transport Phenomena in Porous Media by Networks Consisting of Non-Uniform Capillaries, Soc. Pet. Eng. paper 6191, 1976

Dullien,F.A.L. and G.K.Dhawan, Characterization of Pore Structure by a Combination of Qualitative Photomicrography and Mercury Porosimetry, J. Coll. Interfac. Sci., vol. 47, p. 337, 1974

Dullien,F.A.L. and G.K.Dhawan, Bivariate Pore-Size Distributions of Some Sandstones, J. Coll. Interfac. Sci., vol. 52, p. 129, 1975

Eshelby,J.D., The Determination of the Elastic Field of an Ellipsoidal Inclusion and Related Problems, Proc. Roy. Soc. London, vol. 241, p. 376, 1957

Fatt,I., The Effect of Overburden Pressure on Relative Permeability, Trans. AIME, vol. 198, p.325, 1953

Fatt,I., The Network Model of Porous Media: I. Capillary Pressure Characteristics, Trans. AIME, vol. 207, p. 144, 1956a

Fatt,I., The Network Model of Porous Media: II. Dynamic Properties of Single Size Tube Network, Trans. AIME, vol. 207, p. 160, 1956b

Fatt,I., The Network Model of Porous Media: III. Dynamic Properties of Networks with Tube Radius Distribution, Trans. AIME, vol. 207, p. 164, 1956c

Fatt,I., Effect of Overburden and Reservoir Pressure on Electrical Logging Formation Factor, Bull. AAPG, vol. 41, p. 2456, 1957

Fatt,I., Pore Structure in Sandstones by Compressible Sphere-Pack Models, Bull. AAPG, vol. 42, p. 1914, 1958a

Fatt,I., Compressibility of Sandstones at Low to Moderate Pressures, Bull. AAPG, vol. 42, p. 1924, 1958b

Fatt,I., Pore Volume Compressibilities of Sandstone Reservoir Rocks, Trans. AIME, vol. 213, p. 362, 1958c

Fatt,I. and D.H.Davis, Reduction in Permeability with Overburden Pressure, Trans. AIME, vol. 195, p. 329, 1952

Ferrell,H.H., M.Felsenthel and J.W.Wolfe,Jr., Effect of Overburden Pressure on Flow Capacity in a Deep Oil Reservoir, J. Pet. Tech., vol. 14, p. 962, 1962

Forsythe,G.F. and C.B.Moler, Computer Solutions of Linear Algebraic Systems, Prentice-Hall, New Jersey, 1967

Gassman,F., Uber die Elastizitat Poroser Medien, Mitteilungen aus dem Institut fur Geophysik, vol. 17, p. 1, 1951

Geertsma,J., The Effect of Fluid Pressure Decline on Volumetric Changes

of Porous Rocks, Trans. AIME, vol. 210, p. 331, 1957

Goodier,J.N., Concentration of Stress around Spherical Inclusions and Flaws, Trans. Am. Soc. Mech. Engrs., vol. 55, p. 39, 1933

Gray,D.H., I.Fatt and G.Bergamini, The Effect of Stress on Permeability of Sandstone Cores, Trans. AIME, vol. 228, p. 95, 1963

Greenberg,R.J. and W.F.Brace, Archie's Law for Rocks Modeled by Simple Networks, J. Geophys. Res., vol. 74, p. 2099, 1969

Hadley,K., Comparison of calculated and observed crack densities and seismic velocities in Westerly granite, J. Geophys. Res., vol. 81, p. 3484, 1976

Han, Teh-Hua, personal comm., Dept. of Geophysics, Stanford Univ.

Handin,J., R.V.Hager, M.Friedman and J.N.Feather, Experimental Deformation of Sedimentary Rocks Under Confining Presure: Pore Pressure Tests, Bull. AAPG, vol. 47, p. 717, 1963

Haring,R.E. and R.A.Greenkorn, A Statistical Model of a Porous Medium with Nonuniform Pores, AIChE J., vol. 16, p. 477, 1970

Harris,C.C., Latin Square as a Network Model of Random Packing, Nature, vol. 205, p. 353, 1965

Hertz, H., J. Math (Crelle's J.), vol. 92, 1881

Iczkowski,R.P., Electrical Conductivity of Partially Saturated Porous Solids, Ind. Eng. Chem. Fundam., vol. 9, p. 674, 1970

Jaeger,J.C. and N.G.W.Cook, Fundamentals of Rock Mechanics, Chapman and Hall, London, 1976

Jennings,J.B., H.B.Carrol and C.J.Raible, The Relationship of Permeability to Confining Pressure in Low Permeability Rocks, SPE/DOE Low Permeability Symposium, 1981

Jones,F.O., W.W.Owens, A Laboratory Study of Low Permeability Gas Sands, 1979 SPE Symposium on Low Permeability Gas Reservoirs, 1979

Jones,T.D., Some Compressional and Shear Velocities in Berea, Massilon, and St. Peter Sandstone, Stanford Rock Physics report, vol. 5, p. 165, 1978

Kirkpatrick,S., Percolation and Conduction, Rev. Mod. Phys., vol. 45, p. 574, 1973

Knight,R.J., The Dielectric Constant of Sedimentary Rocks - 5 Hz to 13 MHz, Ph.D. thesis, Stanford University, 1984

Koplik,J., On Effective Medium Theory of Random Linear Networks, Schlumberger-Doll preprint, 1981a

Koplik,J., Creeping Flow in Two-Dimensional Networks, Schlumberger-Doll preprint, 1981b

Koplik,J., Note on the Permeability of Random Networks, Schlumberger-Doll preprint, 1982

Korringa,J., R.J.S.Brown, D.D.Thompson and R.J.Runge, Self-Consistent Imbedding and the Ellipsoidal Model for Porous Rocks, J. Geophys. Res., vol. 84, p. 5591 1979

Kozeny,J., Royal Academy of Science, Vienna, Proc. Class I, vol. 136, p. 271, 1927

Ksenzhek,O.S., Capillary Equilibrium in Porous Media with Intersecting Pores, Russ. J. Phys. Chem., vol. 37, p. 691, 1963

Lobkowicz,F. and A.C.Melissinos, Physics for Scientists and Engineers, Vol. 2, W.B. Saunders Co., Philadelphia, 1975

Lamb,H., Hydrodynamics, Dover Publications, New York, 1932

Larson,R.G., L.E.Scriven and H.T.Davies, Percolation Theory of Residual Phases in Porous Media, Nature, vol. 268, p. 409, 1977

Lin,C.Y. and J.C.Slattery, Three-Dimensional, Randomized, Network Model for Two-Phase Flow through Porous Media, 2nd Joint SPE/DOE Enhanced Oil Recovery Symp., 1981

Madden,T.R., Random Networks and Mixing Laws, Geophysics, vol. 41, p. 1104, 1976

Madden,T.R., Microcrack Connectivity in Rocks: A Renormalization Group Approach to the Critical Phenomena in Crystaline Rocks, J. Geophys. Res., vol. 88, p. 585, 1983

Mavko,G.M. and A.Nur, The Effect of Non-Elliptical Cracks on the Compressibility of Rocks, J. Geophys. Res., 83, 4459, 1978

Mclatchie,A.S., R.A.Hemstock and J.W.Young, The Effective Compressibility of Reservoir Rock and its Effects on Permeability, Trans. AIME, vol. 213, p. 386, 1958

Mellossinos,A.C. and F.Lobkowicz, Physics for Scientists and Engineers Vol.1, W.B.Saunders, Philadelphia, 1975

Mendoza, Jorge, personal comm., Dept. of Geophysics, Stanford Univ.

Mohanty,K.K., H.T.Davies and L.E.Scriven, Physics of Oil Entrapment in Water-Wet Rock, SPE paper 9406, 1980

Morgan,F.D., Capillary Models of Permeability, Stanford Rock Physics report, vol. 22, p. 264, 1984

Murphy,W.F. III, Effects of Microstructure and Pore Fluids on the Acoustic Properties of Granular Materials, Ph.D. thesis Stanford University, 1982

Muskhelishvili,D., Some Basic Problems of the Mathematical Theory of Elasticity, 4th ed., trans. JRM Rodok Groningen, Noordhoff, 1953

New Mexico Institute of Mining and Technology, Three-Dimensional Network Analysis of Interconnected Circular and Slit-Shaped Pores, progress report, 1982

Nicholson,D. and J.H.Petropoulos, Capillary Models for Porous Media: III. Two-phase flow in a three-dimensional network with Gaussian radius distribution, J.Phys. D: Appl.Phys., vol. 4, p. 181, 1971

Nobles,M.A. and H.B.Janzen, Application of a Resistance Network for Studying Mobility Ratio Effects, Trans. AIME, vol. 213, p. 356, 1958

Nur,A., Pore Space Models and the Effects of Pressure on the Relation between Physical Properties, Stanford Rock Physics report, vol. 7, p. 125, 1979

Nur,A., An Exact Effective Stress Law for Elastic Deformation of Rock with Fluids, J. Geophys. Res., vol. 76, p. 6414, 1971

O'Connel,R.J. and B.Budiansky, Seismic Velocities in Dry and Saturated Cracked Solids, J. Geophys. Res., vol. 79, p. 5412, 1974

Owen,J.E., The Resistivity of a Fluid-Filled Porous Body, Trans. AIME, vol. 195, p. 169, 1952

Payatakes,A.C., Dynamic of Oil Ganglia During Immiscible Displacement in Water-Wet Porous Media, Ann. Rev. Fluid Mech., vol. 14, p. 365, 1982

Peikari,B., Fundamentals of Network Analysis and Synthesis, Prentice-Hall, New Jersey, 1974

Pollard,D.D., Equations for Stress and Displacement Fields Around Pressurized Elliptical Holes in Elastic Solids, Math. Geol., vol. 5, p. 11, 1973

Rink,M. and J.R.Schopper, Computations of Network Models of Porous Media, Geophys. Prosp., vol. 16, p. 277, 1968

Rose,W., Studies of Waterflood Performance III. Use of Network Models, Ill. State Geol. Surv. Circ., vol. 237, p. 1, 1957

Schopper,J.R., A Theoretical Investigation on the Formation Factor/ Permeability/ Porosity Relationship Using a Network Model, Geophys. Prosp., vol. 14, p. 301, 1966

Seeburger,D., Fluid Flow through Elliptic and Simple Nonelliptic

Fractures, Stanford Rock Physics report, vol. 7, p. 104, 1979

Seeburger,D., A Pore Space Model for Rock Permeability and Bulk Modulus, J. Geophys. Res., vol. 89, p.527, 1984

Shankland,T.J. and H.S.Waff, Conductivity in Fluid-Bearing Rocks, J. Geophys. Res., vol. 79, p. 4863, 1974

Shante,V.K.S. and S.Kirkpatrick, An Introduction to Percolation Theory, Advan. Phys., vol. 20, p. 325, 1971

Schmidt, Ehud, personal comm., Dept. of Geophysics, Stanford Univ.

Simon,R. and F.J.Kelsey, The Use of Capillary Tube Networks in Reservoir Performance Studies: I. Equal Viscosity Miscible Displacements, Soc. Pet. Eng. J., vol. 11, p. 99, 1971

Simon,R. and F.J.Kelsey, The Use of Capillary Tube Networks in Reservoir Performance Studies: II. Effect of Heterogeneity and Mobility on Miscible Displacement Efficiency, Soc. Pet. Eng. J., vol. 12, p. 345, 1972

Singhal,A.K. and W.H.Somerton, Quantitative Modelling of Immiscible Displacement in Porous Media: A Network Approach, Rev. Inst. Franc. Pet., vol. 32, p. 897, 1977

Snyder,L.S. and W.E.Stewart, Velocity and Pressure Profiles for Newtonian Creeping Flow in Regular Packed Beds of Spheres, AIChE J., vol. 12, p. 167, 1966

Sorensen,J.P. and W.E. Stewart, Computation and Forced Convection in Slow Flow through Ducts and Packed Beds - II. Velocty Profile in a Simple Cubic Array of Spheres, Chem. Eng. Sci., vol. 29, p. 819, 1974

Strang,G., Linear Algebra and Its Applications, Acedemic Press, New York, 1976

Timoshenko,S.P. and J.N.Goodier, Theory of Elasticity, McGraw-Hill, New York, 1970

Van Brakel,J., Pore Space Models for Transport Phenomena in Porous Media Review and Evaluation with Special Emphasis on Capillary Liquid Transport, Pow. Tech., vol. 11, p. 205, 1975

Walls,J., Effects of Pore Pressure, Confining Pressure and Partial Saturation of the Permeability of Sandstones, Ph.D. thesis, Stanford University, 1982

Walls,J., Permeability Measurements on Some Selected Sandstone Samples, Stanford Rock Physics report, vol. 7, p. 57, 1979

Walls,J. and A.Nur, Pore Pressure and Confining Pressure Dependence of Permeability in Sandstone, 7th Formation Evaluation Symposium, Cand.

Well Log. Soc., 1979

Walls,J., A.Nur, and T.Bourbie, Pulse Decay Permeability: Analytical Solution and Experimental Test, Soc. Pet. Eng. J., October 1982

Walsh,J.B., The Effect of Cracks on the Compressibility of Rock, J. Geophys. Res., vol. 70, p. 381, 1965a

Walsh,J.B., The Effect of Cracks on the Uniaxial Elastic Compression of Rocks, J. Geophys. Res., vol. 70, p. 399, 1965b

Walsh,J.B., New Analysis of Attenuation in Partially Melted Rock, J. Geophys. Res., vol. 74, p. 4333, 1969

Watt,J.P., G.F.Davis and R.J.O'Connel, The Elastic Properties of Composite Materials, Rev. Geophys. Sp. Phys., vol. 14, p. 541, 1976

Wienbrandt,R.M. and I.Fatt, A Scanning Electron Microscope Study of the Pore Structure of Sandstone, J. Pet. Tech., vol. 21, p. 543, 1969

Wilhelmi,B. and W.H.Somerton, Simultaneous Measurement of Pore and Elastic Properties of Rocks Under Triaxial Stress Conditions, Trans. AIME, vol. 240, p. 283, 1967

Willenson,J.F., Percolation Theory and Capillary-Dominated Flow in 3-D, Schlumberger-Doll preprint, 1981

Winsauer,W.O., H.MShearin,Jr., P.H.Masson and M.Williams, Resistivity of Brine-Saturated Sands in Relation to Pore Geometry, Bull. AAPG, vol. 36, p. 253, 1952

Wu,T.T., The Effect of Inclusion Shape on the Elastic Moduli of a Two-Phase Material, Int.J.Solids Struc., vol. 3, p. 1, 1966

Wyble,D.O., Effect of Applied Pressure on the Conductivity, Porosity, and Permeability of Sandstones, Trans. AIME, vol. 213, p. 430, 1958

Wyllie,M.R.J., A.R.Gregory and G.H.F.Gardner, An Experimental Investigation of Factors Affecting Elastic Wave Velocities in Porous Media, Geophysics, vol. 23, p. 459, 1958

Wyllie,M.R.J. and M.B.Spangler, Application of Electrical Resistivity Measurements to Problem of Fluid Flow in Porous Media, Bull. AAPG, vol. 36, p. 359, 1952

Yale,D.P.,Elastic Moduli and Mircrocrack Anisotropy in Milford, N.H. Granite, B.S. Thesis, Yale University, 1980

Yale,D.P., Network Modelling of Flow and Deformation in Porous Rocks, Bull. Am. Phys. Soc, vol.28, p.1317, 1983

Yale,D.P., Network Modelling of Flow, Storage and Deformation

in Porous Rocks, Ph.D. Thesis, Stanford University, 1984a

Yale,D.P., Pore Space Network Modelling of Transport and Elastic Properties of Porous Sedimentary Rocks - Part I Theory, Stanford Rock Physics report, vol. 22, p. 219, 1984b

Yale,L.B., Stanford Rock Physics Rock Catalog, vol. 1, 1984a

Yale,L.B., Stanford Rock Physics Rock Catalog, vol. 2, 1984b

Young,D.M., Iterative Solution of Large Linear Systems, Academic Press, New York, 1971

Yuan, H.H., The Influence of Pore Coordination on Petrophysical Properites, SPE paper 10074, 1981

Zoback,M.D., High Pressure Deformation and Fluid Flow in Sandstone, Granite and Granular Material, Ph.D. thesis, Stanford University, 1975

APPENDIX B

Petrographic Information for Rock Samples Measured In This Study

The petrographic description of the 14 samples in Table 4 whose source is "Yale (1984)" (this study) is listed in the following appendix. This information was given to us by Leslie Yale and is from the SRP Rock Catalog, volumes 1 and 2. Further information about these rocks can be found in those volumes. Some small differences exist between our and L. Yale's sample names as follows:

This study	Appendix B
Berea 500	Berea 5-600
Fahler 142	Fahler 18E142
Tertiary 807	Gulf Coast sandstone 14807
Indiana DV	Indiana dark
Massillon DV	Massillon sandstone dark
Massillon DH	Massillon sandstone dark

Our two Massillon samples were taken perpendicular to "DV" and parallel to "DH" the bedding planes of the rock. With the exception of the Indiana DV (taken perpendicular) and Berea 100H (taken parallel), all other cores showed no distinct bedding.

ROCKNAME Beaver sandstone

Descript: QUARTZARENITE--fine to medium grained, well sorted, moderate porosity cemented by quartz overgrowth

Framework Grains

Quartz	78%
Chert	0%
Feldspar	tr.
Carbonate	0%
Lithics	1%
Opaques	0%
Other	

Contacts: long > cc >> sut = tan

Cement/: quartz overgrowth--16% clay--very fine grained rims on original
Matrix quartz grains--trace

Alter-: none apparent
ation

Pore interparticle--void space largely filled with quartz overgrowths--5%

ROCKNAME Berea 100 sandstone

Descript: SUBLITHARENITE--very fine to fine grained,very well sorted,moderate porosity with qtz overgrowth,carbonate,clay,and minor chlorite cement

Framework Grains

Quartz	53%
Chert	2%
Feldspar	3%
Carbonate	0%
Lithics	8% argillaceous
Opaques	tr.
Other	glauconite, heavy minerals--tr.

Contacts: cc > sut > long > tan

Cement/: qtz overgrowth--11% clay--v. fine grained interparticle rim cement
Matrix minor fine grained sericite on grain boundaries--6% carbonate--interparticle--7% chlorite--as alteration of lithics, qtz and fldsp--1%

Alter-: feldspars are corroded, replaced by clay and calcite, quartz altered
ation to carbonate (zeolite?)

Pore interparticle--.05-.15 to .25mm--9% over half the clay is within all argillaceous lithic grains or altered feldspar grains

ROCKNAME Berea 5-600 sandstone

Descript: QUARTZARENITE--fine to medium grained, well sorted, very high porosity with Fe oxide, quartz overgrowth, and clay cement

Framework Grains

Quartz	66%	
Chert	1%	
Feldspar	1%	
Carbonate	0%	
Lithics	1%	argillite, chert
Opaques	0%	
Other		

Contacts: cc > sut > long > tan

Cement/Matrix: quartz overgrowths--5% clay--1% Fe oxide--8%

Alteration: corrosion of quartz, feldspar

Pore interparticle--.2-.4mm to .5mm--15% grain dissolution of feldspar and rims of quartz--2%

ROCKNAME Boise sandstone

Descript: ARKOSE--fine to medium grained, very well sorted, high porosity with minor carbonate-clay cement

Framework Grains

Quartz	28%	
Chert	0%	
Feldspar	44%	
Carbonate	0%	
Lithics	1%	argillaceous
Opaques	tr.	
Other	biotite, muscovite, heavy minerals--2%	

Contacts: long > cc > tan > sut

Cement/Matrix: "clay"--replacement of feldspar--6% carbonate--replacement of feldspar--3% chlorite--tr.

Alteration: feldspar altered to clay, carbonate lithics altered to chlorite and muscovite

Pore interparticle--13% very little cementation of original pore space

ROCKNAME Fahler 18E142

Descript: QUARTZARENITE--fine grained, very well sorted, low porosity with quartz overgrowth, carbonate and clay cement

Framework Grains

Quartz	35%	
Chert	8%	
Feldspar	3%	
Carbonate	0%	
Lithics	3%	mudstone
Opaques	0%	
Other		

Contacts: long = cc = sut >>> tan

Cement/ Matrix: qtz overgrowths--23% carbonate--blocky interpart. local replacement of qtz--12% clay--7% opaques--2% chlorite--very fine to medium grained books--1% Fe oxide with clay--1% sericite in pore space--2%

Alteration: local carbonate replacement of quartz grains, all feldspar altered

Pore interparticle--.125mm--3% early quartz overgrowth has destroyed most of original porosity

ROCKNAME Fahler 18E154

Descript: SUBLITHARENITE--very fine to fine grained, very well sorted, low porosity with carbonate, quartz, clay, Fe oxide, opaque cement

Framework Grains

Quartz	24%	
Chert	8%	
Feldspar	2%	
Carbonate	0%	
Lithics	4%	argillac. chert--2% argillite--2%
Opaques	1%	
Other	tr.	muscovite

Contacts: cc = long > sut >> tan

Cement/ Matrix: chalcedony--1% opaque--3% Fe oxide--4% carbonate--blocky grains cement and replacement of quartz, chert grains--25% quartz overgrowth--20% kaolinite--3% clay--medium grained repl. of chert--5%

Alteration: feldspar altered to clay quartz, chert grains replaced by carbonate

Pore intergrannular--1%

ROCKNAME Fahler 18E161

Descript: SUBLITHARENITE--medium grained, well sorted, very low porosity with quartz overgrowth, carbonate, and clay cement

Framework Grains

Quartz	25%	
Chert	32%	
Feldspar	1%	
Carbonate	0%	
Lithics	13%	argillaceous chert--5% argillite--7% phyllite--1%
Opaques	0%	
Other	0%	

Contacts: cc = sut = long >> tan

Cement/Matrix: qtz overgrowth--12% carbonate--fine to medium grained interparticle --5% chert/chalcedony--locally developed by chert grains--3% opaque --irregular cement intergrain replacement--3% clay--3% clay/mica--2%

Alteration: feldspar altering to clay

Pore: very low porosity due to 1) lithic clast deformation, 2) chert grain deformation, 3) quartz, carbonate, chert cement

ROCKNAME Fahler 18E162

Descript: SUBLITHARENITE--fine to medium grained, well sorted, low dissolution porosity with quartz overgrowth, Fe oxide, clay cement

Framework Grains

Quartz	46%	
Chert	6%	
Feldspar	0%	
Carbonate	0%	
Lithics	8%	argillaceous/Fe oxide rich chert--1% muscovite schist--tr.
Opaques		
Other		lithics cont. siltstone--1% phyllitic chert--1% argillite--1%

Contacts: cc = long > sut >> tan

Cement/Matrix: quartz overgrowth--25% Fe oxide cement--interparticle--8% clay cement--very fine to fine grained interparticle--4% chlorite--replacement of feldspar--tr.

Alteration: feldspar altered to chlorite--tr.

Pore: dissolution--moldic character--2% less extensive quartz overgrowth with remaining pore space filled by Fe oxide and lack of calcite cmt.

ROCKNAME Fahler 18E189

Descript: SUBLITHARENITE--medium grained, well sorted, very low porosity with quartz, carbonate, chalcedony, Fe oxide cement

Framework Grains

Quartz	27%	
Chert	27%	
Feldspar	3%	
Carbonate	0%	
Lithics	11%	argillite--7% argillaceous chert--4%
Opaques	0%	
Other	muscovite--tr.	

Contacts: cc = sut = long >> tan

Cement/Matrix: qtz overgrowth--13% opaque--4% carbonate--9% fine grained quartz-chalcedony adjacent to chert grains--4% clay--fine to medium grained clays as cement adjacent to clay altered lithics--2%

Alteration: feldspars intensely altered to clay + carbonate opaques (hematite, magnetite) and/or carbonate replace chert grains locally

Pore very low porosity, permeability cement type controlled by local grain i.e. chert cement near chert grains

ROCKNAME Fahler 18E192

Descript: QUARTZARENITE--fine grained, well sorted, very low porosity with quartz overgrowth, carbonate, Fe oxide, clay, pyrite cement

Framework Grains

Quartz	28%	
Chert	3%	
Feldspar	0%	
Carbonate	0%	
Lithics	2%	argillaceous
Opaques	0%	
Other		

Contacts: cc > long > sut >> tan

Cement/Matrix: qtz overgrowth--22% clay--v. f. grained interparticle or rim cement --11% Fe oxide(hm,goethite)--interparticle, intergrown with clay--9% pyrite--framboidal--4% clay--fibrous interparticle--2% carbonate--19%

Alteration: none noted

Pore none noted--very extensive quartz overgrowth, carbonate, and Fe oxide cement

ROCKNAME Gulf Coast sandstone 14807

Descript: SUBARKOSE--fine grained, well sorted, high intergranular porosity with clay, quartz overgrowth and pyrite cement

Framework Grains

Quartz	52%
Chert	5%
Feldspar	9%
Carbonate	0%
Lithics	3% argillite--tr., clay rich chert--3%
Opaques	1%
Other	muscovite, glauconite, garnet, biotite

Contacts: cc = long > tan > sut

Cement/: Matrix pyrite--v. f. grained, disseminated in pore space--1% quartz overgrowths--partly corroded and discontinuous--7% clay--rims clasts plugs pore space--9% Fe oxide--plugs pore space--tr. carbonate--tr.

Alteration: feldspar locally altered to clay

Pore interparticle--12% grain dissolution--2% late corrosion (grain dissolution) of quartz overgrowths has enhanced porosity

ROCKNAME Indiana dark sandstone

Descript: SUBARKOSE--fine grained, well sorted, moderate porosity with hematite and clay cement

Framework Grains

Quartz	57%
Chert	tr.
Feldspar	7%
Carbonate	0%
Lithics	tr.
Opaques	tr.
Other	heavy minerals tr.

Contacts: long = tan > cc > sut

Cement/: Matrix hematite(+clay?)--interparticle replacement of feldspar,lithics--22% clay--rims clasts, replacement of clast margin of feldspar--5%

Alteration: feldspar and chert rich lithics altered to clay + hematite

Pore interparticle--8% hematite is likely a mix of hematite and clay
Indiana dark has less pressure solution and greater total % cement

ROCKNAME Massillon sandstone dark (banded)

Descript: QUARTZARENITE--medium grained, well sorted, high porosity with Fe oxide, clay, quartz overgrowth, and chert cement

Framework Grains

Quartz	61%	
Chert	1%	
Feldspar	1%	
Carbonate	0%	
Lithics	1%	micaceous
Opaques	0%	
Other		

Contacts: cc > long = sut > tan

Cement/: Matrix Fe oxide--interparticle--15% clay--interparticle, medium grained, locally plugs porosity--5% chert--interparticle, locally plugs porosity--1% quartz overgrowths--corroded by later dissolution

Alter-: ation corrosion of quartz grains

Pore interparticle--12% dissolution--tr. quartz overgrowths corroded by later dissolution

ROCKNAME Massillon sandstone dark (banded)

Descript: QUARTZARENITE--medium grained, well sorted, high porosity with Fe oxide, clay, quartz overgrowth, and chert cement

Framework Grains

Quartz	61%	
Chert	1%	
Feldspar	1%	
Carbonate	0%	
Lithics	1%	micaceous
Opaques	0%	
Other		

Contacts: cc > long = sut > tan

Cement/: Matrix Fe oxide--interparticle--15% clay--interparticle, medium grained, locally plugs porosity--5% chert--interparticle, locally plugs porosity--1% quartz overgrowths--corroded by later dissolution

Alter-: ation corrosion of quartz grains

Pore interparticle--12% dissolution--tr. quartz overgrowths corroded by later dissolution

APPENDIX C

Experimental Petrophysical Data in Tabular Form

All the experimental data sets listed in Table 4 and represented in Figures 17 through 23 are listed in this appendix. The differential pressure (confining pressure - pore pressure) that each measurement was taken at is listed in the "PRESS." column. Permeabilities are in milli-Darcies (mD) or microDarcies (uD). The change in properties with pressure is shown in the "NORM." columns and it is this data that is plotted in figures 17 through 23. Note that the absolute values of resistivity formation factor are listed in the "FF" columns but that normalized conductivity formation factor is listed in the "NORM." columns. All data not measured in this study (Yale 1984) has been digitized from published figures.

INDIANA DH
YALE (1984)

PRESS. (BARS)	PERM (mD)	NORM. PERM
10.	30.30	1.000
40.	29.80	.984
90.	29.54	.975
190.	29.08	.960
290.	28.66	.946
390.	27.95	.922
490.	27.61	.911

PRESS. (BARS)	FF	NORM. COND
10.	12.09	1.000
20.	12.16	.994
45.	12.30	.983
70.	12.37	.978
120.	12.44	.972
170.	12.49	.968
220.	12.51	.966
270.	12.54	.964
320.	12.55	.963
370.	12.57	.962
420.	12.60	.960
470.	12.60	.959

PRESS (BARS)	PORO.	NORM. POR
10.	.2670	1.000
40.	.2646	.991
90.	.2633	.986
190.	.2617	.980
290.	.2604	.975
390.	.2591	.971
490.	.2578	.966

TORPEDO
DOBRYNIN (1962)

PRESS. (BARS)	PERM (mD)	NORM. PERM
0.	45.00	1.000
68.	41.40	.920
136.	39.60	.880
204.	38.25	.850
272.	37.35	.830
442.	36.00	.800
714.	34.20	.760
986.	32.85	.730

PRESS. (BARS)	FF	NORM. COND
0.	42.50	1.000
34.	44.22	.961
102.	45.90	.926
204.	47.59	.893
306.	48.46	.877
442.	49.30	.862
714.	49.77	.854
986.	49.88	.852

PRESS (BARS)	PORO.	NORM. POR
0.	.2020	1.000
34.	.2012	.996
102.	.1996	.988
204.	.1984	.982
306.	.1976	.978
442.	.1961	.971
741.	.1953	.967
986.	.1941	.961

BRANFORD
WYBLE (1958)

PRESS. (BARS)	PERM (mD)	NORM. PERM
0.	2.50	1.000
17.	2.36	.943
34.	2.24	.894
51.	2.13	.851
68.	2.04	.817
102.	1.89	.754
136.	1.75	.698
170.	1.63	.653
204.	1.53	.613
238.	1.44	.576
272.	1.37	.549
306.	1.33	.531
340.	1.30	.520

PRESS. (BARS)	FF	NORM. COND
0.	95.10	1.000
17.	99.17	.959
34.	102.92	.924
51.	106.73	.891
68.	109.82	.866
102.	114.86	.828
136.	120.69	.788
170.	125.46	.758
204.	128.51	.740
238.	131.35	.724
272.	132.64	.717
306.	133.01	.715
340.	133.38	.713

PRESS (BARS)	PORO.	NORM. POR
0.	.1090	1.000
17.	.1068	.980
51.	.1049	.962
68.	.1041	.955
102.	.1029	.944
136.	.1013	.929
170.	.1001	.918
204.	.0992	.910
238.	.0989	.907
272.	.0984	.903
306.	.0980	.899
340.	.0977	.896
34.	.1057	.970

FAHLER 162
YALE (1984)

PRESS. (BARS)	PERM (uD)	NORM. PERM	PRESS. (BARS)	FF	NORM. COND	PRESS. (BARS)	PORO.	NORM. POR
25.	273.9	1.000	10.	293.4	1.000	10.	.0297	1.000
60.	123.2	.450	60.	404.2	.726	60.	.0263	.886
110.	74.6	.272	110.	485.4	.605	110.	.0250	.842
160.	51.7	.189	160.	564.7	.520	160.	.0240	.808
210.	40.2	.147	210.	625.6	.469	210.	.0235	.791
260.	34.0	.124	260.	668.1	.439	260.	.0231	.778
310.	29.1	.106	310.	729.0	.403	310.	.0228	.768
			360.	758.5	.387	360.	.0227	.764

TRIASSIC 41
CHIERICI (1967)

PRESS. (BARS)	PERM (mD)	NORM. PERM	PRESS. (BARS)	FF	NORM. COND	PRESS (BARS)	PORO.	NORM. POR
0.	42.40	1.000	0.	144.00	1.000	0.	.2120	1.000
50.	39.90	.941	50.	150.94	.954	50.	.2073	.978
150.	36.59	.863	150.	161.98	.889	150.	.2027	.956
250.	34.13	.805	250.	167.64	.859	250.	.1997	.942
450.	31.21	.736	450.	173.91	.828	450.	.1955	.922

CAMBRIAN 16
CHIERICI (1967)

PRESS. (BARS)	PERM (mD)	NORM. PERM	PRESS. (BARS)	FF	NORM. COND	PRESS (BARS)	PORO.	NORM. POR
0.	9.45	1.000	0.	308.00	1.000	0.	.1370	1.000
50.	8.67	.917	50.	332.61	.926	50.	.1340	.978
150.	7.83	.829	150.	358.97	.858	150.	.1304	.952
250.	7.38	.781	250.	376.99	.817	250.	.1286	.939
450.	7.03	.744	450.	399.48	.771	450.	.1265	.923

FAHLER 154
YALE (1984)

PRESS. (BARS)	PERM (uD)	NORM. PERM	PRESS. (BARS)	FF	NORM. COND	PRESS. (BARS)	PORO.	NORM. POR
25.	9.2	1.000	10.	128.8	1.000	10.	.0442	1.000
60.	5.8	.630	60.	167.8	.768	60.	.0403	.912
110.	3.8	.411	110.	191.5	.673	110.	.0387	.876
160.	2.7	.288	160.	211.9	.608	160.	.0377	.853
210.	2.1	.233	210.	228.8	.563	210.	.0372	.842
260.	1.8	.200	260.	242.4	.531	260.	.0368	.833
310.	1.6	.177	310.	252.5	.510	310.	.0363	.821
			360.	262.7	.490	360.	.0361	.817

FAHLER 192
YALE (1984)

PRESS. (BARS)	PERM (uD)	NORM. PERM	PRESS. (BARS)	FF	NORM. COND	PRESS. (BARS)	PORO.	NORM. POR
25.	7.1	1.000	10.	262.5	1.000	10.	.0458	1.000
60.	5.3	.744	60.	282.9	.928	60.	.0418	.913
110.	4.0	.560	110.	335.8	.782	110.	.0402	.878
160.	3.3	.459	160.	363.0	.723	160.	.0390	.852
210.	2.8	.391	210.	385.2	.681	210.	.0384	.838
260.	2.5	.349	260.	421.0	.623	260.	.0379	.828
310.	2.3	.329	310.	429.5	.611	310.	.0376	.821
			360.	441.4	.595	360.	.0376	.821

TENSLEEP
FATT (1957)

PRESS. (BARS)	PERM (mD)	NORM. PERM	PRESS. (BARS)	FF	NORM. COND	PRESS (BARS)	PORO.	NORM. POR
0.	120.00	1.000	0.	19.00	1.000	0.	.1460	1.000
40.	113.88	.949	40.	19.41	.979	40.	.1456	.997
67.	110.70	.923	67.	19.64	.967	67.	.1453	.995
104.	107.75	.898	104.	19.88	.956	104.	.1452	.995
135.	105.37	.878	135.	20.01	.950	135.	.1449	.992
168.	103.60	.863	168.	20.12	.944	168.	.1446	.991
199.	102.56	.855	199.	20.18	.942	199.	.1446	.991
240.	101.21	.843	240.	20.27	.937	240.	.1446	.991
271.	100.32	.836	271.	20.31	.936	271.	.1444	.989
308.	99.34	.828	308.	20.36	.933	308.	.1444	.989
341.	98.59	.822	341.	20.40	.931	341.	.1442	.988

PLIOCENE 35
CHIERICI (1967)

PRESS. (BARS)	PERM (mD)	NORM. PERM	PRESS. (BARS)	FF	NORM. COND	PRESS (BARS)	PORO.	NORM. POR
0.	36.90	1.000	0.	157.00	1.000	0.	.2010	1.000
50.	35.24	.955	50.	163.20	.962	50.	.1970	.980
150.	32.88	.891	150.	165.79	.947	150.	.1940	.965
250.	31.40	.851	250.	172.34	.911	250.	.1918	.954
450.	29.70	.805	450.	175.42	.895	450.	.1871	.931

TRIASSIC 26
CHIERICI (1967)

PRESS. (BARS)	PERM (mD)	NORM. PERM	PRESS. (BARS)	FF	NORM. COND	PRESS (BARS)	PORO.	NORM. POR
0.	67.70	1.000	0.	17.30	1.000	0.	.1800	1.000
50.	65.74	.971	50.	17.82	.971	50.	.1777	.987
150.	62.76	.927	150.	18.23	.949	150.	.1751	.973
250.	61.20	.904	250.	18.87	.917	250.	.1737	.965
450.	58.97	.871	450.	19.20	.901	450.	.1710	.950

TRIASSIC 27
CHIERICI (1967)

PRESS. (BARS)	PERM (mD)	NORM. PERM	PRESS. (BARS)	FF	NORM. COND	PRESS (BARS)	PORO.	NORM. POR
0.	72.30	1.000	0.	20.10	1.000	0.	.1810	1.000
50.	69.48	.961	50.	20.53	.979	50.	.1788	.988
150.	66.30	.917	150.	21.22	.947	150.	.1759	.972
250.	66.30	.917	250.	21.47	.936	250.	.1747	.965
450.	62.61	.866	450.	21.82	.921	450.	.1725	.953

MASSILLON DV
YALE (1984)

PRESS. (BARS)	PERM (mD)	NORM. PERM	PRESS. (BARS)	FF	NORM. COND	PRESS (BARS)	PORO.	NORM. POR
20.	6.85	1.000	10.	27.35	1.000	20.	.1901	1.000
40.	6.37	.930	20.	27.80	.984	30.	.1892	.995
90.	5.87	.857	45.	29.20	.937	40.	.1886	.992
140.	5.63	.822	70.	30.11	.908	60.	.1877	.988
190.	5.36	.783	120.	31.21	.876	90.	.1869	.983
240.	5.15	.752	170.	31.82	.860	140.	.1859	.978
290.	5.05	.737	220.	32.18	.850	190.	.1853	.975
390.	4.90	.715	270.	32.45	.843	240.	.1848	.972
490.	4.87	.711	320.	32.73	.836	290.	.1842	.969
			370.	32.88	.832	340.	.1838	.967
			420.	33.02	.828	390.	.1833	.964
			470.	33.16	.825	490.	.1825	.960

KIRKWOOD
WYBLE (1958)

PRESS. (BARS)	PERM (mD)	NORM. PERM	PRESS. (BARS)	FF	NORM. COND	PRESS (BARS)	PORO.	NORM. POR
0.	12.30	1.000	0.	40.50	1.000	0.	.1520	1.000
17.	10.71	.871	17.	42.23	.959	17.	.1508	.992
34.	9.94	.808	34.	43.88	.923	34.	.1497	.985
51.	9.31	.757	51.	45.15	.897	51.	.1487	.978
68.	8.77	.713	68.	46.13	.878	68.	.1480	.974
102.	8.13	.661	102.	48.10	.842	102.	.1458	.959
136.	7.68	.624	136.	49.45	.819	136.	.1453	.956
170.	7.27	.591	170.	50.31	.805	170.	.1441	.948
204.	6.95	.565	204.	51.27	.790	204.	.1436	.945
238.	6.73	.547	238.	51.99	.779	238.	.1430	.941
272.	6.49	.528	272.	52.46	.772	272.	.1424	.937
306.	6.32	.514	306.	52.67	.769	306.	.1421	.935
340.	6.19	.503	340.	53.01	.764	340.	.1420	.934

FAHLER 142
YALE (1984)

PRESS. (BARS)	PERM (uD)	NORM. PERM	PRESS. (BARS)	FF	NORM. COND	PRESS. (BARS)	PORO.	NORM. POR
25.	18.0	1.000	10.	164.9	1.000	10.	.0762	1.000
60.	10.1	.559	60.	188.2	.876	60.	.0716	.940
110.	5.6	.311	110.	201.7	.817	110.	.0698	.916
160.	3.8	.213	160.	211.4	.780	160.	.0688	.903
210.	2.9	.163	210.	221.1	.746	210.	.0681	.894
260.	2.5	.139	260.	228.9	.720	260.	.0677	.888
310.	2.1	.114	310.	230.8	.714	310.	.0673	.883
			360.	230.8	.714	360.	.0672	.882

FAHLER 189
YALE (1984)

PRESS. (BARS)	PERM (uD)	NORM. PERM
25.	19.8	1.000
110.	8.7	.436
160.	6.2	.310
210.	4.9	.245
260.	4.2	.210
310.	3.7	.187

PRESS. (BARS)	FF	NORM. COND
10.	738.9	1.000
110.	1114.6	.663
160.	1239.8	.596
210.	1295.3	.570
260.	1347.2	.548
310.	1352.5	.546
360.	1357.9	.544

PRESS. (BARS)	PORO.	NORM. POR
25.	.0185	1.000
110.	.0168	.908
160.	.0159	.859
210.	.0154	.832
260.	.0150	.811
310.	.0148	.800
360.	.0149	.805

MASSILLON DH
YALE (1984)

PRESS. (BARS)	PERM (mD)	NORM. PERM
10.	129.60	1.000
40.	124.25	.959
65.	122.96	.949
90.	121.97	.941
140.	120.88	.933
190.	119.89	.925
290.	118.70	.916
390.	117.61	.908
490.	116.12	.896

PRESS. (BARS)	FF	NORM. COND
10.	23.79	1.000
20.	24.05	.989
45.	24.66	.965
70.	25.11	.948
120.	25.59	.930
170.	25.82	.922
220.	25.96	.916
270.	26.03	.914
320.	26.13	.911
370.	26.19	.908
420.	26.25	.906
470.	26.30	.905

PRESS (BARS)	PORO.	NORM. POR
10.	.1609	1.000
20.	.1607	.999
40.	.1598	.993
65.	.1591	.989
90.	.1585	.985
140.	.1578	.981
190.	.1572	.977
290.	.1565	.972
390.	.1558	.968
490.	.1552	.964

BEREA 100H
YALE (1984)

PRESS. (BARS)	PERM (mD)	NORM. PERM
10.	49.00	1.000
70.	47.21	.963
180.	46.30	.945
280.	45.95	.938
380.	45.54	.929
480.	45.04	.919

PRESS. (BARS)	FF	NORM. COND
20.	17.19	1.000
45.	17.46	.984
70.	17.74	.969
120.	18.04	.953
170.	18.20	.945
220.	18.26	.942
270.	18.31	.939
320.	18.36	.936
370.	18.36	.936
420.	18.38	.935
470.	18.38	.935

PRESS (BARS)	PORO.	NORM. POR
10.	.1650	1.000
55.	.1629	.987
110.	.1620	.982
160.	.1612	.977
210.	.1607	.974
260.	.1603	.972
360.	.1596	.968
460.	.1590	.964

MIOCENE 7
CHIERICI (1967)

PRESS. (BARS)	PERM (mD)	NORM. PERM	PRESS. (BARS)	FF	NORM. COND	PRESS (BARS)	PORO.	NORM. POR
0.	4.42	1.000	0.	383.00	1.000	0.	.0830	1.000
50.	4.19	.949	50.	401.89	.953	50.	.0813	.979
150.	3.93	.889	150.	429.37	.892	150.	.0789	.950
250.	3.72	.842	250.	449.00	.853	250.	.0775	.934
450.	3.52	.797	450.	476.96	.803	450.	.0762	.918

FAHLER 161
YALE (1984)

PRESS. (BARS)	PERM (uD)	NORM. PERM	PRESS. (BARS)	FF	NORM. COND	PRESS. (BARS)	PORO.	NORM. POR
25.	10.3	1.000	10.	424.3	1.000	10.	.0230	1.000
60.	7.3	.710	60.	689.4	.615	60.	.0194	.843
110.	5.2	.504	110.	916.5	.463	110.	.0180	.783
160.	4.1	.397	160.	1088.8	.390	160.	.0170	.739
210.	3.5	.346	210.	1184.9	.358	210.	.0167	.726
260.	3.1	.307	260.	1302.6	.326	260.	.0164	.713
310.	2.8	.278	310.	1378.8	.308	310.	.0161	.700
			360.	1416.9	.299	360.	.0160	.696

BOISE
YALE (1984)

PRESS. (BARS)	PERM (mD)	NORM. PERM	PRESS. (BARS)	FF	NORM. COND	PRESS (BARS)	PORO.	NORM. POR
10.	901.90	1.000	10.	11.99	1.000	10.	.2576	1.000
20.	897.30	.995	35.	12.12	.990	20.	.2571	.998
40.	890.63	.988	60.	12.37	.969	40.	.2565	.996
90.	882.51	.979	110.	12.58	.953	65.	.2558	.993
190.	865.82	.960	160.	12.64	.949	90.	.2554	.991
290.	855.63	.949	210.	12.66	.947	140.	.2547	.989
390.	852.57	.945	260.	12.73	.942	190.	.2542	.987
490.	842.28	.934	310.	12.79	.938	240.	.2537	.985
			360.	12.83	.934	290.	.2532	.983
			460.	12.85	.933	340.	.2528	.981
						390.	.2522	.979
						440.	.2517	.977
						490.	.2512	.975

TRIASSIC 38
CHIERICI (1967)

PRESS. (BARS)	PERM (mD)	NORM. PERM	PRESS. (BARS)	FF	NORM. COND	PRESS (BARS)	PORO.	NORM. POR
0.	400.00	1.000	0.	12.70	1.000	0.	.2050	1.000
50.	393.60	.984	50.	13.33	.953	50.	.2025	.988
150.	384.80	.962	150.	13.55	.937	150.	.1991	.971
250.	377.60	.944	250.	13.69	.928	250.	.1980	.966
450.	369.20	.923	450.	13.82	.919	450.	.1960	.956

TERTIARY 807
YALE (1984)

PRESS. (BARS)	PERM (mD)	NORM. PERM	PRESS. (BARS)	FF	NORM. COND	PRESS (BARS)	PORO.	NORM. POR
10.	152.20	1.000	10.	14.90	1.000	10.	.2180	1.000
40.	146.05	.960	20.	15.06	.989	40.	.2148	.985
90.	141.52	.930	45.	15.63	.953	90.	.2121	.973
140.	139.19	.915	70.	16.04	.929	140.	.2106	.966
190.	136.60	.898	120.	16.51	.903	190.	.2096	.962
290.	134.76	.885	170.	16.84	.885	290.	.2082	.955
390.	132.98	.874	220.	17.04	.875	390.	.2072	.950
490.	131.27	.863	270.	17.17	.868	490.	.2064	.947
			320.	17.33	.860			
			370.	17.42	.855			

CAMBRIAN 6
CHIERICI (1967)

PRESS. (BARS)	PERM (mD)	NORM. PERM	PRESS. (BARS)	FF	NORM. COND	PRESS (BARS)	PORO.	NORM. POR
0.	23.00	1.000	0.	89.20	1.000	0.	.0810	1.000
50.	22.29	.969	50.	94.39	.945	50.	.0802	.990
150.	21.46	.933	150.	99.44	.897	150.	.0789	.974
250.	21.02	.914	250.	103.84	.859	250.	.0778	.961
450.	20.59	.895	450.	107.73	.828	450.	.0769	.949

BEREA 500
YALE (1984)

PRESS. (BARS)	PERM (mD)	NORM. PERM	PRESS. (BARS)	FF	NORM. COND	PRESS (BARS)	PORO.	NORM. POR
10.	494.60	1.000	10.	20.13	1.000	10.	.1970	1.000
20.	488.12	.987	40.	20.49	.982	20.	.1964	.997
50.	476.79	.964	90.	20.64	.975	40.	.1956	.993
90.	472.99	.956	140.	21.14	.952	65.	.1948	.989
140.	467.55	.945	190.	21.63	.931	90.	.1942	.986
190.	462.90	.936	240.	22.17	.908	140.	.1932	.981
290.	456.57	.923	290.	22.65	.889	190.	.1926	.978
390.	450.04	.910	340.	22.91	.879	240.	.1922	.976
490.	442.22	.894	390.	23.33	.863	290.	.1918	.974
			440.	24.34	.827	340.	.1914	.972
			490.	25.12	.801	390.	.1911	.970
						440.	.1908	.968
						490.	.1904	.966

CAMBRIAN 14
CHIERICI (1967)

PRESS. (BARS)	PERM (mD)	NORM. PERM	PRESS. (BARS)	FF	NORM. COND	PRESS (BARS)	PORO.	NORM. POR
0.	31.90	1.000	0.	51.90	1.000	0.	.1090	1.000
50.	31.13	.976	50.	54.01	.961	50.	.1073	.984
150.	30.05	.942	150.	55.69	.932	150.	.1058	.971
250.	29.48	.924	250.	59.31	.875	250.	.1047	.961
450.	29.22	.916	450.	61.28	.847	450.	.1033	.948

TRIASSIC 34
CHIERICI (1967)

PRESS. (BARS)	PERM (mD)	NORM. PERM	PRESS. (BARS)	FF	NORM. COND	PRESS (BARS)	PORO.	NORM. POR
0.	352.00	1.000	0.	13.80	1.000	0.	.1990	1.000
50.	349.89	.994	50.	14.24	.969	50.	.1950	.980
150.	342.85	.974	150.	14.57	.947	150.	.1924	.967
250.	337.57	.959	250.	14.78	.934	250.	.1906	.958
450.	329.47	.936	450.	14.95	.923	450.	.1885	.947